

10. SITE 782¹

Shipboard Scientific Party²

HOLE 782A

Date occupied: 16 March 1989
Date departed: 21 March 1989
Time on hole: 4 days 13 hr 30 min
Position: 30°51.66'N, 141°18.85'E
Bottom felt (rig floor; m, drillpipe measurement): 2970.0
Distance between rig floor and sea level (m): 11.1
Water depth (drillpipe measurement from sea level, m): 2958.9
Total depth (rig floor, m): 3446.8
Penetration (m): 476.8
Number of cores: 50
Total length of cored section (m): 476.8
Total core recovered (m): 282.0
Core recovery (%): 59.1
Oldest sediment cored:
Depth (mbsf): 399.5
Nature: vitric nannofossil chalk
Earliest age: middle Eocene(?)
Measured velocity (km/s): 1.5–2.0
Hard rock:
Depth (mbsf): 399.7
Nature: andesite

HOLE 782B

Date occupied: 21 March 1989
Date departed: 23 March 1989
Time on hole: 23 hr 30 min
Position: 30°51.60'N, 141°18.34'E
Bottom felt (rig floor; m, drillpipe measurement): 2977.0
Distance between rig floor and sea level (m): 11.1
Water depth (drillpipe measurement from sea level, m): 2965.9
Total depth (rig floor, m): 3438.9
Penetration (m): 468.9
Number of cores: 2
Total length of cored section (m): 468.9
Total core recovered (m): 0.5
Core recovery (%): 1.0
Oldest sediment cored:
Depth (mbsf): 459.3
Nature: nannofossil chalk (wash core)
Hard rock:
Depth (mbsf): 459.3
Nature: andesite

Principal results: Site 782 lies on the eastern margin of the Izu-Bonin forearc basin, about halfway between the active volcanic arc and the Izu-Bonin trench. Two holes were drilled: Hole 782A, a 476.8-m hole that was cored fully and described; and Hole 782B, a 468.9-m hole, of which only the last 9.5 m was cored and described, but which was used for two logging runs. However, significant penetration of the glassy, siliceous basement rocks proved impossible. A simple subdivision into two lithologic units was made: one sedimentary (Unit I), the other volcanic basement (Unit II). The sedimentary unit, split into Subunits IA through IC, comprises nannofossil marls and nannofossil chalks, with both dispersed volcanic debris and a total of more than 100 ash layers; the volcanogenic component becomes coarser grained and more abundant near the base, with some interbedding of tuffaceous sediment. Stratigraphic age of the sediments is Pleistocene to middle Eocene, with hiatuses between the uppermost Oligocene and middle Miocene, and between the lower Oligocene and upper Oligocene. Sedimentation rates are low in the bottom part of the succession, increasing upward to a maximum of 47 m/m.y. in the late Pliocene. The volcanic basement comprises angular to subrounded clasts (possibly including pillow fragments) of andesite and dacite-rhyolite that are slightly vesicular and typically contain phenocrysts of plagioclase, orthopyroxene, and clinopyroxene in a glassy groundmass. Geochemical data show that these are transitional between the tholeiitic and calc-alkaline volcanic-arc series.

Interstitial fluids in the sediments exhibit typical effects of water-mineral reactions, with potassium and magnesium decreasing steadily with depth, calcium increasing, and silica increasing to a maximum at about 300 mbsf. Ammonia increases to a maximum at about 150 m as a result of bacterial breakdown of organic matter. Most physical properties of the sediments vary systematically downhole: bulk densities increase from 1.6 to 1.95 kg/cm³, porosities decrease from 70% to 60%, and magnetic susceptibilities and electrical resistivities increase. Logging data show physical and chemical discontinuities at about 300 and 370 m. The latter corresponds to the Oligocene hiatus and is marked by increases in seismic velocity, density, and silica and potassium contents, perhaps reflecting the increased volcanic influx during the Eocene. Magnetic inclination data from Hole 782A cluster around +50° and -50°, indicating little or no translation of the site since the late Eocene. However, declinations are scattered because of core disturbance; thus, no data for the extent of rotation were obtained.

BACKGROUND AND SCIENTIFIC OBJECTIVES

Site 782 is located at 30°51.66'N, 141°18.85'E, at 2958.9 m below sea level (bsl) on the outer half of the Izu-Bonin forearc, about 70 km west of the axis of the Izu-Bonin Trench (Fig. 1). It is the first of a series of sites within the Izu-Bonin forearc region that was drilled during Legs 125 and 126. The purpose of this effort was to study the history of the Izu-Bonin forearc and to compare drilling results in the Izu-Bonin forearc region with those gained in the Mariana forearc region during Leg 60 of the Deep Sea Drilling Project. By drilling at Site 782 we sought to determine the following:

1. The stratigraphy of the forearc and, hence, both the temporal variations in sedimentation, depositional environment, and paleoceanography and the history of intensity and chemistry of arc volcanism;

¹ Fryer, P., Pearce, J. A., Stokking, L. B., et al., 1990. *Proc. ODP, Init. Repts.*, 125: College Station, TX (Ocean Drilling Program).

² Shipboard Scientific Party is as given in list of participants preceding the contents.

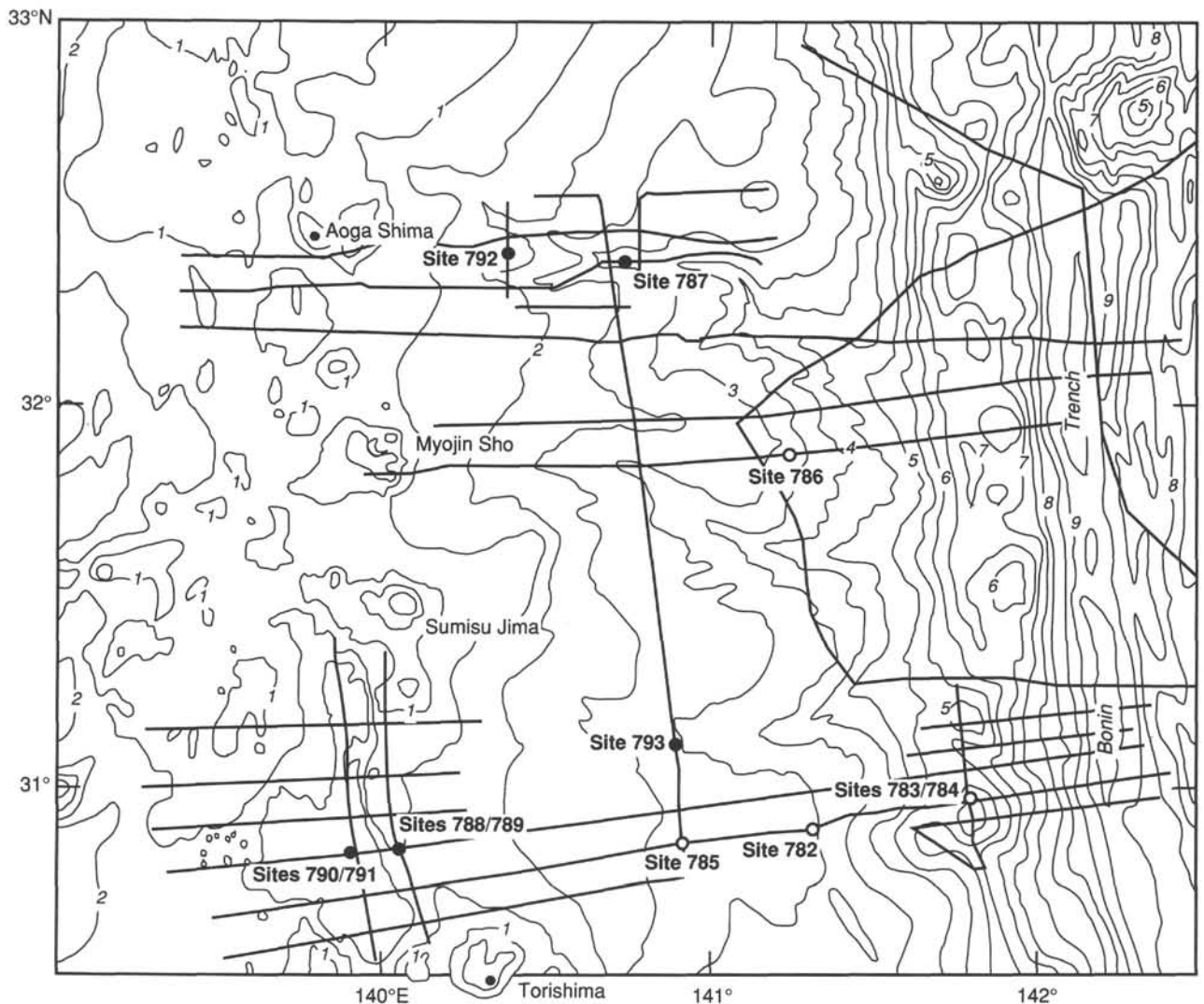


Figure 1. Bathymetry map of the Izu-Bonin forearc and forearc areas from about 30.5°N to 33°N. The locations of sites for Legs 125 and 126 are shown on this map, as are the locations of MCS lines run by B. Taylor. Contour interval is 0.5 km.

2. The uplift/subsidence history of the outer half of the forearc to provide information about forearc flexure and basin development, as well as about the extent of any vertical tectonic activity that may have taken place since formation of the forearc terrane;

3. The nature of igneous basement forming the forearc to answer questions concerning the nature of volcanism in the initial stages of subduction, the origin of boninites, and the formation of the 200-km-wide arc-type forearc crust; and

4. The microstructural deformation and the large-scale rotation and translation of the forearc terrane since the Eocene.

The first of these objectives has been addressed partly through detailed studies of sediments retrieved at Site 782. These sediments contain a record of the history of intensity and composition of arc volcanism, which should help to place constraints on hypotheses regarding the controls over variations in such arc-related phenomena as subduction rates and episodes of backarc spreading.

The complex relationships among tectonic and volcanic phenomena in island arcs, such as changes in subduction rate, periodicity of backarc rifting, pulses of arc volcanism, and

variations in sedimentation rates in forearc environments, are difficult to correlate. Several conflicting models suggest possible interrelationships. For instance, Karig (1975) proposed that periods of arc volcanic maxima correlated with periods of marginal basin formation and high subduction rates. By contrast, Scott and Kroenke (1981) suggested that initial periods of backarc spreading are coincident with minimal arc volcanism. Contrary to both, Hussong and Uyeda (1981) inferred that arc volcanism has probably been continuous since the Eocene, but that the initiation of backarc spreading by arc rifting produced drastic subsidence of the arc volcanoes, which resulted in deep-water eruptions with limited lateral transport of volcanic material. Obviously, a unique solution to such complex interrelations as these cannot be determined without integrating the existing geophysical and geochemical studies with the stratigraphic information gained from drilling. Studies of the chronology and geochemistry of tephra deposits in the forearc basin sites should provide constraints for these various models. In addition, such studies will test whether boninitic (Beccaluva et al., 1980), alkalic (Stern et al., 1984), and/or bimodal basalt and rhyodacitic (Gill et al., 1984; Fryer et al., 1985) volcanism characterize particular types of arc tectonic phenomena, such as periods of arc rifting.

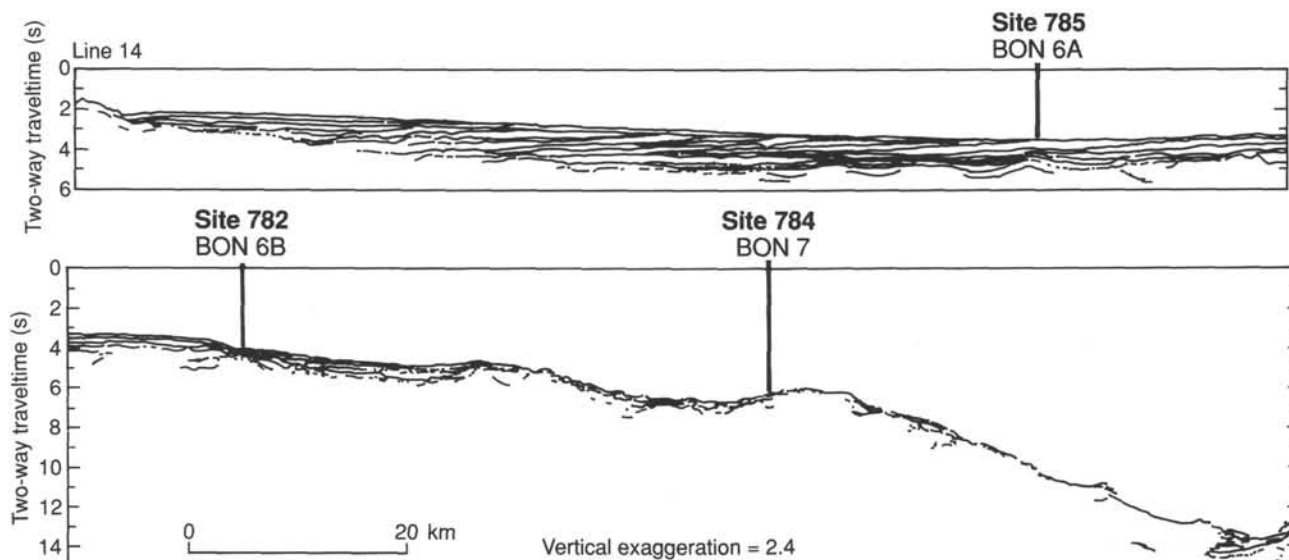


Figure 2. Line drawing of the seismic profile through Site 782.

The second objective can be investigated through a combination of sediment analysis and evaluation of logging results linked to the study of multichannel seismic-reflection data from the forearc. Multichannel seismic (MCS) surveys of the Izu-Bonin forearc revealed a complicated basement that is often seismically stratified and cut by dipping reflectors. These reflection characteristics are unlike those of normal oceanic crustal sections and suggest that Eocene volcanism may have been accompanied or followed by tectonic activity. Alternatively, the Eocene volcanic deposits may have been superimposed on an older terrane stranded in the forearc region (Ogawa and Naka, 1984). The Izu-Bonin forearc basin Site 782 (Fig. 1) was selected in the hope of sampling the hitherto unstudied upper forearc basement to constrain some of the parameters required for modeling forearc evolution. For example, in the Izu-Bonin forearc, the presence of shallow-water Eocene fossils on the Izu-Bonin Islands, and of a well-developed submarine canyon system and lower-slope terrace elsewhere in the forearc (see Fig. 1), suggests that fairly stable conditions have prevailed since the anomalous Eocene phase of arc-basin development. This hypothesis can be tested at Site 782 by determining the uplift-subsidence history and by comparing the results with those from other holes across the forearc, using backstripping techniques on cored/logged holes and seismic stratigraphic analyses of interconnecting MCS profiles (Fig. 2). Microstructures in the drill cores also should help to determine the intensity of faulting in space and time across the forearc terrane.

In addition, several unanswered questions arise regarding a number of other structural aspects of forearc evolution. Were the volcanic arc and forearc regions developed by igneous construction or by differential uplift? Did forearc basins form in response to spreading or to differential subsidence? Was flexural loading by arc volcanoes or by coupling with the subducting plate an important process during construction of the forearc? Determining the forearc vertical displacement history should provide some of the information about forearc flexure and basin development necessary to answer these questions.

The third objective at this site, to answer questions about the nature of volcanism in the initial stages of subduction, can be achieved by evaluating three main alternative hypotheses for the origin and evolution of the Izu-Bonin forearc terrane.

The active volcanic arc (Izu arc) and the forearc terrane might have been continuous originally, but may have been separated subsequently by forearc spreading. The volcanic arc and forearc terrane may have been built separately, but nearly synchronously, on former Philippine Sea Plate crust. The terrane might form part of a continuous Eocene arc volcanic province, possibly with overprints of later forearc volcanism. Each scenario of forearc development implies a different crustal structure for the forearc.

Another question is how do the various models for forearc evolution relate to ophiolite formation? Many scientists now ascribe a majority of ophiolites to subduction-related settings because of their chemistry and associated sediments. Pearce et al. (1984) proposed that supra-subduction zone (SSZ) ophiolites (defined as those having the geochemical characteristics of island arcs, but the structure of oceanic crust) formed by seafloor spreading during the initial stages of subduction, prior to the development of any volcanic arc. Boninites, whose type locality is the Izu-Bonin Islands, are a common occurrence in SSZ ophiolites. They may require variable degrees of hydrous partial melting of a refractory source to produce wet magmas. These magmas then rise to shallow depth while maintaining fairly high temperatures to avoid amphibole crystallization. These unusual conditions may prevail only during initial subduction or arc rifting. However, the eruptive style and exact tectonic setting of the Eocene volcanism are unclear.

With the exception of dredge hauls from inner trench walls and large fault scarps (Bloomer, 1983; Bloomer and Hawkins, 1983; Bloomer and Fisher, 1987; Johnson and Fryer, 1988), our direct knowledge of intraoceanic forearc basement is based primarily on data from the Mariana and Tonga frontal arc islands (Guam, Saipan, and 'Eua) and the Izu-Bonin Islands, all of which expose Eocene island-arc tholeiites and boninites (Reagan and Meijer, 1984; Ewart et al., 1977; Shiraki et al., 1980) and from DSDP Leg 60, Sites 458 through 461, which sampled Eocene arc tholeiites and lower Oligocene boninites and arc tholeiites from the Mariana outer-forearc. Only in dredge hauls at one site in the Mariana forearc near Conical Seamount has the deep forearc basement been sampled (Johnson and Fryer, 1988). From the available data, one may assume that the present 150- to 220-km-wide Izu-Bonin-Mariana forearc formed in large part by volcanism in the initial

stages of arc development during the Eocene and early Oligocene. Similar volcanism has not taken place since and, to our knowledge, cannot be studied as an active phenomenon anywhere on Earth at present. However, basement beneath the thickly sedimented upper-slope basin between the volcanic arc and the region of the break in slope of the inner trench wall has never been sampled. Thus, drilling at Site 782 should extend our knowledge of forearc basement to this area.

The fourth objective of the site, the study of microstructures and plate rotations, can be addressed through a study of the paleomagnetic properties of the cored materials. Measurements of the paleomagnetic properties of subaerial portions of the Izu-Bonin and Mariana forearcs have shown at least 20° of northward drift and 30° to more than 90° of clockwise rotation since the Eocene (see summary in Keating et al., 1983). How and when these motions took place, and the nature of their relationship to the overall structural evolution of the forearc, are enigmatic. One model suggests that the islands acted as "ball-bearings" between the Pacific and Philippine Sea plates. Karig and Moore (1975), and later Ogawa and Naka (1984), suggested that the islands might be an exotic terrain introduced from the south by oblique motion. However, marine geophysical data indicate a structural continuity of the Izu-Bonin Islands with the outer-arc high (Honza and Tamaki, 1985) and support Keating et al.'s model (1983) that the Izu-Bonin Islands (and therefore the Philippine Sea Plate) were situated near the Equator during the Eocene, roughly perpendicular to their present trend. If true, this hypothesis has major implications for reconstructions of the Philippine Sea and surrounding plates, and the related issues of initial subduction and West Philippine Basin evolution. We hope that studies of the paleomagnetism of the cores will permit testing of this model and its further refinement.

OPERATIONS

Transit from Site 781 to Site 782

The 770-nmi transit from Site 781 to Site 782 was completed in 75 hr, 45 min. Site 782 was established at 0900 Universal Time Coordinated (UTC), 16 March 1989, by dropping a beacon. Because a GPS window did not exist and no good satellite location fixes were obtained during the approach to the site, additional surveying was performed after the beacon drop to ensure that the site location was correct.

Hole 782A

The vessel was positioned over the beacon at 1300UTC, 16 March. A standard APC/XCB bottom-hole assembly (BHA), including a nonmagnetic drill collar, was prepared with a soft-formation bit and lockable flapper valve (LFV). The trip into the hole began at 1330UTC, 16 March, with 45- to 50-kt winds, 15- to 18-ft seas, and 20-ft swells. The topography of the seafloor was such that several echoes were recorded by the precision depth recorder (PDR); therefore, the drill string was tripped in cautiously until weight was taken by the sediments. The first APC core barrel retrieved was completely full and considered a misrun. The BHA was lifted 9.5 m, and another APC core was taken, which produced a water core. The BHA was then lowered 5 m and a third APC core was taken. When retrieved, the core barrel was found to contain 10 m of core. Operations were hampered by inclement weather, and considerable time was required to retrieve the first two core barrels. Therefore, we declared the mud line at 2958.9 mbsl, and Hole 782A was officially spudded at 2200UTC, 16 March. Core orientation began with Core 125-782-5H and continued through Core 125-782-9H. Heat flow was measured after Cores 125-782-4H at 38.3 mbsf and 125-782-7H at 66.8 mbsf.

Approximately 12 hr of coring time was lost during the first 36 hr of drilling at Hole 782A. Rough seas and the heave of the ship caused the latch safety-release pins on the sinker bars to shear during deployment of the APC. During retrieval of the sinker-bar assembly to change shear pins, the core barrels remained in the BHA and were subjected to the heave of the ship, causing core disturbance. After nine cores, the XCB was deployed. The first retrieval of the XCB also resulted in a sheared pin. Finally, with calmer weather and the use of the XCB, coring proceeded without sheared pins.

Excellent recovery was achieved as the hole was advanced to 399.5 mbsf. At that depth, an extensive ash layer was encountered and recovery declined dramatically. A noticeable reduction in the drilling rate occurred at 470 mbsf when drilling in andesite, and the bit became plugged. The core barrel was dropped during recovery and attempts to latch onto it were futile. All circulation was lost, so we decided to trip out of the hole.

The pipe was pulled to 457 mbsf, where it became stuck during removal of a connection. Further attempts to free the drill string failed, and it had to be severed at 1340UTC, 20 March. An explosive charge was used to sever the second joint of drill pipe above the drill collar.

The drill pipe was pulled out of the hole and, with the severed joint back on board at 2230UTC, 20 March, Hole 782A officially ended. The APC had been deployed nine times, with 85.5 m cored and 90 m of recovered core for a recovery rate of 105% (Table 1). The XCB was deployed 41 times, with 391 m cored and 188 m of recovered core for a recovery rate of 48%. The hole was advanced to a final depth of 476.8 mbsf (Table 1).

Hole 782B

Because we had not achieved our basement objective at Site 782, a standard RCB BHA with a mechanical bit release (MBR) and bit was prepared for coring a second hole. The vessel was offset 100 m to the south, and the pipe trip back to the seafloor began at 2230UTC, 20 March. The seafloor was reached at 0700UTC, 21 March, at 2965.9 mbsl. Hole 782B had been drilled to 459.3 mbsf, when problems began in the form of bit plugging and increasing torque. Only one 9.6-m-RCB core was cut, with 0.1 m of recovered core for a recovery rate of 1%. The hole was drilled to 459.3 m and cored 9.6 m to a final depth of 468.9 mbsf.

A wiper trip from 3375.9 to 3424.9 mbsf was made to prepare the hole for logging. The MBR released without any problems, and the hole was filled with KCl mud. The logging equipment was prepared, the BHA was raised to 71 mbsf, and logging began. Two successful logging runs were conducted. The first used the dual induction tool (DIT), the dual lithodensity tool (HLDT), the sonic digital tool (SDT), and the natural gamma-ray spectrometry (NGT) tool; the second run used the induced gamma-ray spectroscopy tool (GST), the general purpose inclination tool (GPIT), the aluminum clay tool (AC), the compensated neutron porosity tool (CNT), and the natural gamma-ray spectrometry tool (NGT). The third run employed the magnetic susceptibility tool, which flooded 100 m below the keel and had to be retrieved, ending the logging program.

The Schlumberger equipment was rigged down, and the pipe trip out of the hole began at 0800UTC, 23 March. Site 782 officially ended at 1345UTC, 23 March, when the BHA was back on deck and the vessel departed for Site 783.

LITHOSTRATIGRAPHY

Introduction

The stratigraphic section recovered at Site 782 is divided into two lithologic units: Unit I (Holocene? to middle Eocene)

Table 1. Coring summaries, Site 782.

Core no.	Date (March 1989)	Time (UTC)	Depth (mbsf)	Length cored (m)	Length recovered (m)	Recovery (%)
125-782A-1H	17	0130	0-9.8	9.8	9.80	100.0
2H	17	0230	9.8-19.3	9.5	9.95	105.0
3H	17	0345	19.3-28.8	9.5	10.0	106.0
4H	17	0445	28.8-38.3	9.5	10.03	105.6
5H	17	0800	38.3-47.8	9.5	10.04	105.7
6H	17	0935	47.8-57.3	9.5	10.01	105.3
7H	17	1315	57.3-66.8	9.5	10.04	105.7
8H	17	1945	66.8-76.3	9.5	10.11	106.4
9H	17	2245	76.3-85.8	9.5	9.93	104.0
10X	18	0105	85.8-95.7	9.9	2.52	25.4
11X	18	0200	95.7-105.3	9.6	4.06	42.3
12X	18	0300	105.3-115.0	9.7	5.07	52.2
13X	18	0345	115.0-124.6	9.6	5.05	52.6
14X	18	0415	124.6-134.3	9.7	6.17	63.6
15X	18	0510	134.3-143.9	9.6	5.07	52.8
16X	18	0550	143.9-153.6	9.7	4.26	43.9
17X	18	0630	153.6-163.2	9.6	7.87	82.0
18X	18	0700	163.2-172.9	9.7	2.78	28.6
19X	18	0745	172.9-182.5	9.6	5.40	56.2
20X	18	0830	182.5-192.1	9.6	0.87	9.1
21X	18	0900	192.1-201.8	9.7	7.16	73.8
22X	18	0945	201.8-211.5	9.7	1.64	16.9
23X	18	1020	211.5-221.0	9.5	9.85	103.0
24X	18	1100	221.0-230.7	9.7	2.68	27.6
25X	18	1140	230.7-240.3	9.6	9.42	98.1
26X	18	1230	240.3-250.0	9.7	9.82	101.0
27X	18	1310	250.0-259.6	9.6	3.94	41.0
28X	18	1350	259.6-269.2	9.6	9.37	97.6
29X	18	1435	269.2-278.8	9.6	9.69	101.0
30X	18	1525	278.8-288.5	9.7	3.35	34.5
31X	18	1700	288.5-294.0	5.5	4.42	80.3
32X	18	2145	294.0-303.5	9.5	8.86	93.2
33X	18	2245	303.5-313.1	9.6	9.82	102.0
34X	18	2345	313.1-322.5	9.4	1.92	20.4
35X	19	0050	322.5-332.1	9.6	9.83	102.0
36X	19	0230	332.1-341.6	9.5	7.92	83.3
37X	19	0400	341.6-351.2	9.6	9.87	103.0
38X	19	0515	351.2-360.9	9.7	0.00	0.0
39X	19	0645	360.9-370.5	9.6	2.64	27.5
40X	19	0800	370.5-380.2	9.7	6.29	64.8
41X	19	0915	380.2-389.8	9.6	9.82	102.0
42X	19	1035	389.8-399.5	9.7	3.45	35.5
43X	19	1200	399.5-409.2	9.7	0.21	2.2
44X	19	1325	409.2-418.8	9.6	0.21	2.2
45X	19	1515	418.8-428.5	9.7	0.40	4.1
46X	19	1655	428.5-438.2	9.7	0.00	0.0
47X	19	1900	438.2-447.9	9.7	0.00	0.0
48X	19	2100	447.9-457.6	9.7	0.00	0.0
49X	19	2305	457.6-467.1	9.5	0.15	1.6
50X	20	0830	467.1-476.8	9.7	0.17	1.8
Coring total				476.8	282.00	59.1
125-782B-1W	22	0100	0-459.3	459.3	0.40	(wash core)
2R	22	0200	459.3-468.9	9.6	0.10	1.0
Coring total				9.6	0.10	1.0
Washing total				459.3	0.40	
Combined total				468.9	0.50	

and Unit II (the andesitic basement rocks, Table 2). Variability within the three subunits of Unit I represents gradational changes in the relative dominance of various sedimentary components. All of the sediment types found at Site 782 are present in each subunit.

Unit I

Cores 125-782A-1H-1, 0 cm, to 125-782A-43X-CC, 16 cm; depth, 0-409.2 mbsf.

Age: Holocene(?) to middle Eocene.

This unit extends from the sediment/water interface to 409.2 mbsf and includes the entire sedimentary sequence overlying andesitic basement. Nannofossil age determinations

place the top of this unit as Holocene(?) or late Pleistocene and the base as middle Eocene. The dominant lithology of this unit is nannofossil marl or nannofossil chalk. Ash layers are found throughout Unit I (see Table 3). There are no striking breaks of the lithology, although burrowing, vitric components and induration all increase downsection.

Subunit IA (Cores 125-782A-1H-1 to 125-782A-16X-CC, 9 cm; depth, 0-153.6 mbsf).

Age: Holocene(?) to early Pliocene.

The uppermost part of this subunit is composed of gray (5Y 5/1) to yellow-greenish (5Y 7/1), homogeneous nannofossil marl. Core recovery was more than 100% in the 0- to 100-m interval, probably because of the lithologic homogeneity.

Table 2. Lithologic units recovered at Site 782.

Lithologic unit/subunit	Core section, interval (m)	Depth (mbsf)	Dominant lithology	Stratigraphic age
IA	125-782A-1H-1, 0 to 125-782A-16X-CC, 9	0 to 153.6	Nannofossil marls	Holocene(?) to lower Pliocene
	125-782A-17X-1, 0 to 125-782A-35X-5, 145	153.6 to 337.0		upper Miocene to middle Miocene
IC	125-782A-35X-5, 145 to 125-782A-43X-CC, 16	337.0 to 409.2	Nannofossil chalks, vitric nannofossil chalks	upper Oligocene to middle Eocene
	125-782A-43X-CC, 16 to 125-782A-50X-1, 42	409.2 to 476.8		Andesitic rocks

Faint horizontal laminations, some graded bedding, and sporadic burrowing were the only sedimentary structures observed.

The section contains volcanic ash layers less than 1 to 8 cm thick, of light and dark colored vitric fragments, often with feldspar, and commonly graded (see Table 3). Inverse grading occurs locally as a result of density segregation during gravitational flow and settling of pumice and smaller vitric/crystal grains. Other characteristic structures of the lower part of Subunit IA include vertical burrows and slumps. Burrows commonly are filled with ash and locally are filled with nannofossil marl. Sedimentary stratigraphy and structures are largely missing in the upper 15 cores because of severe coring disturbance.

In smear slides, the main components present other than calcareous nannofossils, radiolarians, and foraminifers are glass (10%), carbonate grains (7%), opaque minerals (7%), feldspar (5%), with minor pyroxene (2%) and chlorite (1%), and traces of quartz, zoisite/epidote, serpentine, aragonite, and glauconite.

Subunit IB (Cores 125-782A-17X-1, 0 cm, to 125-782A-35X-5, 145 cm; depth, 153.6–337.0 mbsf).

Age: late to middle Miocene.

Subunit IB is characterized by extensive bioturbation, by an increase in the amount of volcanic detritus, and by the proportion of alternating light gray (5Y 7/1) and dark gray (5Y 4/1) sequences having thicknesses of 1 dm to several decimeters. Greenish colors are not present; the major lithology remains nannofossil marl (as in Subunit IA); volcanic debris as ash layers and interspersed allochthonous material remains somewhat constant. The increased induration may be the cause of poorer core recovery. Burrows are more common in Subunit IB than in Subunit IA. These burrows are typically horizontal and are rarely larger than about 1 mm, although larger ones are present.

Although rare laminations do occur in the subunit, any primary depositional textures that were present would certainly have been destroyed by this intense bioturbation. Volcanic ash is present, both as separate layers and dispersed and mixed within the nannofossil chalk. The color of the strata depends largely on the relative abundances of the components forming the sediment: large proportions of nannofossils cause lighter colors, whereas abundant glass particles cause darker colors.

In smear slides, components present (other than nannofossils, radiolarians, and foraminifers) are glass (20%), feldspar (8%), opaque minerals (5%), with minor pyroxene (3%),

epidote/zoisite, and traces of chlorite, glauconite, amphibole, and zeolite.

Subunit IC (Cores 125-782A-35X-5, 145 cm, to 125-782A-43X-CC, 16 cm; depth, 337.0–409.2 mbsf).

Age: late Oligocene to middle Eocene.

Subunit IC is predominantly vitric nannofossil chalk with frequent intercalations of volcanic ash. Volcanogenic minerals, which include pyroxene (7%), feldspar (5%), glass (approximately 25%) and their alteration products (zeolites, 2–50%; and serpentines, 0–12%), become more abundant with depth. Because of the greater variability of the strata compared with the overlying subunits, the colors of the sediments vary between brownish, grayish, and greenish hues over relatively short intervals.

Breccialike zones and intervals in Intervals 125-782A-39X-1, 21–121 cm, and 125-782A-42X-1, 12–40 cm, may be drilling breccia or primary structures. However, near the base of Subunit IC, pebble-rich sands and gravelly conglomerates are intercalated within the nannofossil chalks and become the dominant lithologies in the bottom of Subunit IC. Serpentine-filled veins and interstitial pore spaces are common in these strata. A thin basaltic layer directly overlies the basaltic basement in Core 125-782A-43X-CC. Core recovery in this interval was less than 50%.

In smear slides, components other than nannofossils, radiolarians, and foraminifers are glass (25%), opaque minerals (8%), pyroxene (7%), feldspar (5%), with minor epidote/zoisite (6%), zeolite (except 50% in one sample), serpentine (except 12% in one sample), amphibole, and traces of quartz.

Unit II

Cores 125-782A-43X-CC, 16 cm, to 125-782A-50X-1, 42 cm; depth, 409.2–476.8 mbsf.

For a description of the rocks recovered from this lithologic unit, see "Igneous and Metamorphic Petrology" section (this chapter).

BIOSTRATIGRAPHY

Evidence from calcareous nannofossils, planktonic foraminifers, and diatoms indicates that the sediments overlying the igneous rock range in age from late Pleistocene to middle Eocene (Fig. 3). Epoch boundary markers are found in Samples 125-782A-4H-CC (Pleistocene), 125-782A-16X-CC (Pliocene), 125-782A-35X-5, 120–121 cm (Miocene), and 125-782A-39X-CC (Oligocene). Hiatuses may exist between the

Table 3. Preliminary compilation of ash layers found in lithologic Unit I at Site 782.

Core, section, interval (cm)	Depth (mbsf)	Volcanic layer
125-782A-1H-1, 90	0.9	1
1H-3, 24	3.24	2
1H-3, 130	4.3	3
2H-4, 86	15.16	4
2H-4, 90	15.2	5
2H-4, 103-104	15.33	6
2H-4, 114	15.44	7
2H-4, 131	15.61	8
2H-5, 107-115	16.87-16.95	9
2H-5, 127-150	17.3	10
2H-6, 0-8	18.1	11
2H-6, 85-86	18.16	12
5H-6, 18-19	45.98	13
6H-3, 21-27	51.01-51.07	14
6H-4, 84-91	53.14-53.21	15
6H-6 55-57	55.85-55.87	16
6H-6, 87-90	56.17-56.20	17
7H-3, 67-69	60.97-60.98	18
7H-3, 106-110	61.36-61.40	19
7H-4, 79-84	62.53-62.64	20
7H-7, 59-61	66.89-66.91	21
8H-4, 94-95	72.24	22
8H-4, 122-123	72.52	23
11X-1, 54-57	96.24-96.27	24
11X-1, 110-117	96.80-96.87	25
11X-2, 37-38	97.57	26
11X-3, 0-1	98.7	27
11X-3, 9.5-10	98.8	28
11X-3, 51-54	99.21-99.24	29
12X-1, 20	105.5	30
12X-1, 28-29	105.58	31
12X-2, 9-10	106.8	32
12X-2, 16-17	106.96	33
12X-CC, 22-23	110.27	34
13X-2, 103-104	117.53	35
13X-3, 51.5-52.5	118.52	36
14X-2, 10-11	126.2	37
14X-2, 82-83	126.52	38
14X-2, 112-116	117.22-127.26	39
14X-2, 140-144	127.50-127.54	40
14X-3, 41-45	128.01-128.05	41
14X-5, 15-18	130.0-130.65	42
15X-2, 105.5-106.5	136.86	43
15X-2, 115	136.95	44
15X-2, 117	136.97	45
15X-3, 8-16	137.38-137.54	46
15X-3, 101-105	138.31-138.35	47
15X-3, 113-115	138.41-138.43	48
15X-4, 13.5-17.0	138.93-138.97	49
16X-3, 96-97	147.86	50
17X-1, 54-55	154.14	51
17X-2, 3-5	155.13-155.15	52
17X-2, 102-103	156.12	53
17X-2, 124-125	156.34	54
17X-3, 121	157.81	55
17X-4, 0-2	158.08-158.12	56
17X-4, 73-74	158.83	57
17X-5, 139-141	160.99-161.01	58
18X-1, 10-16	163.36-163.38	59
19X-1, 147-148	174.37	60

Table 3. (continued).

Core, section, interval (cm)	Depth (mbsf)	Volcanic layer
19X-2, 23-27	174.63-174.67	61
19X-3, 104-105	176.94	62
19X-CC, 13-14	178.08	63
20X-CC, 10	183.26	64
21X-1, 51-53	192.61-192.62	65
21X-1, 64-66	192.74-192.76	66
21X-2, 48-51	194.08-194.10	67
21X-2, 82-86.5	194.42-194.46	68
21X-2, 96-97	194.56	69
21X-2, 127-128	194.87	70
21X-3, 0-1	195.1	71
21X-3, 72	195.82	72
21X-5, 42-45	198.52-198.55	73
23X-2, 15-16	213.15	74
23X-3, 23-26	214.73-214.76	75
23X-3, 93-94	215.33	76
23X-4, 107-109	217.07-217.09	77
23X-4, 132-133	217.32	78
23X-5, 40-45	217.90-217.95	79
23X-5, 83-86	218.33-218.36	80
23X-6, 67-68	219.67	81
23X-6, 134-137	220.34-220.37	82
23X-6, 141-144	220.41-220.44	83
24X-1, 44-45	221.44	84
24X-2, 2-3	222.7	85
25X-4, 32-36	235.52-235.56	86
25X-4, 114	236.34	87
26X-1, 138	241.68	88
26X-1, 140	241.7	89
26X-2, 83-85	242.63-242.65	90
28X-1, 98-99	260.58	91
28X-3, 17	262.77	92
29X-3, 9-10	273.1	93
29X-3, 43-46	272.63-272.66	94
29X-3, 90	273.1	95
29X-4, 85-90	274.55-274.67	96
29X-5, 12-15	275.32-272.35	97
29X-6, 19-21	276.89-276.91	98
29X-6, 30-41	277.00-277.11	99
29X-7, 35-37	278.55-278.57	100
30X-2, 9-10	280.39	101
30X-2, 30-31	280.6	102
31X-1, 17	288.67	103
31X-1, 22-24	288.72-288.74	104
32X-2, 41-46	295.91-295.96	105
32X-4, 124	299.74	106
32X-6, 32-35	301.82-301.85	107
33X-3, 82-85	307.82-307.35	108
33X-5, 87-88	310.37	109
33X-7, 27-29.5	312.77-312.80	110
34X-CC, 20-26.5	314.79-314.85	111
37X-5, 85-87	348.45-348.47	112
39X-2, 9	362.49	113
39X-2, 44-45.5	362.88	114
39X-2, 70-71	363.1	115
41X-4, 23-24	384.93	116

These ash layers represent primary ash-fall deposits from a nearby volcanic event. Not listed are additional layers at this site that are interpreted as reworked volcanoclastic debris, presumably deposited by turbidity currents, bottom currents, debris flows, and so forth.

late Oligocene and middle Miocene and between the early Oligocene and late Oligocene.

Calcareous Nannofossils

Pleistocene through middle Eocene nannofossil assemblages are present in Hole 782A.

Pleistocene

Pleistocene nannofossil assemblages are abundant and moderately to well-preserved in Samples 125-782A-1H-1, 20

cm, to 125-782A-4H-CC on the basis of the presence of *Emiliania huxleyi*, *Gephyrocapsa oceanica*, *G. caribbeanica*, *Pseudoemiliania lacunosa*, *Helicosphaera sellii*, and other species. Samples 125-782A-1H-1, 20 cm, to 125-782A-1H-CC, 125-782A-2H-1, 53 cm, and 125-782A-2H-CC to 125-782A-4H-CC define the late Pleistocene (Zone CN15), middle Pleistocene (CN14b subzone), and early Pleistocene (CN14a subzone), respectively.

Gephyrocapsa oceanica is absent in Sample 125-782A-5H-3, 86 cm, whereas *Pseudoemiliania lacunosa*, *Calcidiscus*

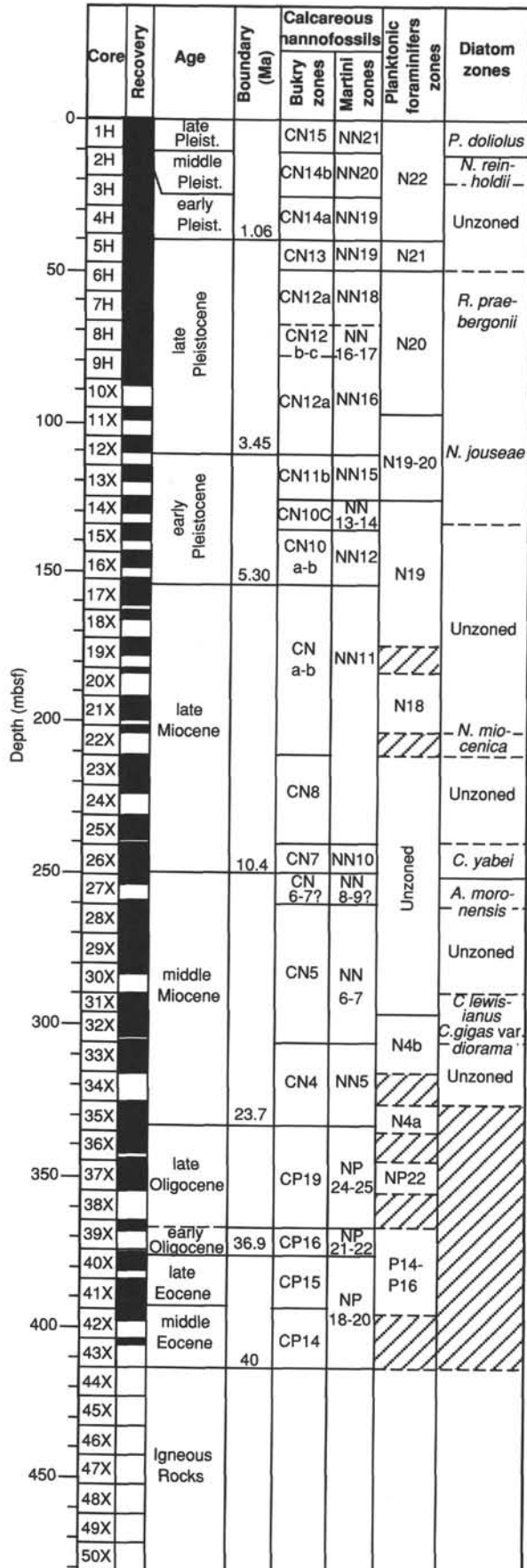


Figure 3. Biostratigraphic summary for Site 782.

macintyreii, and *Gephyrocapsa caribbeanica* are common; this sample was assigned to the late Pliocene (CN13a subzone), following Backman, Duncan, et al. (1988). Thus, the Pliocene/Pleistocene boundary is located within Sections 125-782A-5H-1 or 125-782A-5H-2.

Pliocene

Late Pliocene nannofossil assemblages are present from Sample 125-782A-5H-3, 86 cm, to 125-782A-11X-CC. The abundant and moderately to well-preserved assemblages are characterized by marker species of late Pliocene age, *Discoaster asymmetricus*, *D. brouweri*, *D. pentaradiatus*, *D. surculus*, *D. tamalis*, and *Ceratolithus separatus* (CN12a subzone). The last occurrence of *Discoaster brouweri*, together with *D. triradiatus*, is present in Sample 125-782A-6H-CC; the CN12/CN13 boundary thus is present in Core 125-782A-6H.

The last occurrence of *Reticulofenestra pseudumbilica* (top of Zone CN11), which coincides approximately with the lower Pliocene/upper Pliocene boundary, is present in Sample 125-782A-12X-CC. This moderately preserved assemblage is characterized by *Sphenolithus abies*, *Discoaster asymmetricus*, and *Pseudoemiliania lacunosa*, together with *Discoaster brouweri* and *D. pentaradiatus*. The first occurrence of *Discoaster tamalis* and the last occurrence of *Reticulofenestra pseudumbilica* and *Sphenolithus* spp. overlap in this sample. This association, together with *Amaurolithus delicatus* and *A. tricorniculatus*, is common to abundant down to Sample 125-782A-16X-CC, where the first occurrence of *Ceratolithus acutus* can be found. In Sample 125-782A-17X-CC, the last occurrence of *Discoaster quinquerramus*, *D. berggreni*, and *Triquetrorhabdulus rugosus*, together with the first occurrence of *Amaurolithus tricorniculatus*, was found. Thus, the Miocene/Pliocene boundary is located within Core 125-782A-17X.

Miocene

Few-to-abundant, moderately preserved late Miocene nannofossil assemblages are present in Samples 125-782A-17X-CC to 125-782A-26X-CC. The top of this assemblage has been defined by the last occurrence of *Discoaster quinquerramus* together with *Triquetrorhabdulus rugosus*; the bottom lies between the first occurrence of *Catinaster coalitus* and the first occurrence of *Catinaster calyculus*, within Zone CN6.

The first occurrence of *Discoaster quinquerramus* in Sample 125-782A-22X-CC defines the Zone CN8/CN9 boundary. We expected *Discoaster berggreni*, *D. surculus*, and *D. neohamatus* to appear before *Discoaster quinquerramus*, indicating drilling disturbances in these cores.

Sample 125-782A-25X-7, 7 cm, contains the first occurrence of *Discoaster pentaradiatus* together with *D. prepentaradiatus*. Sample 125-782A-26X-4, 92-94 cm, is characterized by the last occurrence of *Discoaster hamatus* (although very rare) and *Catinaster coalitus* (marker species for Zone CN7), together with *Catinaster calyculus* and *Discoaster calcaris*. Therefore, the Zone CN7/CN8 boundary has been placed between Samples 125-782A-25X-7, 7 cm, and 125-782A-26X-4, 92-94 cm.

Middle Miocene nannofossil assemblages were found in Samples 125-782A-27X-1, 110 cm, to 125-782A-35X-5, 125 cm, whereas the early Miocene is completely missing. Sample 125-782A-35X-5, 125 cm, is middle Miocene in age (Zone CN4) on the basis of the occurrence of *Sphenolithus heteromorphus*, together with *Calcidiscus macintyreii*, *C. leptoporus*, and *Discoaster variabilis*. The presence of specimens of *Reticulofenestra pseudumbilica* larger than 7 mm indicates that this sample is located in the upper part of Zone

CN4. Reworked species of Zone CN2 *Discoaster druggi* and *Sphenolithus belemnoides* also are present. The top of Zone CN4 can be found in Sample 125-782A-33X-CC, in which the last occurrence of *Sphenolithus heteromorphus* was found. The last occurrence of *Cyclocargolithus floridanus* (Sample 125-782A-30X-2, 21 cm) and the first occurrence of *Discoaster kugleri* (Sample 125-782A-29X-CC) indicate the Zone CN5a/CN5b boundary. Drilling disturbances are common in middle Miocene cores.

However, Sample 125-782A-35X-6, 10 cm, belongs to the late Oligocene on the basis of the last appearance of *Dictyococcithes bisectus*. If Zones CN1 to CN4 are partly missing, a hiatus having a duration of more than 7.5 Ma must be present between the middle Miocene and upper Oligocene.

Oligocene

Abundant, moderately to well-preserved nanofossil assemblages are present from Samples 125-782A-35X-6, 10 cm, to 125-782A-39X-CC. The last sample is early Oligocene in age (Zone CP16) on the basis of the occurrence of *Ericsonia formosa* and *Isthmolithus recurvus* and the lack of the Eocene marker *Discoaster saipanensis*. Because of the occurrence of common specimens of *Ericsonia subdisticha*, this may represent Zone CP16a. Samples 125-782A-35X-6, 10 cm, through 125-782A-39X-2, 11 cm, were assigned to the late Oligocene (Zone CP19) on the basis of the occurrence of *Sphenolithus ciperoensis*, *S. distentus*, and *Helicosphaera recta*. A hiatus between early and late Oligocene might be present within Core 125-782A-39X because Zones CP17 and CP18 and Subzone CP16b/c are missing, but this may also result from poor core recovery.

Eocene

The section from Samples 125-782A-40X-CC to 125-782A-43X-CC has been interpreted as late to middle Eocene in age (Zones CP14–CP15) on the basis of the occurrence of *Discoaster bifax*, *Chiasmolithus oamaruensis*, *Discoaster barbadiensis*, *D. saipanensis*, and *Criboecentrum reticulatum*. Middle Eocene marker species (*Chiasmolithus expansus*, *C. grandis*, and *C. solithus*) were found in Sample 125-782A-41X-4, 16–17 cm, but not in Sample 125-782A-41X-3, 43–44 cm. The CP14/CP15 zonal boundary (middle Eocene/late Eocene boundary) thus is located between these two samples. The assemblages are rare to common in abundance and are poor to moderate in preservation. These samples directly overlie the volcanic basement.

Foraminifers

The Cenozoic planktonic foraminiferal stratigraphy for Hole 782A is summarized in Table 4. The relatively poor preservation and generally low abundance of planktonic foraminifers in the pre-Quaternary cores do not permit one to determine specific ages, thus precluding an accurate biostratigraphic subdivision of Hole 782A. An asterisk (*) is used to denote that the species listed in these columns are the species used to define (based on presence or absence) the age of the sample in question. No ages were determined for samples of poor preservation on the basis of the absence of species.

The planktonic foraminiferal results from Hole 782A place the sedimentary sequence between the Quaternary (Zone P22) and the middle Eocene (Zone P14–low Zone P16). Temperate-to-warm subtropical planktonic foraminiferal forms dominate the whole of the sedimentary sequence, with tropical forms tending to constitute only a small proportion of sample assemblages. The poor preservation, low abundances, and high number of barren samples below the middle-early Pliocene Sample 125-782A-13X-CC correlate with the large amounts of volcanoclastic material present in these samples.

Diatoms

Diatoms are rare to common and poorly to well preserved in Cores 125-782A-1H through 125-782A-34X. Cores 125-782A-35X through 125-782A-43X are barren of diatoms. The diatom assemblage in Hole 782A is characterized by common *Thalassionema nitzschioides* and few *Coscinodiscus* spp., *Nitzschia* spp., *Thalassiosira* spp., and others. Fragments of *Ethmodiscus rex* are present in most samples.

Because of the absence of age-diagnostic species in many samples, large intervals have been left unzoned. However, one may date the sedimentary interval in Hole 782A as ranging from the Quaternary to at least the middle Miocene.

Sample 125-782A-1H-CC was assigned to the *Pseudoeunotia doliolus* Zone by the presence of *P. doliolus* and the absence of *Nitzschia reinholdii*. *N. reinholdii* is present in Sample 125-782A-2H-CC, together with *P. doliolus*; this sample thus was placed in the *N. reinholdii* Zone. Both zones are Quaternary in age.

Samples 125-782A-6H-CC and 125-782A-7H-CC can be assigned a late Pliocene age (*Rhizosolenia praebergonii* Zone) on the basis of the occurrence of *R. praebergonii*. The boundary between the *R. praebergonii* Zone and the *Nitzschia jouseae* Zone was tentatively placed at Sample 125-782A-8H-CC on the basis of the absence of *R. praebergonii* and the occurrence of a fragment that may be *Actinocyclus ellipticus* f. *lanceolatus*.

Samples 125-782A-9H-CC through 125-782A-14X-CC contain *N. jouseae* and are early to late Pliocene in age (*N. jouseae* Zone).

Nitzschia miocenica appears in Sample 125-782A-22X-CC, and *Coscinodiscus yabei* appears in Sample 125-782A-26X-CC; therefore, these samples were assigned to the late Miocene.

Actinocyclus moronensis was found in Sample 125-782A-27X-CC, and *Coscinodiscus lewisianus* is present in Samples 125-782A-31X-CC and 125-782A-32X-CC, where it can be observed with *Coscinodiscus plicatulus* and *Denticulopsis nicobarica*, dating this interval to the middle Miocene (*C. lewisianus*/*C. gigas* var. *diorama* zones).

IGNEOUS AND METAMORPHIC PETROLOGY

Angular to subrounded clasts of moderately to highly phyrlic, two-pyroxene andesite and dacite were recovered from the bottom of Holes 782A and 782B. These clasts range from about 20 to 50 mm, are gray to greenish-brown and black, contain 60% to 90% glass, and typically are slightly vesicular (less than 10 vol%).

It is possible that some of these clasts are disrupted fragments of pillow lavas. Elongation of the vesicles and some alignment of groundmass feldspar laths define a flow texture in a few of the clasts, but other evidence for the original morphology of the materials was not available.

Euhedral, oscillatory-zoned plagioclase up to 5 mm long is the most abundant (less than 25 modal%) phenocryst phase, followed by subequal proportions of about 3 to 5 modal% of euhedral clinopyroxene and pink-green pleochroic orthopyroxene (less than 2–3 mm in size). Euhedral magnetite (less than 1 mm in size) is a minor (less than 3 modal%) phenocryst type. These phases also form glomerocrystic clusters up to 10 mm wide.

The groundmass of the andesites and dacites is predominantly glass, with numerous quench-textured feldspar laths and minor amounts of dusty iron-titanium oxides. Some chloritic alteration along anastomosing cracks in the glass is present in many of the samples. Fresh, pale brown glass inclusions less than 0.2 mm in diameter are present in the

Table 4. Summary of foraminiferal data for Site 782.

Core, section	Abundance	Preservation	Diagnostic species present*	Diagnostic species absent*	Zone(s)	Age/age range
125-782A-1H-CC	Abundant	Good	<i>Globorotalia truncatulinoides</i>	—	N22	Pleistocene
125-782A-2H-CC	Abundant	Good	<i>Globorotalia truncatulinoides</i>	—	N22	Pleistocene
125-782A-3H-CC	Abundant	Good	<i>Globorotalia truncatulinoides</i>	—	N22	Pleistocene
125-782A-4H-CC	Abundant	Good	<i>Globorotalia truncatulinoides</i>	—	N22	Pleistocene
125-782A-5H-CC	Common	Moderate	<i>Globorotalia tosaensis</i>	<i>Globorotalia truncatulinoides</i>	N21	late Pliocene
125-782A-6H-CC	Abundant	Moderate	<i>Globorotalia crassaformis</i>	<i>Globorotalia truncatulinoides</i>	upper N19–N21	middle early Pliocene-late Pliocene
125-782A-7H-CC	Common	Moderate	<i>Globorotalia crassaformis</i>	<i>Globorotalia truncatulinoides</i>	upper N19–N21	middle early Pliocene-late Pliocene
125-782A-8H-CC	Few	Moderate	<i>Globorotalia crassaformis</i>	<i>Globorotalia truncatulinoides</i>	upper N19–N21	middle early Pliocene-late Pliocene
125-782A-9H-CC	Few	Moderate	<i>Globorotalia crassaformis</i>	<i>Globorotalia truncatulinoides</i>	upper N19–N21	middle early Pliocene-late Pliocene
125-782A-10X-CC	Few	Moderate	<i>Globorotalia crassaformis</i> <i>Globigerinoides extremus</i> <i>Globorotalia crassaformis</i>	<i>Globorotalia truncatulinoides</i>	upper N19–N21	middle early Pliocene-late Pliocene
125-782A-11X-CC	Common	Moderate	<i>Globorotalia crassaformis</i> <i>Neogloboquadrina acostaensis</i>	—	upper N19–N19/20	middle early Pliocene-late early Pliocene
125-782A-12X-CC	Common	Moderate	<i>Globorotalia crassaformis</i> <i>Sphaeroidinellopsis praedeheiscens</i>	—	upper N19–N19/20	middle early Pliocene-late early Pliocene
125-782A-13X-CC	Common	Moderate	<i>Globorotalia crassaformis</i> <i>Globigerinoides bulloideus</i>	—	upper N19	middle early Pliocene
125-782A-14X-CC	Rare	Moderate	<i>Globorotalia crassaformis</i>	<i>Globorotalia truncatulinoides</i>	upper N19–N21	early Pliocene-late Pliocene
125-782A-15X-CC	Barren	—	—	—	—	—
125-782A-16X-CC	Barren	—	—	—	—	—
125-782A-17X-CC	Rare	Poor	<i>Sphaeroidinellopsis seminula</i>	—	N9–N21	early middle Miocene-late Pliocene
125-782A-18X-CC	Common	Poor	<i>Orbulina universa</i> <i>Globigerina nepenthes</i> <i>Globorotalia</i> (H.) margaritidae	<i>Globorotalia crassaformis</i>	lower N19	earliest early Pliocene
125-782A-19X-CC	Barren	—	—	—	—	—
125-782A-20X-CC	Rare	Poor	<i>Sphaeroidinellopsis seminula</i> <i>Globorotalia tumida</i>	—	N18–N21	late Miocene-late Pliocene
125-782A-21X-CC	Few	Poor	<i>Globorotalia</i> cf. <i>tumida</i> <i>Sphaeroidinellopsis kochi</i>	—	N18–N19	late Miocene-early Pliocene
125-782A-22X-CC	Barren	—	—	—	—	—
125-782A-23X-CC	Rare	Poor	<i>Sphaeroidinellopsis kochi</i>	—	N14–N19	late middle Miocene-early Pliocene
125-782A-24X-CC	Rare	Moderate	<i>Globigerina nepenthes</i> <i>Globigerina nepenthes</i>	—	N14–N19	late middle Miocene-early Pliocene
125-782A-25X-CC	Rare	Moderate	<i>Orbulina universa</i>	—	N9–N22	early middle Miocene-recent
125-782A-26X-CC	Rare	Moderate	<i>Globigerina nepenthes</i>	—	N14–N19	late middle Miocene-early Pliocene
125-782A-27X-CC	Barren	—	—	—	—	—
125-782A-28X-CC	Barren	—	—	—	—	—
125-782A-29X-CC	Barren	—	—	—	—	—
125-782A-30X-CC	Barren	—	—	—	—	—
125-782A-31X-CC	Barren	—	—	—	—	—
125-782A-32X-CC	Rare	Moderate	<i>Dentaloglobigerina altispira</i>	—	N4B–N21	early Miocene-late Pliocene
125-782A-33X-CC	Few	Poor	<i>Globorotalia</i> (F.) peripheroronda <i>Globoquadrina deheiscens</i>	—	N4B–N10	early Miocene-earliest middle Miocene
125-782A-34X-CC	Barren	—	—	—	—	—
125-782A-35X-CC	Few	Poor	<i>Globorotalia</i> (J.) <i>mayeri</i> <i>Catapsydrax dissimilis</i>	—	N4A–N6	latest Oligocene-middle early Miocene
125-782A-36X-CC	Barren	—	—	—	—	—
125-782A-37X-CC	Few	Poor	<i>Catapsydrax dissimilis</i> <i>Globoquadrina venezuelana</i>	—	P22–N6	late Oligocene-middle early Miocene
125-782A-38X-CC	No Recovery	—	—	—	—	—
125-782A-39X-CC	Few	Poor	<i>Catapsydrax dissimilis</i>	—	P13–N6	late middle Eocene-early Miocene
125-782A-40X-CC	Few	Poor	<i>Catapsydrax dissimilis</i>	—	P13–N6	late middle Eocene-early Miocene
125-782A-41X-CC	Common	Moderate	<i>Catapsydrax unicavus</i> <i>Globigerinoides</i> cf. <i>mexicanus</i>	—	P14–lower P16	late early Eocene-early late Eocene
125-782A-42X-CC	—	—	—	—	—	—
125-782A-43X-CC	—	—	—	—	—	—

*See text for explanation.

majority of the plagioclase phenocrysts, and these inclusions typically contain one or more shrinkage bubbles. Interstitial fresh glass is also present in the glomerocrystic clusters. Trace amounts of euhedral apatite are present as inclusions in some plagioclase phenocrysts and as a microphenocryst phase in the groundmass. Ilmenite and sulfide minerals are also present in trace quantities in some of the samples.

Note that the phase assemblage characteristic of the basement clasts is also typical of the overlying ashes and glass fragments in the sediments (see "Lithostratigraphy" section, this chapter).

IGNEOUS AND METAMORPHIC GEOCHEMISTRY

Various igneous rocks were encountered in both Holes 782A and 782B. Of these rocks, those that were taken from the core-catcher sample (Core 125-782A-49X-CC) are residues after the hole was washed through and hence may not have been sampled *in situ*. Eight samples were selected for ship-board X-ray fluorescence (see "Explanatory Notes" chapter, this volume). All samples were analyzed for abundance of major elements, but because of their small size, trace-element analysis was conducted on only three of the samples. Abundances of major and trace elements are presented in Table 5.

Major Elements

Two distinct rock types that form high- and low-silica groups were found. Both groups, however, have low potassium, titanium, and magnesium contents. The low-silica group (between 56.50 and 58.42 wt% SiO₂) has moderate-to-low values of magnesium (between 2.70 and 3.12 wt% MgO); the high-silica group (between 66.20 and 72.00 wt% SiO₂) contains virtually no magnesium (between 0 and 0.69 wt% MgO). The variation in titanium is greater for the low-silica group (from 0.64 to 1.13 wt% TiO₂) than for the high-silica group (from 0.34 to 0.43 wt% TiO₂). Potassium ranges from 0.57 to 1.08 wt% and 0.53 to 0.77 wt% K₂O for the high- and low-silica groups,

respectively. The rocks are andesites and dacites-rhyolites on the basis of the silica and potassium contents and span the tholeiitic and calc-alkaline fields (Fig. 4). It is possible that the two groups are related by fractional crystallization.

Compared with the lavas recovered from the Mariana forearc at Sites 458 and 459, DSDP Leg 60 (see "Introduction" chapter, this volume), the rocks from Site 782 fall at the lower potassium end of the Leg 60 field. However, these rocks contain considerably less MgO at similar silica values (Fig. 5), and hence probably have a source that is distinct from that of the Leg 60 rocks.

Trace Elements

Two samples from the high-silica group and one sample from the low-silica group were analyzed for their abundance of trace elements. To avoid the possible effects of fractional crystallization on the trace-element ratios, only the most mafic sample (125-782A-49X-CC, 3–5 cm) is presented in a multi-element diagram (Fig. 6) normalized to a normal mid-ocean ridge basalt (N-MORB). Relative to N-MORB, the rock has high abundances of large-ion-lithophile (LIL) elements and low abundances of the high-field-strength (HFS) elements, particularly niobium, zirconium, yttrium, and titanium. The light-to-heavy rare-earth-element ratio, represented by cerium/yttrium (which is similar to cerium/ytterbium), is only slightly higher than N-MORB, implying little if any light rare-earth-element enrichment. These trace-element characteristics thus are consistent with derivation from a parent magma derived from the forearc mantle wedge that was selectively enriched by LIL elements from the downgoing slab.

SEDIMENT/FLUID GEOCHEMISTRY

Sediment Geochemistry

Sediments from Site 782 were analyzed on board ship for inorganic carbon and for total carbon, nitrogen, and sulfur using the techniques described in the "Explanatory Notes"

Table 5. Abundances of major and trace elements for rocks recovered at Site 782.

Core: Interval (cm):	44X-CC, 13–17	45X-1, 30–32	45X-1, 32–35	49X-CC, 58	49X-CC, 3–5	49X-CC, 37–42	782B-2R-1, 16–29	782A-41X-CC, 44–47
(in wt%)								
SiO ₂	70.27	66.2	66.92	55.61	55.94	55.63	70.84	72.00
TiO ₂	0.37	0.43	0.40	0.64	0.65	0.76	0.38	0.34
Al ₂ O ₃	13.77	15.11	14.23	14.56	14.58	15.1	14.24	13.98
Fe ₂ O ₃ (total)	2.92	4.45	4.05	9.99	10.17	10.42	2.64	2.57
MnO	0.05	0.10	0.10	0.14	0.14	0.16	0.03	0.03
MgO	0.11	0.69	0.68	2.68	2.84	3.08	0.01	0.01
CaO	3.14	3.88	3.37	6.91	6.86	7.37	3.22	2.37
Na ₂ O	4.56	4.29	3.94	2.35	2.4	2.54	4.45	4.46
K ₂ O	0.69	0.67	1.08	0.77	0.75	0.53	0.79	0.57
P ₂ O ₅	0.05	0.05	0.07	0.01	0.03	0.05	0.05	0.03
LOI	1.32	0.64	3.49	1.28	3.63	2.18	1.01	1.37
Total	98.52	99.12	100.68	99.49	100.83	99.34	98.21	98.56
Mg#	0.06	0.21	0.22	0.32	0.33	0.34	0.01	0.01
(in ppm)								
Nb			0.9		2.2			0.3
Zr			111		58			115
Y			26		17			27
Sr			202		176			144
Rb			11.1		8.1			3.5
Zn			104		90			69
Cu			11		116			13
Ni			0		8			3
Cr			0		0			0
V			32		459			5
Ti			2820		4320			2220
Ce			20		15			17
Ba			35		30			51

LOI = loss on ignition. (Analyzed on board the *Resolution* by D. Sims using X-ray fluorescence.)

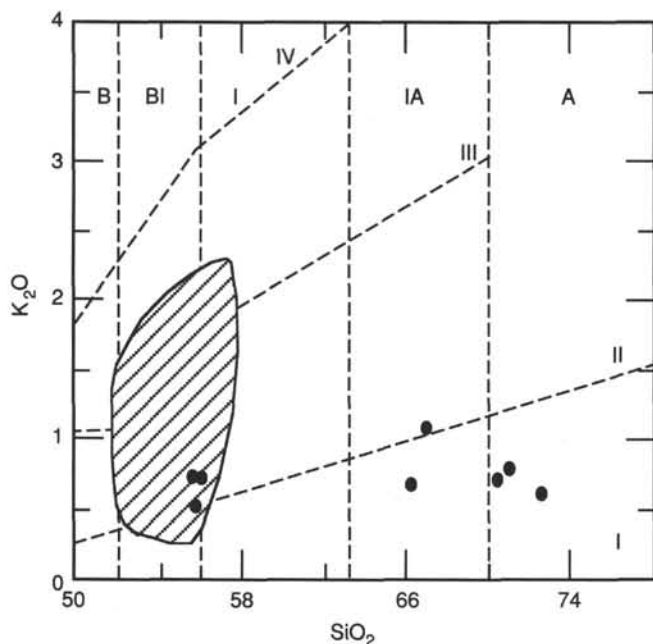


Figure 4. K_2O - SiO_2 igneous-rock classification diagram for destructive and collision margins (after Peccerillo and Taylor, 1976). The vertical boundaries mark the fields for basic (B), intermediate (BI), intermediate (I), intermediate-acid (IA), and acid (A) rocks; boundaries having positive slopes mark the slopes for tholeiitic (I), calc-alkaline (II), high-potassium calc-alkaline (III), and shoshonitic (IV) series. Data from Site 782 fall between the tholeiitic and calc-alkaline series, but at low abundances of potassium. The field for Mariana forearc basement rocks (recovered during DSDP Leg 60, Sites 458 and 459; after Wood et al., 1981) (hatched area) is also plotted for comparison.

(this volume). The organic carbon content was then calculated by difference. These results are presented in Table 6 and in Figure 7. The $CaCO_3$ content of the sediments varies from 10 to 70 wt%. Abrupt changes were observed at 14, 115, 210, 307, and 330 mbsf. Between these depths, changes are gradual or nonexistent. The organic carbon content is less than 0.2 wt%, except for intervals at 0 to 25 and 200 to 300 mbsf, where values approach 0.5 and 0.8 wt%, respectively. Two samples at 119 and 391 mbsf have much higher values of 2.5 and 1.4 wt%, respectively. The profile of nitrogen content with depth resembles that of organic carbon. Values range from less than 0.01 to 0.22 wt%. Sulfur is below the detection limit of 0.06 wt% in all samples.

Fluid Geochemistry

The concentration of methane measured for 5-cm³ sediment headspace samples is uniformly low, less than 20 $\mu L/L$ (Table 7). Methane was the only hydrocarbon detected.

Interstitial waters at Site 782 exhibit changes with depth (Table 8) that are typical of many deep-sea sites having moderate rates of sedimentation and organic carbon deposition. Depth profiles show the effects of three main processes: (1) bacterial oxidation of organic matter using various oxidants, including seawater sulfate; (2) precipitation of $CaCO_3$; and (3) alteration of volcanic material in the sediments and basement. Oxidation of organic matter produces bicarbonate alkalinity and ammonia while consuming oxidants in the order oxygen, nitrate, nitrite, MnO_2 , $FeOOH$, sulfate. The enhanced alkalinity causes $CaCO_3$ to precipitate. Alteration of volcanic material by seawater at low temperatures removes magnesium, potassium, and hydroxyl from solution in ex-

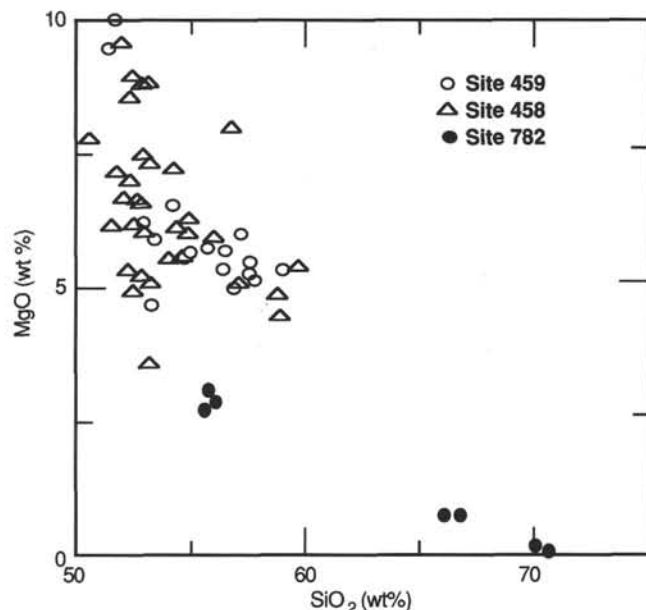


Figure 5. MgO - SiO_2 co-variation diagram separating the andesites and dacites-rhyolites recovered from the basement at Site 782 compared with rocks from Mariana forearc basement recovered during DSDP Leg 60, Sites 458 and 459.

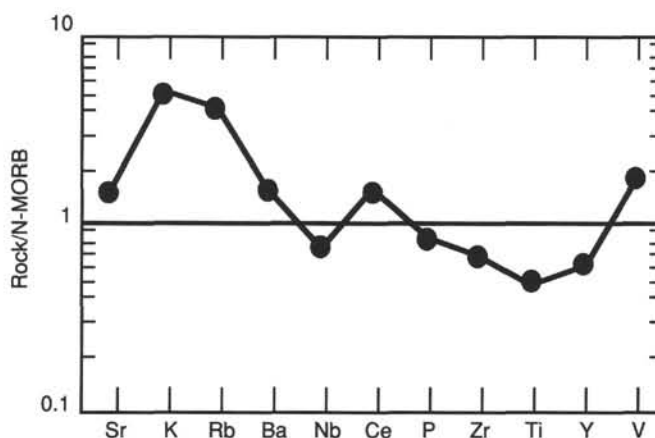


Figure 6. N-MORB normalized patterns for Sample 125-782A-49X-CC, 3–5 cm, the most mafic sample analyzed from Site 782. The high LIL element enrichment and low HFS element abundances are typical of a subduction-related tectonic environment of formation.

change for calcium and silica from the volcanic sediments and basement rocks. The acidity generated by these reactions consumes bicarbonate alkalinity, as does the precipitation of $CaCO_3$, which is favored in turn by the enhanced concentration of dissolved calcium. The depth profiles for the various dissolved species are determined largely by the relative rates of these competing reactions.

At Site 782, oxidation of organic matter causes alkalinity to increase by one-third in the near-surface sediments (Fig. 8). Below that, it decreases steadily toward basement, where it is consumed by reactions involving the removal of mainly magnesium from seawater. The shallow maximum in alkalinity is underlain by a deeper maximum in ammonia, as is typical in deep-sea sediments, where organic matter is being oxidized.

Table 6. Total nitrogen, carbon, organic carbon, and carbonate carbon in sediments at Site 782.

Core, section, interval (cm)	Depth (mbsf)	Total nitrogen (wt%)	Total carbon (wt%)	Inorganic carbon (wt%)	Organic carbon (wt%)	CaCO ₃ (wt%)
125-782A-1H-1, 76-78	0.76			2.27		18.9
1H-2, 76-78	2.26			2.18		18.2
1H-3, 76-78	3.76	0.11	3.13	2.70	0.43	22.5
1H-4, 76-78	5.26			4.21		35.1
1H-5, 76-78	6.76			1.70		14.2
1H-6, 76-78	8.26			2.06		17.2
1H-7, 29-31	9.29			1.32		11.0
1H-CC, 8-10	9.68			2.98		24.8
2H-1, 74-76	10.54			3.83		31.9
2H-2, 61-63	11.91			4.62		38.5
2H-3, 65-67	13.45	0.08	3.84	3.67	0.17	30.6
2H-4, 61-63	14.91			7.05		58.7
2H-5, 61-63	16.41			5.02		41.8
2H-6, 76-78	18.06			7.16		59.6
2H-7, 30-32	19.10			5.49		45.7
3H-1, 79-81	20.09			4.18		34.8
3H-2, 79-81	21.59			3.32		27.6
3H-2, 79-81	23.09	0.13	4.86	4.56	0.30	38.0
3H-4, 78-90	24.58			2.98		24.8
3H-5, 78-80	26.08			5.32		44.3
3H-6, 78-80	27.58			3.68		30.7
3H-7, 38-40	28.68			7.78		64.8
4H-1, 79-81	29.59			5.73		47.7
4H-2, 79-81	31.09			5.10		42.5
4H-3, 79-81	32.59	0.07	4.57	4.65	0.00	38.7
4H-4, 79-81	34.09			4.58		38.2
4H-5, 79-81	35.59			4.13		34.4
4H-6, 79-81	37.09			6.42		53.5
4H-7, 39-41	38.19			5.30		44.1
5H-1, 78-80	39.08			2.83		23.6
5H-2, 78-80	40.58			5.37		44.7
5H-3, 78-80	42.08	0.10	5.53	5.44	0.09	45.3
5H-4, 78-80	43.58			2.64		22.0
5H-5, 78-80	45.08			5.00		41.7
5H-6, 78-80	46.58			3.41		28.4
5H-7, 36-38	47.66			4.71		39.2
6H-1, 73-75	48.53			2.34		19.5
6H-2, 63-65	49.93			2.75		22.9
6H-3, 97-99	51.77	0.10	2.98	2.83	0.15	23.6
6H-4, 68-70	52.98			2.65		22.1
6H-5, 43-45	54.23			3.12		26.0
6H-6, 53-55	55.83			2.16		18.0
6H-7, 37-39	57.17			4.12		34.3
7H-1, 30-32	57.60			3.68		30.7
7H-2, 30-32	59.10			4.97		41.4
7H-3, 33-35	60.63	0.11	3.19	3.08	0.11	25.7
7H-4, 26-28	62.06			3.40		28.3
7H-5, 79-81	64.09			3.30		27.5
7H-6, 73-75	65.53			1.67		13.9
7H-7, 26-28	66.56			2.76		23.0
8H-1, 74-76	67.54			3.54		29.5
8H-2, 74-76	69.04			4.08		34.0
8H-3, 74-76	70.54	0.12	2.73	2.63	0.10	21.9
8H-4, 74-76	72.04			3.89		32.4
8H-5, 74-76	73.54			4.75		39.6
8H-6, 74-76	75.04			3.28		27.3
8H-7, 35-37	76.15			2.97		24.7
9H-1, 72-74	77.02			1.33		11.1
9H-2, 72-74	78.52			1.44		12.0
9H-3, 78-80	80.08	0.07	1.63	1.47	0.16	12.2
9H-4, 72-74	81.52			4.05		33.7
9H-5, 78-80	83.08			4.02		33.5
9H-6, 78-80	84.58			3.57		29.7
9H-7, 31-33	85.61			3.35		27.9
10X-1, 130-132	87.10			2.29		19.1
10X-2, 36-38	87.66	0.06	2.69	2.58	0.11	21.5
11X-1, 74-76	96.44			2.09		17.4
11X-2, 54-56	97.74			1.21		10.1
11X-3, 69-71	99.39	0.10	3.61	3.39	0.22	28.2
12X-1, 74-76	106.04			3.86		32.2
12X-2, 74-76	107.54			3.25		27.1
12X-3, 67-69	108.97	0.08	4.09	3.92	0.17	32.7
12X-4, 13-15	109.93			3.28		27.3
13X-1, 63-65	115.63			5.38		44.8
13X-2, 80-82	117.30			3.55		29.6

Table 6 (continued).

Core, section, interval (cm)	Depth (mbsf)	Total nitrogen (wt%)	Total carbon (wt%)	Inorganic carbon (wt%)	Organic carbon (wt%)	CaCO ₃ (wt%)
13X-3, 72-74	118.72	0.14	8.59	6.06	2.53	50.5
13X-4, 22-24	119.72			5.02		41.8
14X-1, 74-76	125.34			5.42		45.1
14X-2, 74-76	126.84			4.10		34.2
14X-3, 74-76	128.34	nd	6.30	6.10	0.20	50.8
14X-4, 74-76	129.84			4.63		38.6
14X-5, 8-10	130.58			3.31		27.6
15X-1, 80-82	135.10			4.14		34.5
15X-2, 73-75	136.53			5.06		42.1
15X-3, 80-82	138.10	nd	4.55	4.35	0.20	36.2
15X-4, 8-10	138.88			2.40		20.0
16X-1, 68-70	144.58			4.12	0.04	34.3
16X-2, 55-57	145.95	0.06	2.78	2.74		22.8
16X-3, 68-70	147.58			4.50		37.5
17X-1, 67-69	154.27			5.57		46.4
17X-2, 75-77	155.85			5.73		47.7
17X-3, 75-77	157.35			7.11		59.2
17X-4, 75-77	158.85			4.00		33.3
17X-5, 39-41	159.99	0.07	5.53	5.40	0.13	45.0
17X-6, 9-11	161.19			5.02		41.8
18X-1, 72-74	163.92			3.61		30.1
18X-2, 47-49	165.17	nd	7.29	7.22	0.07	60.1
18X-CC, 12-14	165.80			7.96		66.3
19X-1, 46-48	173.36			5.47		45.6
19X-2, 46-48	174.86			4.54		37.8
19X-3, 32-34	176.22	nd	4.30	4.17	0.13	34.7
19X-4, 32-34	177.72			2.92		24.3
19X-CC, 20-22	178.15			3.82		31.8
20X-1, 48-50	182.98	0.08	4.99	4.87	0.12	40.6
21X-1, 20-22	192.30	0.07	5.58	5.59	0.00	46.6
21X-1, 95-97	193.05	0.06	1.62	1.55	0.07	12.9
21X-2, 20-22	193.80			6.97		58.1
21X-2, 71-73	194.31			5.57		46.4
21X-3, 34-36	195.44			5.72		47.6
21X-4, 46-48	197.06	0.08	3.97	3.85	0.12	32.1
21X-4, 64-66	197.24	nd	6.89	6.75	0.14	56.2
21X-5, 7-9	198.17	0.07	2.62	2.54	0.08	21.2
21X-5, 61-63	198.71	nd	7.11	7.04	0.07	58.6
22X-1, 72-74	202.52	nd	6.85	6.53	0.32	54.4
22X-CC, 39-41	203.35	nd	5.27	5.04	0.23	42.0
23X-1, 99-101	212.49			4.54		37.8
23X-2, 52-54	213.52	nd	3.90	3.39	0.51	28.2
23X-3, 46-48	214.96	nd	1.77	1.49	0.28	12.4
23X-4, 15-17	216.15			1.87		15.6
23X-5, 68-70	218.18			3.83		31.9
23X-6, 87-89	219.87			2.55		21.2
23X-7, 13-15	220.63			2.78		23.2
24X-1, 72-74	221.72	0.08	1.53	1.35	0.18	11.3
24X-1, 136-138	222.36	0.10	5.14	5.02	0.12	41.8
24X-2, 25-27	222.75			4.68		39.0
24X-2, 87-89	223.37			3.76		31.3
25X-1, 73-74	231.43	0.15	2.69	2.25	0.44	18.7
25X-2, 56-58	232.76	0.23	6.15	5.67	0.48	47.2
25X-3, 64-65	234.34			5.00		41.7
25X-4, 57-58	235.77			1.98		16.5
25X-5, 47-49	237.17			3.57		29.7
25X-6, 74-75	238.94			4.72		39.3
26X-1, 69-71	240.99			5.25		43.7
26X-2, 50-52	242.30			3.68		30.7
26X-3, 60-62	243.90			4.38		36.5
26X-4, 96-98	245.76			4.15		34.6
26X-5, 60-62	246.90			4.80		40.0
26X-6, 60-62	248.40			2.50		20.8
26X-7, 37-39	249.67			6.27		52.2
27X-1, 84-86	250.84			4.62		38.5
27X-2, 73-75	252.23			3.07		25.6
27X-3, 27-29	253.27	0.17	1.80	1.54	0.26	12.8
27X-CC, 13-15	253.81			3.08		25.7
28X-1, 78-80	260.38			3.89		32.4
28X-2, 62-64	261.72			1.66		13.8
28X-3, 65-67	263.25			1.62		13.5
28X-4, 65-67	264.75			2.80		23.3
28X-5, 73-75	266.33			3.49		29.1
28X-6, 56-58	267.66			2.49		20.7
29X-1, 56-58	269.76			3.72		31.0
29X-2, 47-49	271.17			4.61		38.4

Table 6 (continued).

Core, section, interval (cm)	Depth (mbsf)	Total nitrogen (wt%)	Total carbon (wt%)	Inorganic carbon (wt%)	Organic carbon (wt%)	CaCO ₃ (wt%)
29X-3, 58-60	272.78			2.83		23.6
29X-4, 59-61	274.29			2.55		21.2
29X-5, 50-52	275.70	0.18	4.36	3.64	0.72	30.3
29X-6, 63-65	277.33	0.13	2.50	2.34	0.16	19.5
29X-7, 28-30	278.48			2.38		19.8
30X-1, 74-76	279.54			5.49		45.7
30X-2, 34-36	280.64			1.92		16.0
30X-CC, 22-24	281.67	0.16	4.67	4.22	0.45	35.2
31X-1, 37-39	288.87			5.25		43.7
31X-2, 68-70	289.66			4.03		33.6
31X-3, 54-56	291.02			3.28		27.3
32X-1, 69-71	294.69			2.56		21.3
32X-2, 65-71	296.15			2.43		20.2
32X-3, 65-67	297.65	0.13	4.73	4.03	0.70	33.6
32X-4, 42-44	298.92	0.11	3.56	3.31	0.25	27.6
32X-5, 70-72	300.70			3.73		31.1
32X-6, 58-60	302.08			4.07		33.9
33X-1, 20-23	303.70			4.97		41.4
33X-2, 16-18	305.16			3.15		26.2
33X-3, 63-67	307.13			1.14		9.5
33X-4, 29-31	308.29			3.98		33.2
33X-5, 134-137	310.84			2.60		21.7
33X-6, 37-40	311.37			3.27		27.2
33X-7, 22-25	312.72			3.64		30.3
33X-CC, 25-28	313.21			1.39		11.6
34X-1, 64-66	313.74	0.07	0.43	0.30	0.13	2.5
34X-CC, 33-35	314.92			0.95		7.9
35X-1, 40-42	322.90			4.11		34.2
35X-2, 37-39	324.37	0.06	5.15	5.16	0.00	43.0
35X-3, 41-43	325.91	0.03	1.82	1.80	0.02	15.0
35X-4, 133-135	328.33			4.58		38.2
35X-5, 138-140	329.88			0.63		5.2
35X-6, 60-62	330.60	0.06	8.26	8.26	0.00	68.8
35X-7, 8-10	331.58	0.09	8.66	8.63	0.03	71.9
35X-CC, 3-5	332.00			8.83		73.6
36X-1, 66-68	332.76			7.42		61.8
36X-2, 76-78	334.36	nd	5.56	5.57	0.00	46.4
36X-3, 62-64	335.72	0.08	8.29	8.38	0.00	69.8
36X-4, 50-52	337.10			6.69		55.7
36X-5, 9-11	338.19			7.10		59.1
36X-CC, 28-30	339.74			4.47		37.2
37X-1, 113-115	342.73			5.21		43.4
37X-2, 75-77	343.85			7.78		64.8
37X-3, 36-38	344.96	0.06	5.25	5.09	0.16	42.4
37X-4, 88-90	346.98	0.05	6.78	6.61	0.17	55.1
37X-5, 89-91	348.49			6.11		50.9
37X-6, 119-121	350.29			5.41		45.1
37X-7, 42-44	351.02			2.63		21.9
37X-CC, 29-31	351.35			6.32		52.6
39X-1, 136-138	362.26			6.93		57.7
39X-2, 29-31	362.69			5.74		47.8
40X-1, 142-144	371.92			4.27		35.6
40X-2, 81-83	372.81			5.28		44.0
40X-3, 62-64	374.12	0.11	4.30	4.31	0.00	35.9
40X-4, 82-84	375.82	0.09	2.62	2.44	0.18	20.3
41X-1, 94-96	381.14			2.05		17.1
41X-2, 37-39	382.07			2.58		21.5
41X-3, 44-46	383.64			2.19		18.2
41X-4, 96-98	385.66			2.44		20.3
41X-5, 83-85	387.03			2.18		18.2
41X-6, 41-43	388.11	0.08	4.15	4.02	0.13	33.5
41X-7, 10-12	389.30	nd	9.55	9.58	0.00	79.8
42X-1, 88-90	390.68	nd	10.57	9.14	1.43	76.1
42X-CC, 6-8	392.77	nd	2.06	1.99	0.07	16.6

nd = not detected. Total sulfur was below the detection limit of 0.06 wt% in all samples analyzed for total carbon, nitrogen, and sulfur.

Seawater sulfate decreases by about 10% as a result of these reactions.

Dissolved magnesium decreases with depth, especially as basement is approached (Fig. 9). This decrease is nearly matched by an increase in dissolved calcium, although this increase does not begin until about 120 mbsf. At shallower depths, calcium decreases as a result of CaCO₃ precipita-

tion. Like magnesium, potassium decreases steadily with depth as a result of uptake into alteration minerals, mainly in basement. The increase in potassium relative to seawater in the near-surface sediments is probably an artifact of sampling and squeezing. Sodium, chlorinity, bromide, and salinity show relatively little change with depth (Figs. 9 and 10).

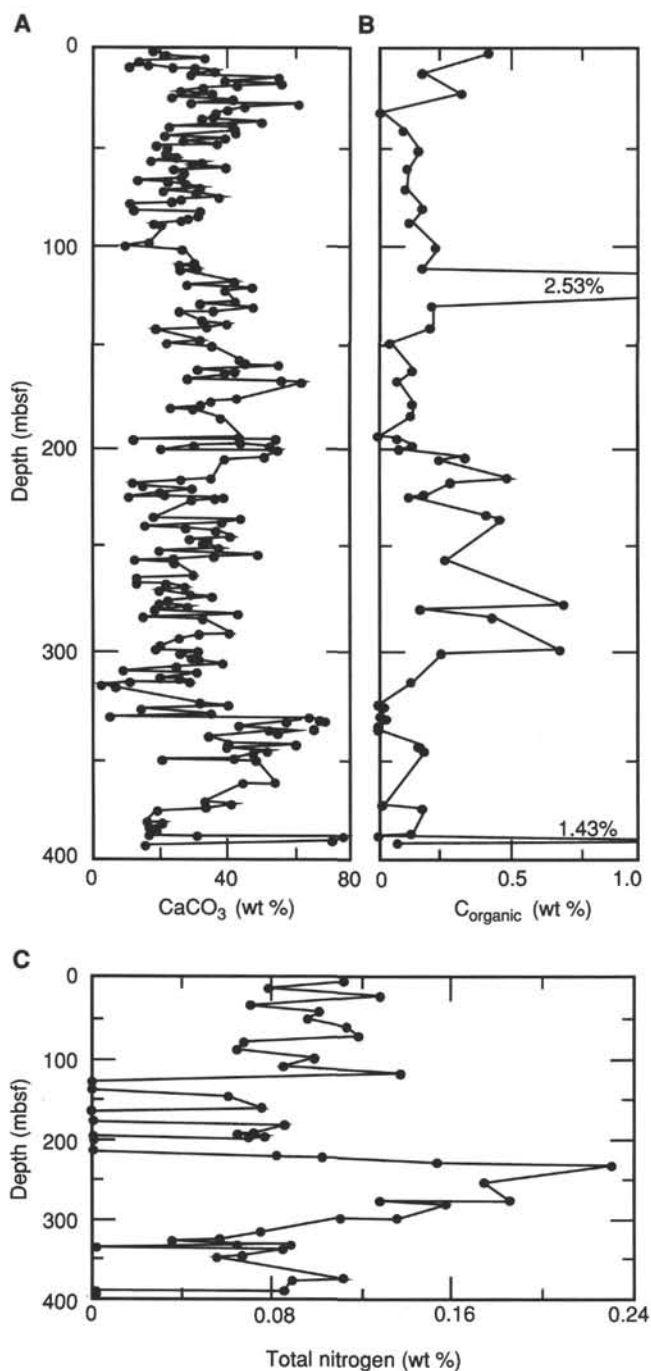


Figure 7. Calcium carbonate (A), total organic carbon (B), and total nitrogen (C) in sediments from Hole 782A.

PALEOMAGNETISM

Magnetic Remanence

Two holes (Holes 782A and 782B) were drilled at Site 782. Hole 782A had an overall core recovery of 59%. We identified many intervals of normal and reversed polarity within the hole. These data, when combined with the biostratigraphic data (see "Biostratigraphy" section, this chapter), enabled us to construct a preliminary magnetostratigraphy for the sediments in the upper 240 m of the hole. Unfortunately, the paleomagnetic data are less reliable below this level because

Table 7. Results of headspace-gas analyses of sediments at Site 782.

Core, section, interval (cm)	Depth (mbsf)	Methane ($\mu\text{L/L}$) ^a	Methane (μM) ^b
125-782A-1H-3, 0-3	3.02	12	1.0
2H-5, 0-3	15.82	11	1.0
3H-4, 140-145	25.23	11	1.0
4H-5, 0-5	34.83	13	1.1
5H-5, 0-5	44.32	12	1.0
6H-5, 0-5	53.82	10	0.9
7H-5, 0-5	63.32	14	1.2
8H-3, 0-3	69.82	16	1.4
9H-3, 0-3	79.32	17	1.5
10X-2, 0-3	87.32	12	1.1
11X-3, 0-3	98.72	12	1.0
12X-3, 0-5	108.33	11	0.9
13X-3, 0-5	118.03	11	0.9
15X-3, 0-5	137.33	11	1.0
16X-3, 0-5	146.93	10	0.9
18X-2, 0-3	164.71	9	0.8
19X-3, 0-3	175.92	10	0.9
23X-5, 0-3	217.52	9	0.8
24X-2, 0-3	222.52	10	0.9
26X-4, 0-3	244.82	9	0.8
29X-5, 0-3	275.22	9	0.8
30X-3, 0-3	281.82	10	0.9
32X-6, 0-3	301.52	12	1.0
35X-4, 0-3	327.02	9	0.8
37X-3, 0-3	344.62	10	0.9
39X-2, 0-3	362.41	11	0.9
41X-5, 0-5	386.22	12	1.0
42X-2, 0-3	391.32	9	0.8

^a Microliters of methane per liter of wet sediment, assuming a sample volume of 4.2 cm³ of sediment.

^b Micromoles of methane per liter of interstitial water, assuming a porosity of 50%.

of poor recovery. We hope that more detailed shorebased work will resolve the stratigraphy. Only a small amount (less than 1 m) of fragments of basement rocks unsuitable for paleomagnetic study was recovered in Hole 782B. The natural remanent magnetization (NRM) of the archive half of each core from Hole 782A was measured using the cryogenic magnetometer. Intensities vary widely from 1 to 800 mA/m. Most samples have values between 10 and 100 mA/m. There is no correlation between intensity and sub-bottom depth (Fig. 11). When the cores then were demagnetized at the 10-mT level and remeasured, intensities measured were about 10% to 40% of their initial values. The low latitude of the site can make determination of polarity difficult if the inclinations are very shallow. However, the magnetic directions in many of the cores have steep enough inclinations to allow one to interpret polarity unambiguously. In many cases, the cores record sharp polarity transitions (Fig. 12).

Many of the cores exhibit signs of drilling disturbance that range from slightly disturbed to disrupted (see the core descriptions and photos). Data from cores described as more than slightly disturbed were rejected for any analysis. However, note that the cores that were recorded as being moderately disturbed display stable magnetic behavior and record changes in magnetic polarity (Fig. 13). This suggests that the disturbance identified in the cores is, in some cases, only a surficial feature.

The magnetostratigraphy for Hole 782A is summarized in Figures 14A and 14B. Also shown are the magnetic polarity scale and the nannofossil zones taken from Berggren et al. (1985). Between 0 and 250 mbsf, the biostratigraphic data allow us to make reliable correlations with the magnetic polarity time scale of Berggren et al. (1985). Below this level, recovery was much poorer, and the biostratigraphic zonations are less precise, making correlations with the observed mag-

netostratigraphy more difficult. In addition, the sediments between 322 and 332 mbsf were deposited over 10 m.y., making any correlation with the magnetic polarity time scale for this interval impossible.

Past work from drill cores from the Philippine Sea Plate (Bleil, 1982) suggests that the Philippine Sea Plate has moved northward with time. Inclination data from Hole 782A have been separated into 100-m sections, grouped into 10° intervals, and plotted on histograms (Fig. 15). At all depths, the inclinations cluster at about +50° and -50°, suggesting that there has been little or no translation of the site since the late Eocene. However, the distribution of inclinations is dominated by normal polarity, suggesting that many of the rocks are carrying an overprint from the present magnetic field. This is particularly evident in the inclination data between 300 and 400 mbsf. In this interval, one finds more sediments having shallow magnetic inclinations; however, these data would not suggest the large amount of translation, as reported by Bleil (1982). Future shorebased work will better determine paleolatitudes for Hole 782A. Cores 125-782A-5H through 125-782A-9H were oriented using the multishot camera. However, these cores were frequently disturbed by the drilling process, which is reflected by the scatter in declinations. Thus, no rotation data could be obtained.

Magnetic Susceptibility

Whole-core magnetic susceptibilities were measured using the multisensor track (MST). Susceptibilities in the interval from 0 to 240 mbsf range between $6\pi \times 10^{-4}$ SI and $50\pi \times 10^{-4}$ SI and show little scatter. Below this, there is a small, but significant, increase in susceptibility as well as in the amount of dispersion. The increase in susceptibility does not correlate with an increase in the number of ash layers, but rather with an increase in the amount of induration in the sediments. A downhole plot of magnetic susceptibility from Hole 782A is presented in Figure 16.

SEDIMENT ACCUMULATION RATES

Estimates of sedimentation rates for Site 782 are based on calcareous nannofossil zones (Table 9) that were used to construct the age-depth curve shown in Figure 17.

Sedimentation rates in the latest Eocene/earliest Oligocene are extremely low, although only two biostratigraphic events are available for this period. A hiatus between the early and late Oligocene may be present (see "Biostratigraphy" section, this chapter). The estimated rate for the upper Oligocene section is about 4.9 m/m.y. The lower Miocene sequence is characterized by a hiatus. Sedimentation rates for the middle Miocene to late Pliocene sequences are estimated to be about 16.5 m/m.y. Thereafter, sedimentation rates increase to about 47.1 m/m.y. in the upper Pliocene section and are even higher in the Pleistocene.

PHYSICAL PROPERTIES

The high percentage of core recovered from Hole 782A allowed us to measure physical properties for the nearly 400 m of sedimentary section. Unfortunately, poor recovery of basement rocks prevented similar measurements. Physical- and index-property measurements are listed in Tables 10 and 11.

Thermal conductivities in the sedimentary section are clustered at about 1 W/mK (Table 11) and increase slightly and show greater scatter with depth (Fig. 18). This increased scatter may be related to drilling disturbance in the more

compacted sediment at deeper levels in the hole. The presence of drilling biscuits supports this hypothesis.

Good quality data were obtained from the gamma-ray attenuation and porosity evaluator (GRAPE), especially for the APC cores (Cores 125-782A-1H through 125-782A-9H). GRAPE bulk densities increase downhole from about 1.6 to 1.95 g/cm³ (Fig. 19). The amount of scatter increases downhole in a pattern similar to that seen in thermal-conductivity measurements and probably is also related to drilling disturbance. Detailed analyses of GRAPE data show a change in slope of density measurements at 373 mbsf (Fig. 20), which may correspond to changes in downhole measurements of velocity, density, and resistivity (see "Downhole Measurements" section, this chapter). The GRAPE density discontinuity at 373 mbsf is not apparent in the index-property data.

Index-property measurements (bulk and grain densities, porosity, and water content) agree well with GRAPE data (Table 10). Bulk densities derived from measurements of discrete samples show a similar increase with depth to those observed in GRAPE data (Fig. 21). Less scatter was observed in the bulk density of discrete samples than in the GRAPE measurements because the discrete samples were taken from coherent blocks, thus avoiding zones of disturbed core. Grain densities display no depth variability, but instead are nearly constant at 2.8 to 2.9 g/cm³.

Compressional-wave velocities were determined for the uppermost portion of the core using the *P*-wave logger on the MST. Velocity was constant at 1550 m/s in the APC cores (Fig. 22). These data are in good agreement with values obtained from logging the hole (see "Downhole Measurements" section, this chapter). No velocity information was retrieved from cores in the interval from 70 to 270 mbsf because of poor coupling of the *P*-wave-logger transducers on XCB cores and because we could not measure velocities in poorly consolidated core on the Hamilton frame.

Hamilton-frame velocities were measured for lithified sedimentary rocks recovered from 265 to 390 mbsf (Table 11), both in the "A" direction (propagation direction parallel to the core axis) and in the "B" direction (normal to the axis of the cores). Both "A" and "B" direction velocities increase from about 1680 to 2000 m/s over the measured interval (Fig. 23). The sample velocities are isotropic.

Electrical resistivity was measured for every other section from the cores of Hole 782A (Table 11). Values range from 16 to 41 ohms, averaging about 20 ohms (Fig. 24). Resistivity increases slightly with depth. No measurements were taken below 278 mbsf because of increasing consolidation, which prevented probe insertion.

DOWNHOLE MEASUREMENTS

Logging Operations

During logging at Site 782 we used two logging strings. The first string consisted of the temperature logging tool (TLT), phasor induction tool (DIT), lithodensity tool (HLDT), and the sonic tool (SDT). The second string consisted of the temperature logging tool (TLT), the natural gamma-ray spectrometry tool (NGT), aluminum clay tool (ACT), general purpose instrumentation tool (GPIT), compensated neutron tool (CNT), and the induced gamma-ray spectrometry (GST) tool.

Logging commenced at 1150UTC on 22 March with the deployment of the first string. When this string reached the seafloor, we halted it for 8 min to record a seawater temperature for reference to the logged values. At 1330UTC the string was out of the drillpipe at 105 mbsf. The sonic logs (both

Table 8. Composition of interstitial waters from sediments at Site 782.

Sample no.	Core, section, interval (cm)	Volume (mL)	Squeeze T (°C)	Depth (mbsf)	pH	Salinity (R.I., %)	Salinity (calc., %)	Chlorinity (mmol/kg)	Alkalinity (meq/kg)	Sulfate (mmol/kg)	Sodium (mmol/kg)	Potassium (mmol/kg)
Surface seawater (17 March 1989)					8.25	35.6	34.654	539.2	2.689	27.78	462.0	10.11
1W-1	782A-1H-3, 145-150	45	3	4.48	7.86	35.4	34.996	545.5	3.279	26.44	468.9	12.11
1W-2	782A-2H-4, 145-150	50	2	15.78	7.71	35.1	35.149	548.4	3.291	26.60	471.3	11.07
1W-3	782A-3H-4, 145-150	51	2	25.28	7.62	35.4	35.259	549.4	3.229	26.93	474.6	10.99
1W-4	782A-4H-4, 145-150	32	2	34.78	7.69	36.0	35.031	546.5	2.829	26.85	470.6	10.74
1W-5	782A-5H-4, 145-150	44	3	44.28	7.75	35.5	35.023	546.5	3.254	26.40	471.0	11.06
1W-6	782A-7H-4, 140-150	52	3	63.25	7.89	35.3	35.233	550.4	3.281	25.86	477.9	11.56
1W-7	782A-11X-2, 145-150	32	4	98.68	7.91	35.1	34.809	546.5	2.987	24.92	470.6	10.55
1W-8	782A-13X-2, 140-150	55	5	117.95	7.83	34.9	34.881	546.5	2.376	25.76	473.4	9.94
1W-9	782A-16X-2, 140-150	63	6	146.85	7.78	35.0	34.767	545.5	2.420	25.21	471.9	9.95
1W-11	782A-19X-2, 140-150	48	6	175.85	7.88	35.0	34.673	544.6	2.271	25.23	470.8	8.73
1W-11	782A-23X-4, 140-150	49	8	217.45	7.82	35.1	34.696	546.5	1.919	24.71	469.0	9.49
1W-12	782A-26X-3, 140-150	51	8	244.75	7.75	35.2	34.733	545.5	2.259	25.08	469.1	9.03
1W-13	782A-29X-4, 140-150	46	8	275.15	7.88	36.1	34.819	547.7	1.754	24.82	471.9	8.98
1W-14	782A-32X-5, 140-150	54	9	301.45	7.65	35.1	34.042	548.7	1.733	26.25	472.9	8.27
1W-15	782A-35X-3, 140-150	50	9	326.95	7.57	35.1	34.877	546.8	2.167	25.28	471.9	7.74
1W-16	782A-39X-1, 140-150	48	10	362.35	7.73	35.2	34.659	543.9	1.426	24.90	469.3	7.54
1W-17	782A-42X-1, 140-150	31	10	391.25	7.82	35.0	34.590	542.9	1.233	24.75	469.3	7.23

short and long) were erratic because of skipped cycle induced by rugose hole conditions. The string touched down at 1414UTC at 453 mbsf; the return logging run began at 1422UTC and reached the pipe at 1534UTC. We completed a short duplicate run in the upper part of the hole and then returned the tool string to the surface at 1607UTC.

The second logging run (using the second, geochemical, string) commenced at 1930UTC and included an 8-min-calibration stop for the TLT near the seafloor. The tool string reached the bottom of the hole (453 mbsf) at 2130UTC. Uphole logging began at 2145UTC and reached the drillpipe at 2356UTC. Logging continued in the drillpipe to 10 m above

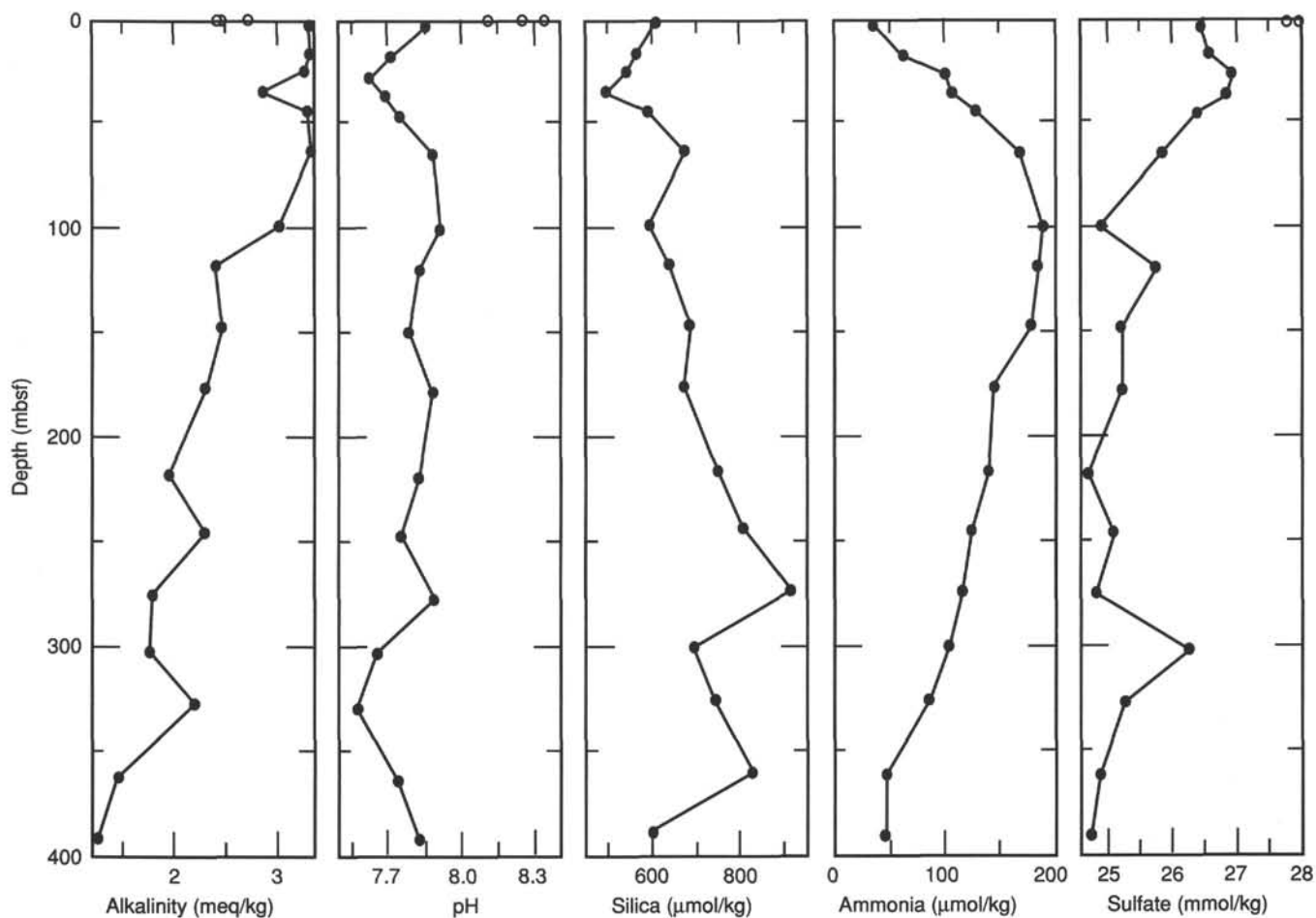


Figure 8. Composition of interstitial waters (alkalinity, pH, silica, sulfate, ammonia) from sediments at Site 782 (solid circles) compared with surface seawater collected 22 February, 4 March, and 17 March 1989 (open circles).

Table 8 (continued).

Calcium (mmol/ kg)	Magnesium (mmol/kg)	Bromide (mmol/kg)	Silica (μ mol/kg)	Ammonia (μ mol/kg)
10.18	52.48	0.81	0	10
9.69	50.62	0.82	610	35
9.62	51.63	0.81	566	61
9.46	51.00	0.92	544	101
9.56	51.30	0.88	493	107
9.27	50.96	0.90	591	128
8.95	49.01	0.86	677	169
9.30	49.76	1.06	595	190
9.26	49.25	0.81	642	185
9.78	48.49	0.90	687	179
10.26	48.64	0.88	673	145
11.17	48.52	0.93	751	138
12.45	47.47	0.91	806	122
13.32	45.82	0.84	917	115
15.07	45.79	0.83	694	102
17.27	42.65	0.86	745	83
20.33	38.81	0.89	827	45
22.31	36.28	0.88	597	42

the seafloor. Two more runs were made in the drillpipe for calibration purposes, one of which required raising the drill string by 2 m. The second pass ended at 0308UTC, 23 March, when the tool string was brought to the surface.

A third logging run (using the magnetic susceptibility tool) then was attempted. The tool failed because of water leakage

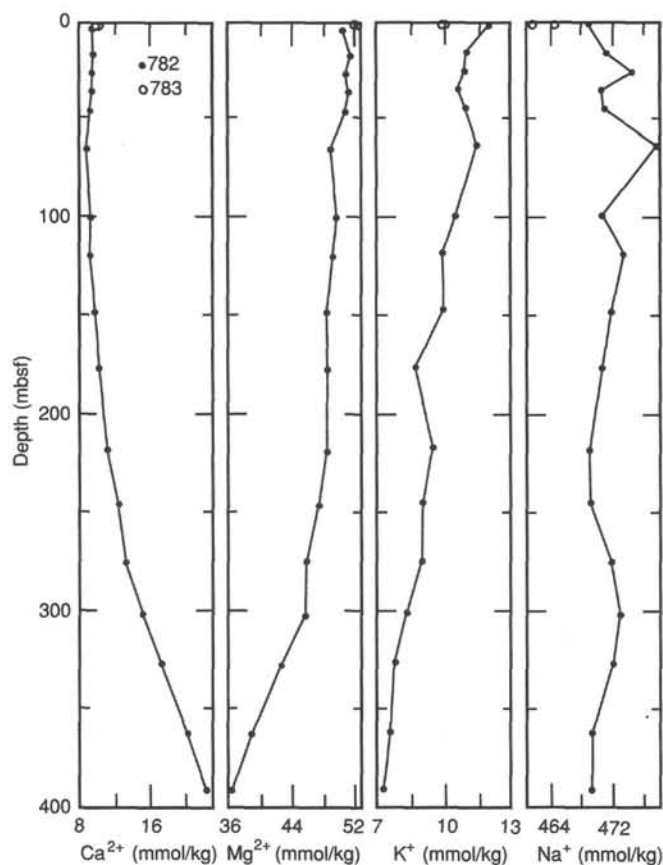


Figure 9. Composition of interstitial waters (calcium, magnesium, potassium, sodium) from sediments at Site 782 (dots) compared with surface seawater collected 22 February, 4 March, and 17 March 1989 (open circles).

into the instrument package, and logging at Site 782 was abandoned.

Results

Logging results for Hole 782B are presented in Figures 25 through 32. The measurements define four units above basement at Site 782: a first unit from above the end of the drill pipe (about 100 mbsf) to 208 mbsf (Figs. 25–28); a second unit from 208 to 305 mbsf; a third unit from 305 mbsf to 373 mbsf (Figs. 29 and 30); and a fourth unit from 373 mbsf to basement at 409 mbsf (Figs. 31 and 32).

First Unit

The first unit (to 208 mbsf) contains lithologic Subunit IA and the upper part of lithologic Subunit IB. The gamma-ray logs show a broad-scale variation within this unit, with the CGR log varying between 6 and 24 API units (averaging about 14), and the SGR log varying between 14 and 25 API units (averaging about 18). The resistivity log values are about 0.8 to 0.9 ohm-m, with a slow increase with depth. The IDPH log consistently has a slightly higher reading throughout this hole; thus, it may have a slight instrument-calibration error. The caliper log shows that the hole is 0.38 to 0.43 m (15 to 17 in.) in diameter, with scattered washouts to more than 0.48 m (19 in.). This log also indicates scattered small anomalies in hole diameter with an approximate 10-m interval (Fig. 25). These anomalies may be related to washouts that occur when pipe sections are being added, and downward progress of the pipe string is momentarily stopped. Bulk density (as shown in the RHOB curve) is fairly constant at 1.65 to 1.7 g/cm³. Porosity (PHI) gradually

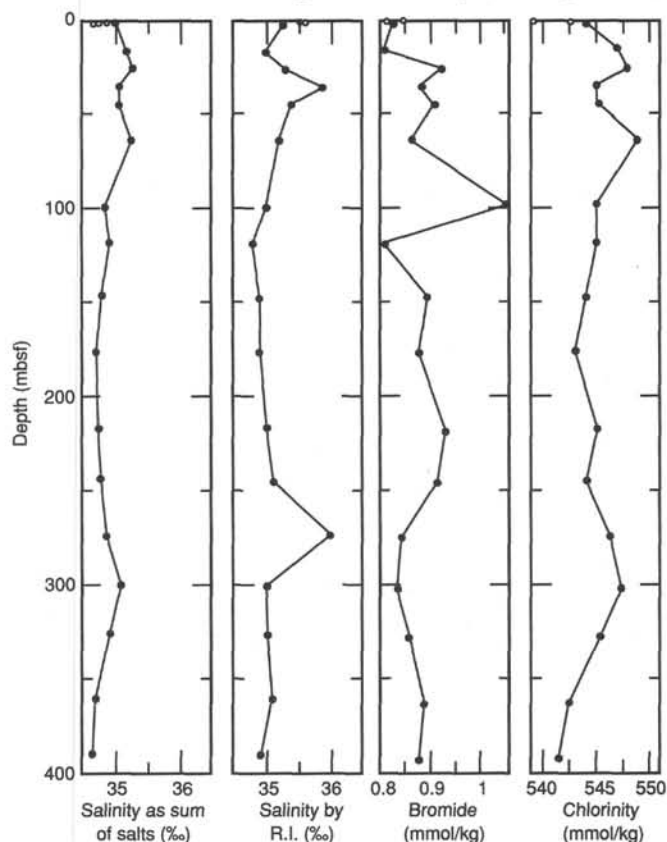


Figure 10. Composition of interstitial waters (salinity, bromide, chlorinity) from sediments at Site 782 (dots) compared with surface seawater collected 22 February, 4 March, and 17 March 1989 (open circles).

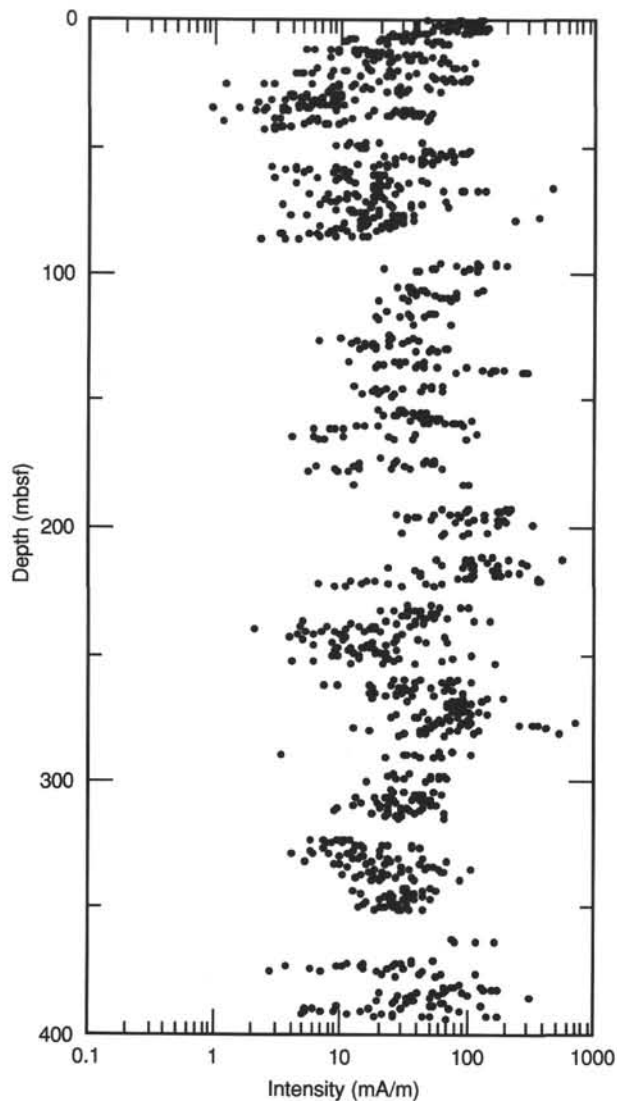


Figure 11. A downhole plot of magnetic intensity for Hole 782A.

decreases with depth to 60% at the base of the unit. The photoelectric effect (PEF) is constant at 2.8 to 3.0. *P*-wave velocity is constant, near 1.65 km/s.

The chemical composition of the unit is variable, despite its uniform appearance and physical properties. SiO_2 content averages about 40%, but varies from 0% to 80%. CaO content averages about 30% and varies from 0% to 50%, generally complementary to SiO_2 . Al_2O_3 content is in the range of 15% to 18%, but sometimes reaches 35%. MgO is variable, ranging between 0% and 16%, but is generally found in a layer of about 10%. Elements having lower abundances and less variation include sulfur at 1%, K_2O at 1% to 1.4%, Fe_2O_3 at 1% to 1.5%, and TiO_2 at 0.5% to 1.0%. Trace elements include gadolinium at about 3 ppm (with a few increases to 10 ppm), uranium at about 1 ppm, and thorium at about 1 ppm.

Second Unit

The second unit (208–305 mbsf) is within lithologic Subunit IB. This unit has a gradational boundary with the overlying first unit, but also has an abrupt boundary with the underlying third unit. The gamma-ray logs are more uniform than in the

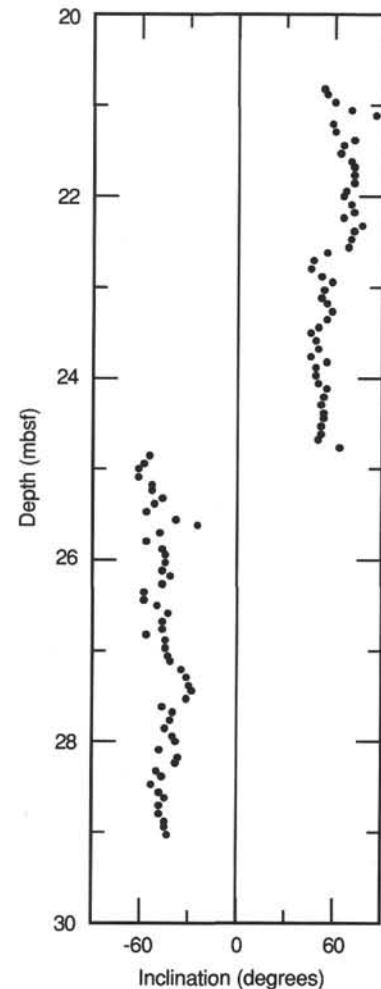


Figure 12. Inclination data from Core 125-782A-3H showing a well-defined polarity transition.

first unit, with CGR values at 20 API units and SGR values at 23 API units. The gamma-ray logs do show two layers of increased values in the bottom few meters of this unit, with values as high as 35 API units in the layer at the very bottom. Resistivity values grade up from 0.8 ohm-m at the upper boundary to 1.0 ohm-m within the unit. Values distinctly increase at the lower boundary. The increasing resistivity with depth reflects increasing consolidation of the sedimentary section. The caliper log shows that the hole is fairly uniform in size (between 0.38 to 0.43 m) in this unit. One washout occurs near the top of the unit and the 10-m-interval anomalies also occur in this unit. Bulk density shows a gradual increase from 1.65 to 1.75 g/cm^3 in the layer just at the bottom of the unit. The photoelectric effect also shows a gradual increase from 2.5 to 3.0 within this unit. Porosity is uniform at 60%, aside from one large increase at 233 mbsf. *P*-wave velocity increases gradually from 1.75 to 1.85 km/s.

The elemental logs show that the dominant composition is SiO_2 at 40%, with a range of from 10% to 70%. Despite the wide range, variability is not as great as in the first unit. CaO is the second most abundant component; it generally varies in a complementary manner to SiO_2 . Typically, CaO values are 30%, and the range is from 0% to 45%. The percentage of Al_2O_3 in the second unit is distinctly higher than in the first unit, averaging about 25%. The variability in Al_2O_3 also is

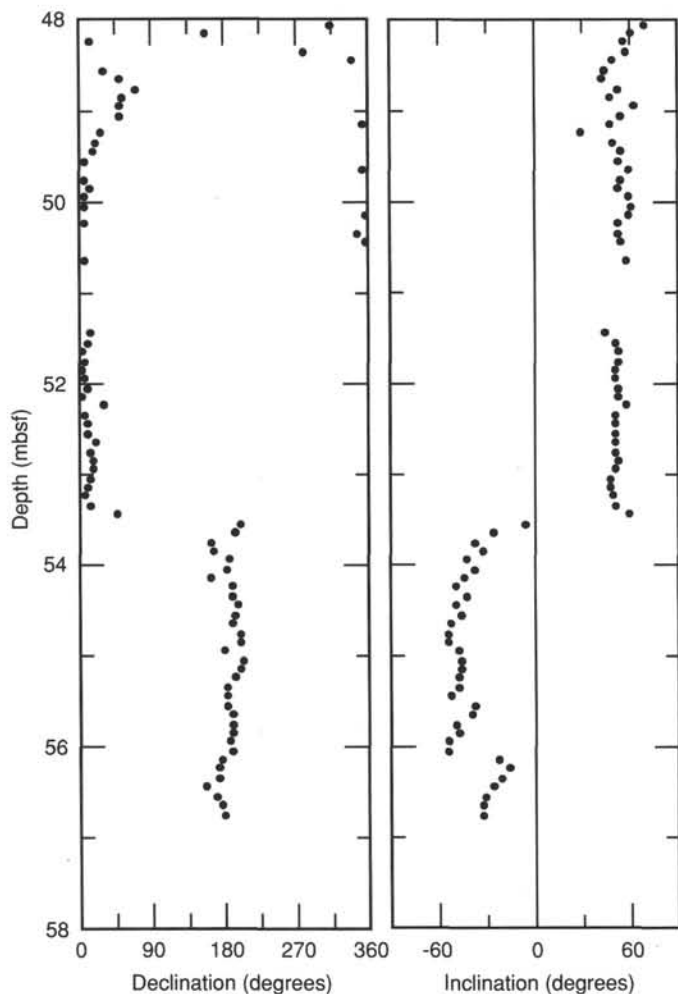


Figure 13. Inclination and declination data from oriented Core 125-782A-6H. This core is described as having moderate drilling disturbance, but note the consistency of the magnetic vector.

higher in the second unit, with six layers having values of more than 40%. MgO continues to occur in layers of about 10%, but these decrease in frequency with increasing depth. Fe₂O₃ is low (less than 1%) in the upper 30 m of this unit, then averages about 2% for the rest of this unit. K₂O is distinctly higher than in the first unit, with values of about 1.6%. Thorium also is higher than in the first unit, with fairly constant values at 2 ppm. Several elements are as abundant as in the first unit: sulfur (1%), TiO₂ (0.7%), uranium (1 ppm), gadolinium (3 ppm).

Third Unit

The third unit extends from 305 to 373 mbsf and spans the transition from lithologic Subunit IB to Subunit IC at 337.0 mbsf. The third unit has distinct differences in composition and physical properties from its neighboring units. The gamma-ray logs abruptly decrease to uniform values of 15 API units for both SGR and CGR. Resistivity values increase abruptly to 1.5 ohm-m at the top of the unit and to 2.0 ohm-m within the unit in two less well-defined steps. The caliper log shows that the hole opens up to a diameter of 0.43 m at the top of the unit, then gradually widens to more than 0.48 m. Bulk density is slightly higher (at 1.75 to 1.8 g/cm³) than in the second unit. The PEF effect is also slightly higher than in the

second unit at 3.0 to 3.2. Porosity values decrease and become more variable, ranging between 40% and 65%. P-wave velocities increase from 1.85 to 2.15 km/s. Velocity values exhibit small-scale variability, with some layers having velocities of 2.8 km/s.

The composition of the third unit is also distinct from the overlying second unit. CaO is higher (at 40%–45%) and then slowly decreases down the section. SiO₂ is lower (at 30%–35%) and is somewhat more variable, ranging from 12% to 55%. SiO₂ increases down the section. Abundance of Al₂O₃ is slightly lower than in the second unit (at 18%) and is not as variable as in that unit. The abundance of MgO continues to occur in layers from 0% to 10%. A number of elements have similar values to those in the second unit: Fe₂O₃ (1%–2%), sulfur (1%), TiO₂ (~0.8%), and gadolinium (~4 ppm). The abundances of the radioactive elements are lower in the third unit than in the second: K₂O (slightly lower at 1.4%), thorium (much lower at 1 ppm), and uranium (much lower at 0.6 ppm trending down to 0 ppm at the base of the unit).

Fourth Unit

The fourth unit defined by logging results extends from 373 to 409 mbsf. This unit contains pebble-rich sands and gravelly conglomerates found at the base of lithologic Subunit IC. Physical-property logs show abrupt changes from values of the third unit. Gamma-ray values are about 20 API units for both SGR and CGR. Resistivity values show a sharp increase, which then tails off and ends at 6 to 7 ohm-m. These values decline sharply to 3 ohm-m at 390 mbsf, then gradually rise to 5 ohm-m at the base of the unit. The P-wave velocity is variable, but averages 2.4 km/s above 390 mbsf and 2.1 km/s below that depth. The caliper log shows that the hole decreases gradually to 0.43 m diameter at 383 mbsf, after which it opens up again. The diameter then sharply decreases to a uniform value of 0.32 m below 397 mbsf. Bulk densities show an irregular increase from 1.75 to 2.1 g/cm³, with scattered layers as high as 2.35 g/cm³. The PEF effect is somewhat less than in the third unit, at 2.5 to 3.0.

Elemental abundances show abrupt changes from the overlying unit. SiO₂ increases down the section from 50% to 70%. CaO shows a dramatic decrease to about 10%. MgO is much higher at 10% to 20% and is present throughout most of the unit. MgO disappears at the base of the section. Al₂O₃ has an increased variability, although the average value is about the same at 20%. Sulfur values are slightly higher at 1.5%; TiO₂ is also slightly higher at 1%. Values of gadolinium are distinctly higher at 6 to 7 ppm. Concentrations of the radioactive elements are higher, with uranium and thorium at about 1 ppm. K₂O increases to 2% and then decreases to 1% down the section.

Basement

The final logging unit is the basement below 409 mbsf (lithologic Unit II). The basement does not stand out from the fourth unit in the same way that the fourth unit is distinct from the third. Gamma-ray values for CGR and SGR increase to 25 API units. Resistivity is constant at 4 to 5 ohm-m to 423 mbsf, where it decreases to 3 ohm-m. Below 433 mbsf, resistivity gradually increases to 9 or 10 ohm-m at the bottom of the hole. The caliper log shows that the hole opens from 0.32 m to 0.48 m, then gradually decreases to 0.28 m. Bulk density is constant near 2.05 g/cm³. The PEF effect increases to 3.2, then decreases to 2.5 below 423 mbsf. P-wave velocity is fairly constant at 2.8 to 3.0 km/s.

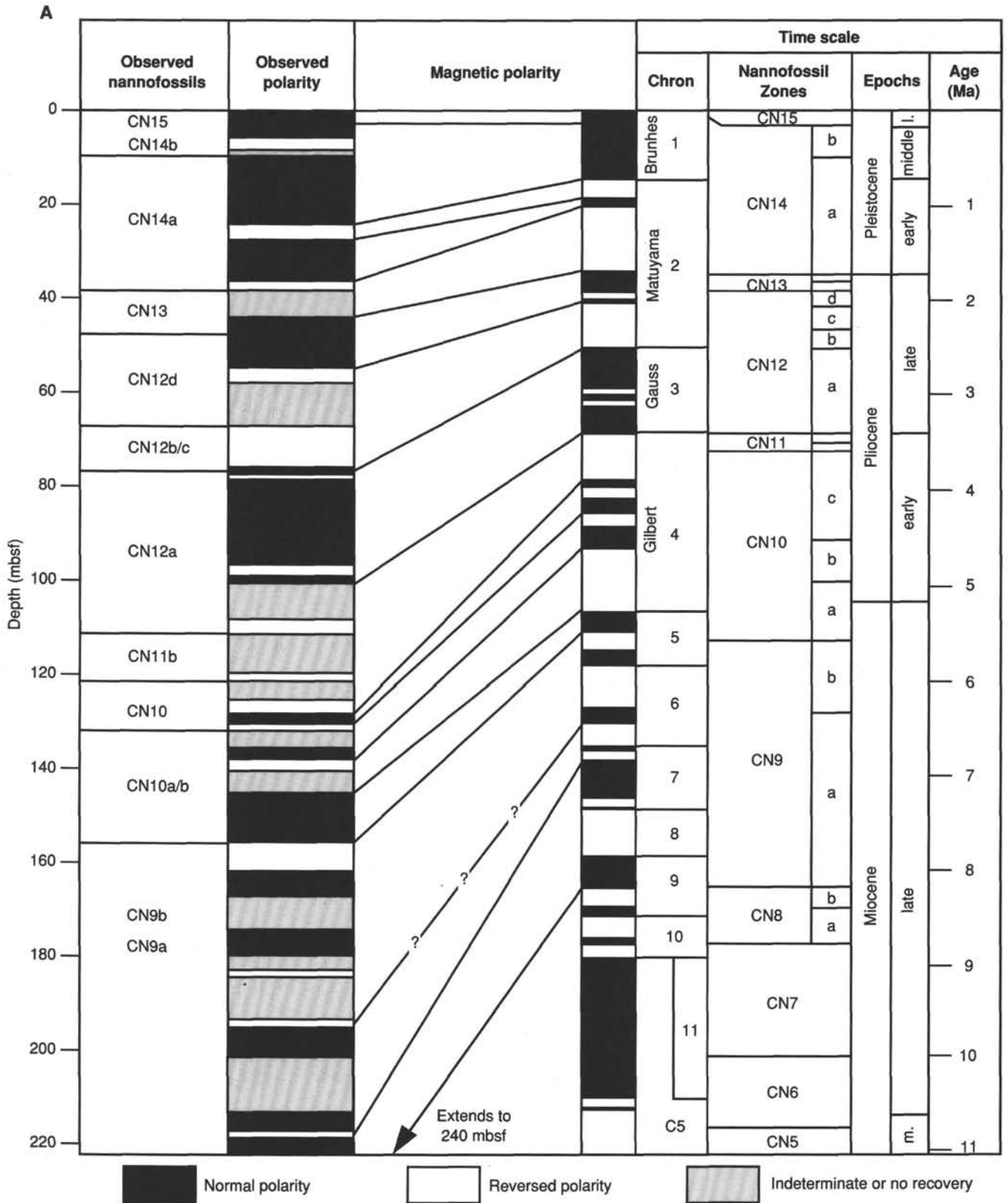


Figure 14. A. Observed magnetostratigraphy of Hole 782A for the interval from 0 to 220 mbsf, correlated with time scale of Berggren et al. (1985). B. Observed magnetostratigraphy of Hole 782A for the interval from 220 to 420 mbsf, correlated with time scale from Berggren et al. (1985).

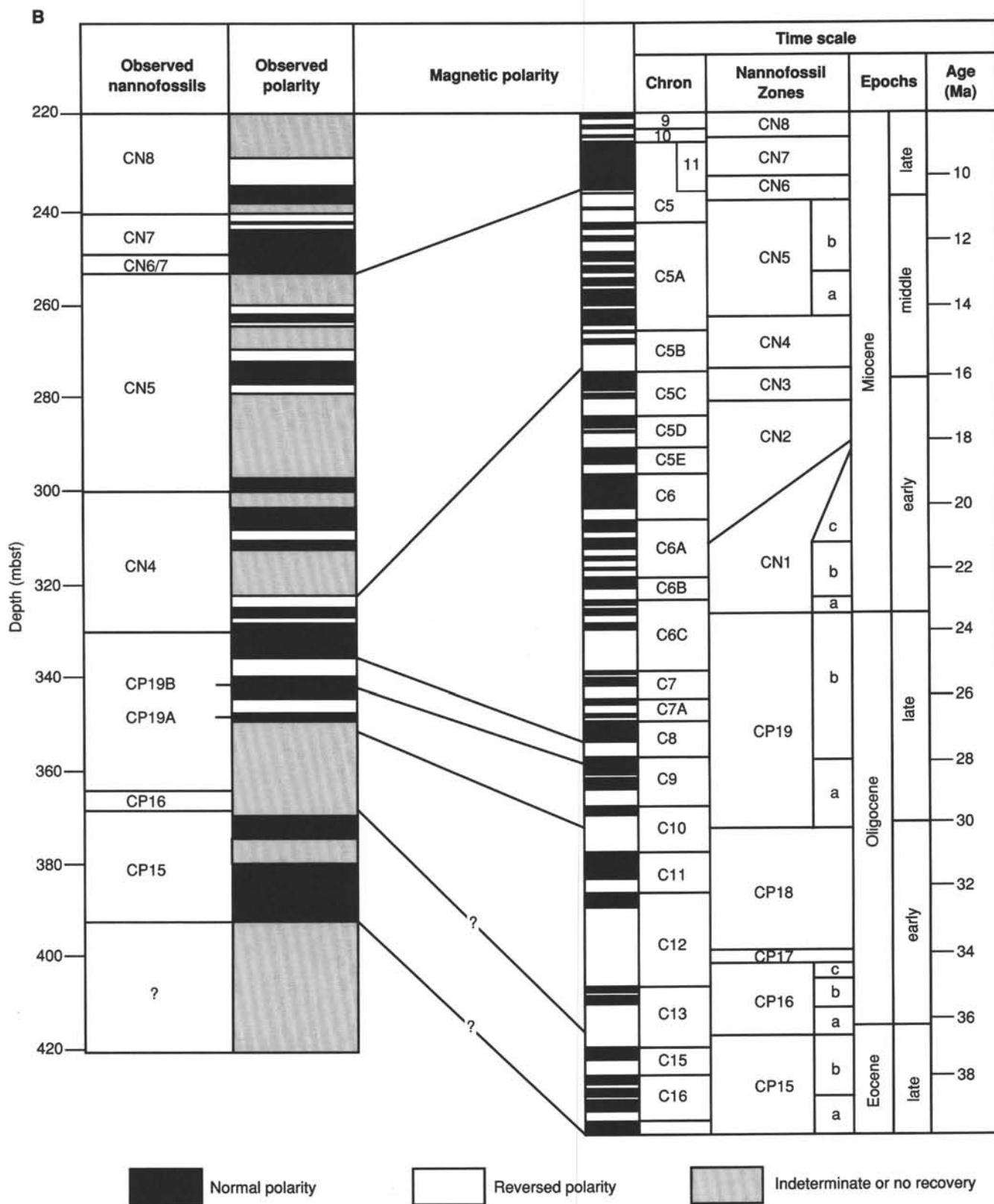


Figure 14 (continued).

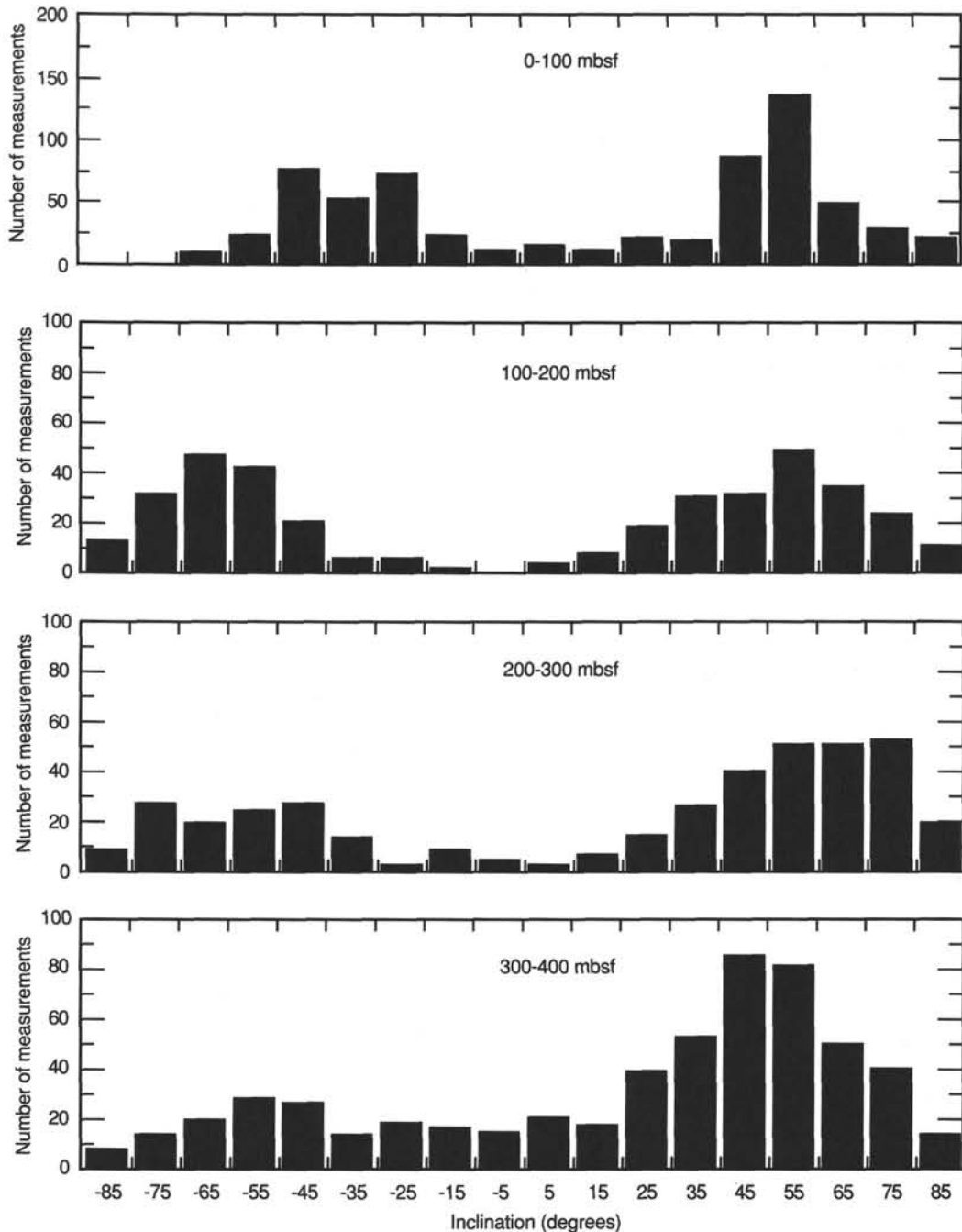


Figure 15. Inclination distribution as a function of depth.

Elemental logs show that SiO_2 is highly variable and ranges between 40% and 70%. CaO is fairly constant at near 10%. Al_2O_3 decreases from 20% down the section, but scattered layers have high values. Abundances of MgO increase from 15% to 20%. Percentages of Fe_2O_3 are higher in the fourth unit, increasing to 4%. Abundance of sulfur is somewhat lower at 1%. TiO_2 is similar at 1%, as is the concentration of gadolinium at 6 ppm. K_2O increases to a uniform 2%, whereas uranium remains steady at 0.7 ppm, and thorium also remains steady at 1 ppm.

Ashes and Magnetic Logs

A three-axis magnetic log is presented in Figure 28, along with an enlarged-scale plot of the vertical component. The

logging string is not stabilized in the hole and has no other reference for orientation; thus, these logs primarily show the rotation of the tool during the logging run. In other areas, such as off the Oman margin during Leg 117, the vertical component was correlated successfully with mineralogy (Prell, Nitsuma, et al., 1989). The data here show only an inverse correlation with the Y component at Hole 782B, indicating a slightly deviated hole.

More than 100 ash layers were recognized in the cores recovered from Site 782 (see "Lithostratigraphy" section, this chapter). We were unable to correlate any of the logs (including the magnetometer logs; Fig. 28) with the ash layers. The tools in the logging string generally have a resolution of 15 cm or more, whereas the ash layers are generally less than 1 cm

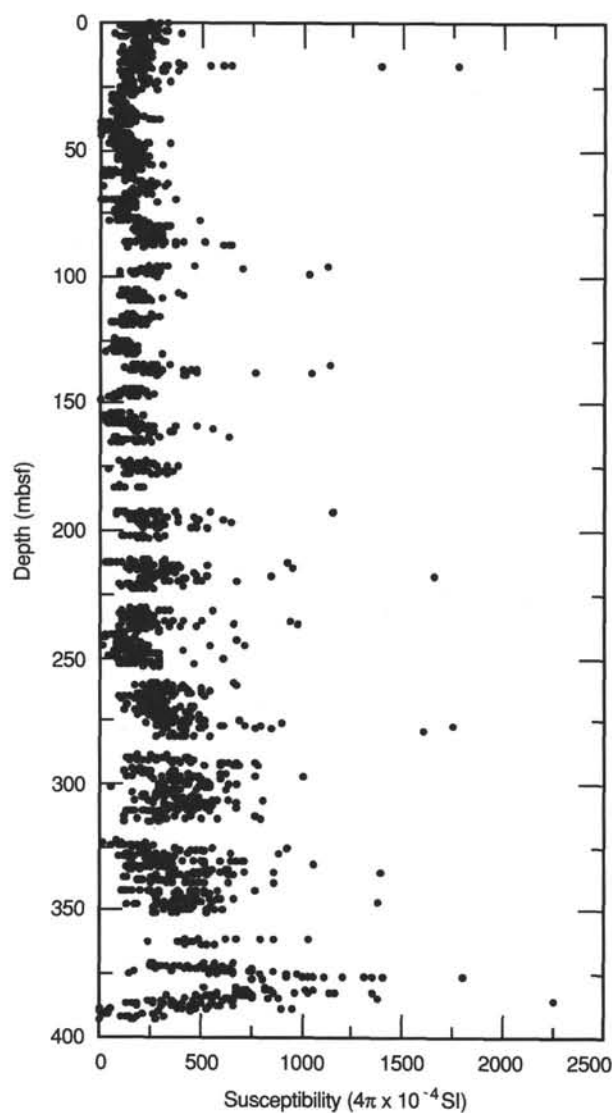


Figure 16. A downhole plot of susceptibility for Hole 782A.

thick. As mentioned previously, the susceptibility tool was deployed but failed to operate.

Heat-Flow Measurements

Two measurements were attempted with the Barnes-Uyeda heat-flow tool at 38.3 and 66.8 mbsf. The results are presented in Figures 33 and 34. Neither run obtained a useful *in-situ* temperature because of excessive motion during logging.

Results from the two TLT runs are shown in Figures 35 and 36. The temperature at the bottom of the hole was about 4.75°C during the first run, but warmed to about 5.75°C during the second run. Engineering data for the hole's drilling and pumping-rate history will be used to construct a time-dependent thermal model for the drill hole. This thermal model will enable us to determine the equilibrium temperature profile for the hole.

Measurements of thermal conductivity (Fig. 37), its inverse thermal resistivity (Fig. 38), and the depth integral of thermal resistivity (Fig. 39) will be used with the temperature profile to determine heat flow at this hole.

Table 9. Biostratigraphic data used to plot the age-depth curve in Figure 17.

Biostratigraphic event		Depth (mbsf)	Age (Ma)
Calcareous nannofossils			
<i>Emiliana huxleyi</i>	FO	9.8	0.26
<i>Pseudoemiliana lacunosa</i>	LO	28.8	0.4
<i>Calcidisais macintyreii</i>	LO	33.2	1.45
<i>Gephyrocapsa oceanica</i>	FO	38.3	1.66
<i>Discoaster brouweri</i>	LO	57.3	1.98
<i>D. surculus</i>	LO	76.3	2.4
<i>Reticulofenestra pseudumbilica</i>	LO	115.0	3.4
<i>P. lacunosa</i>	FO	124.6	3.5
<i>Amaurolithus tricorniculatus</i>	LO	134.4	3.6
<i>D. quingueramus</i>	LO	163.2	5.6
<i>D. neohamatus</i>	LO	221.0	8.3
<i>D. kugleri</i>	LO	251.1	10.8
<i>C. floridanus</i>	LO	280.5	13.0
<i>Sphenolithus heteromorphus</i>	LO	313.1	14.4
<i>D. bisectus</i>	LO	332.1	23.7
<i>S. ciperoensis</i>	FO	363.5	30.1
<i>C. grandis</i>	LO	387.6	39.6
<i>D. bifax</i>	LO	389.8	42.2

For source of age and depth information, see "Biostratigraphy" section, this chapter.

SUMMARY AND CONCLUSIONS

Site 782 (30°51.66'N, 141°18.85'E, 2958.9 mbsl) is located on the eastern margin of the Izu-Bonin forearc basin, about halfway between the active volcanic arc and the Izu-Bonin trench. Two holes were drilled: Hole 782A, a 476.8-m hole that was fully cored and described; and Hole 782B, a 468.9-m hole, of which only the last 9.5 m was cored and described, but that was used for two logging runs (Fig. 40).

Two lithologic units, the first of which is sedimentary and made up of three subunits, the second of which comprises volcanic basement, have been defined at Site 782: Unit I, Subunit IA (0–153.6 mbsf in Hole 782A) is Holocene(?) to lower Pliocene, gray to yellow-greenish, homogeneous, nannofossil marl containing scattered volcanic debris and volcanic ash layers; Unit I, Subunit IB (153.6–337.0 mbsf in Hole 782A) is upper to middle Miocene, light to dark gray, nannofossil marl containing scattered volcanic debris and volcanic ash layers; Unit I, Subunit IC (337.0–409.2 mbsf in Hole 782A) is upper Oligocene to middle Eocene, vitric nannofossil chinks intercalated with tuffaceous sediment and also (near the base) pebble-rich sands, gravelly conglomerates, and numerous ash layers; Unit II (409.2–476.8 mbsf in Hole 782A and 459.3–468.9 mbsf in Hole 782B) comprises angular to subrounded clasts of intermediate-acid lava.

Sedimentation rates increased from the upper Oligocene section (about 5 m/m.y.) through the upper Miocene and lower Pliocene sections (about 16.5 m/m.y.), to the upper Pliocene section (about 47 m/m.y.), with a possible decrease in sedimentation rate in the Pleistocene section. Two possible unconformities were identified in the succession: one between the uppermost Oligocene and middle Miocene sections, the other between the lower Oligocene and upper Oligocene sections. The sediments exhibit common slump structures, burrows, and normal and reverse grading. More than 100 volcanic ash layers were identified in the cored section. Volcanogenic materials in the ash and dispersed within the sediments include primary materials (glass, opaque minerals, feldspar, pyroxenes, and amphibole), together with their alteration products (chlorite, glauconite, zeolite, and epidote group minerals).

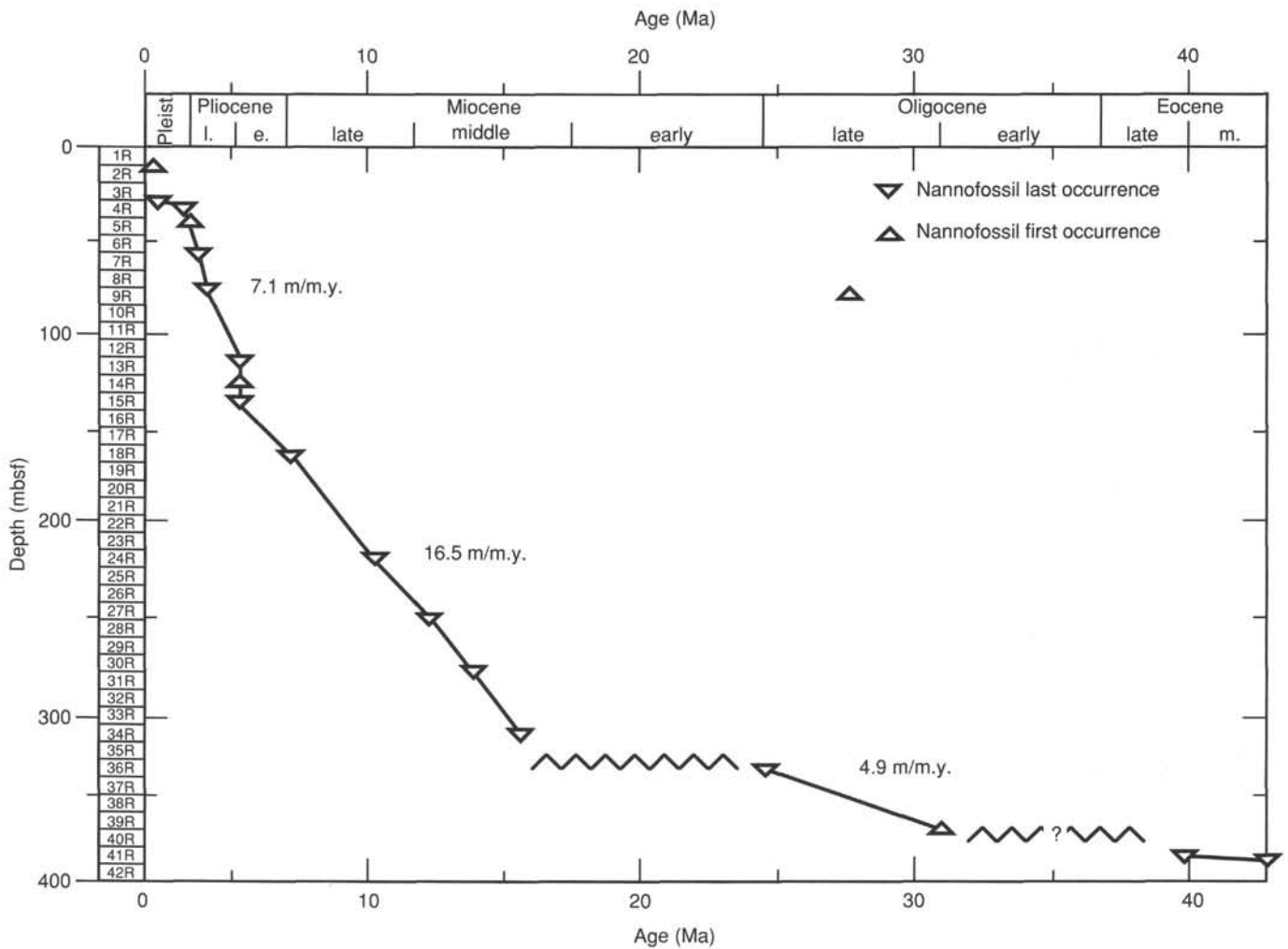


Figure 17. Age and depth curve for Site 782 showing estimated sedimentation rates. Ages determined are described in the text.

The lavas of Unit II typically are slightly vesicular and contain phenocrysts of plagioclase, orthopyroxene, and clinopyroxene in a glassy groundmass. Some may be pillow fragments. Geochemical data show that these phenocrysts fall into two compositional groups, an andesite group and a dacite-rhyolite group, and that they are transitional between the tholeiitic and calc-alkaline volcanic-arc series. The andesites have low magnesium contents and thus are distinct from the high-magnesium bronzite andesites of similar age reported from other, more eastern, parts of the Izu-Bonin-Mariana forearc.

Interstitial fluids in lithologic Unit I have seawater pH, sodium, and chlorinity values throughout the section. In response to water-mineral reactions, potassium (from 12 to 7 mmol/kg) and magnesium (from 50 to 36 mmol/kg) decrease steadily with depth, whereas calcium increases from 9 to 22 mmol/kg and silica increases from 600 to a maximum of 900 mmol/kg at about 300 m. Ammonia increases from 35 to a maximum of 190 mmol/kg at about 150 m as a result of bacterial breakdown of organic matter.

Studies of physical properties in Hole 782A reveal thermal conductivities within Unit I of about 1 W/mK and bulk densities that increase downhole within Unit I from 1.6 to 1.95 g/cm³. Porosities of the sediments decrease downhole from 70% to 60%, with a discontinuity at about 280 mbsf (middle Miocene). Magnetic susceptibilities increase downhole in re-

sponse to the amount of induration of the sediment. Magnetic inclination data from Hole 782A cluster around +50° and -50°, indicating little or no translation of the site since the late Eocene. However, declinations are scattered because of core disturbance; thus, no data for the extent of rotation could be obtained.

Logging enabled us to divide Hole 782B into three distinct units according to its physical and chemical properties: an upper unit from 0 to about 300 mbsf; a middle unit from about 300 to about 370 mbsf; and a lower unit from about 370 mbsf to the lower limit of logging at about 420 mbsf. The boundary between the upper and middle units is marked by a sudden downhole increase in density and resistivity and may correspond to an increase in sediment compaction or to the Miocene unconformity. The boundary between the middle and lower units is marked by an increase and greater variability in compressional-wave velocity and density, together with an increase in silica and potassium. This boundary may correspond to the Oligocene unconformity.

The principal results of this site are (1) the identification of Eocene basement in this part of the forearc basin, (2) the characterization of the uppermost basement as intermediate-acid submarine volcanic rocks of island-arc tholeiite to calc-alkaline affinities, (3) paleomagnetic evidence that no major translation of the site has occurred since the Eocene, and (4) the recognition that the greatest sedimentation rate is seen in

Table 10. Index properties for Hole 782A.

Core, section, interval (cm)	Depth (mbsf)	Bulk density (g/cm ³)	Grain density (g/cm ³)	Porosity (%)	Water content (%)	Void ratio
125-782A-1H-1, 76-78	0.76	1.62	2.83	67.5	44.3	0.67
1H-2, 76-78	2.26	1.62	2.68	64.7	42.5	0.65
1H-3, 76-78	3.76	1.63	2.68	64.3	42	0.64
1H-4, 76-78	5.26	1.62	2.69	64.6	42.3	0.65
1H-5, 76-78	6.76	1.54	2.57	66.9	46.1	0.67
1H-6, 76-78	8.26	1.61	2.61	63.4	41.7	0.63
1H-7, 29-31	9.29	1.63	2.7	64.2	41.8	0.64
1H-CC, 13-8	9.68	1.62	2.55	61.5	40.3	0.61
2H-1, 74-76	10.54	1.57	2.48	62.8	42.4	0.63
2H-2, 61-63	11.91	1.54	2.77	70.7	48.6	0.71
2H-3, 65-67	13.45	1.59	2.72	67.1	44.8	0.67
2H-4, 61-63	14.91	1.58	2.61	65.6	44.2	0.66
2H-5, 61-63	16.41	1.64	2.61	61.5	39.7	0.61
2H-6, 76-78	18.06	1.61	2.73	66	43.5	0.66
2H-7, 30-32	19.1	1.69	2.77	62.5	39.3	0.63
3H-1, 79-81	20.09	1.31	2.01	71.4	57.8	0.71
3H-2, 79-81	21.59	1.62	2.62	63.1	41.4	0.63
3H-3, 79-81	23.09	1.57	2.66	67	45.2	0.67
3H-4, 78-80	24.58	1.55	2.63	68	46.7	0.68
3H-5, 78-80	26.08	1.59	2.58	64.6	43.3	0.65
3H-6, 78-80	27.58	1.65	2.63	61.7	39.7	0.62
3H-7, 38-40	28.68	1.61	2.64	64	42.2	0.64
4H-1, 79-81	29.59	1.61	2.75	66.3	43.6	0.66
4H-2, 79-81	31.09	1.57	2.62	66.1	44.6	0.66
4H-3, 79-81	32.59	1.6	2.69	65.8	43.6	0.66
4H-4, 79-81	34.09	1.62	2.7	64.7	42.3	0.65
4H-5, 79-81	35.59	1.6	2.57	63.3	42.1	0.63
4H-6, 79-81	37.09	1.64	2.67	63	40.7	0.63
4H-7, 39-41	38.19	1.59	2.59	64.2	42.9	0.64
5H-1, 74-76	39.04	1.62	2.6	63.1	41.5	0.63
5H-2, 74-76	40.54	1.6	2.59	63.8	42.4	0.64
5H-3, 74-76	42.04	1.6	2.56	63	41.7	0.63
5H-4, 74-76	43.54	1.61	2.66	64.7	42.7	0.65
5H-5, 74-76	45.04	1.62	2.69	65.1	42.8	0.65
5H-6, 74-76	46.54	1.6	2.75	67.1	44.5	0.67
5H-7, 36-38	47.66	1.65	2.39	54.5	35	0.54
6H-1, 73-75	48.53	1.6	2.63	64.7	43	0.65
6H-2, 63-65	49.93	1.62	2.68	64.6	42.4	0.65
6H-3, 97-99	51.77	1.61	2.41	58.2	38.4	0.58
6H-4, 68-70	52.98	1.63	2.58	61.8	40.3	0.62
6H-5, 43-45	54.23	1.48	2.61	71.5	51.2	0.72
6H-5, 53-56	55.83	1.74	2.69	57.4	35	0.57
6H-7, 37-39	57.17	1.59	2.55	63.5	42.4	0.63
7H-1, 30-32	57.6	1.69	2.75	61.9	38.9	0.62
7H-2, 30-32	59.1	1.67	2.73	62.8	39.9	0.63
7H-3, 33-35	60.63	1.63	2.63	62.7	40.8	0.63
7H-4, 26-28	62.06	1.65	2.72	63.7	41	0.64
7H-5, 79-81	64.09	1.68	2.74	62.4	39.5	0.62
7H-6, 73-75	65.53	1.67	2.65	60.6	38.5	0.61
7H-7, 26-28	66.56	1.67	2.6	59.7	38	0.6
8H-1, 74-76	67.54	1.58	2.54	64.1	43.2	0.64
8H-2, 74-76	69.04	1.63	2.66	63.7	41.6	0.64
8H-3, 74-76	70.54	1.59	2.57	64.1	42.9	0.64
8H-4, 74-76	72.04	1.63	2.65	63.1	41.1	0.63
8H-5, 74-76	73.54	1.63	2.66	63.4	41.2	0.63
8H-6, 74-76	75.04	1.55	2.62	67.8	46.5	0.68
8H-7, 35-37	76.15	1.71	2.58	56.3	35	0.56
9H-1, 72-74	77.02	1.64	2.59	61.5	40	0.62
9H-2, 72-74	78.52	1.62	2.65	63.5	41.5	0.63
9H-3, 78-80	80.08	1.61	2.67	65.1	43.1	0.65
9H-4, 72-74	81.52	1.6	2.59	64.2	42.7	0.64
9H-5, 78-80	83.08	1.66	2.66	61.9	39.7	0.62
9H-6, 78-80	84.58	1.67	2.73	62.5	39.7	0.63
9H-7, 31-33	85.61	1.58	2.62	65.9	44.4	0.66
10X-1, 130-132	87.1	1.63	2.76	65.7	42.8	0.66
10X-2, 36-38	87.66	1.54	2.67	69.5	48.1	0.69
11X-1, 74-76	96.44	1.6	2.62	64.3	42.5	0.64
11X-2, 54-56	97.74	1.6	2.74	67	44.5	0.67
11X-3, 69-71	99.39	1.57	2.63	66.3	44.8	0.66
12X-1, 74-76	106.04	1.59	2.75	67.9	45.5	0.68
12X-2, 74-76	107.54	1.61	2.65	64.7	42.7	0.65
12X-3, 67-69	108.97	1.64	2.64	62.4	40.5	0.62
12X-4, 13-15	109.93	1.63	2.69	63.8	41.5	0.64
13X-1, 62-64	115.62	1.59	2.71	67	44.8	0.67
13X-2, 80-82	117.3	1.6	2.59	63.8	42.4	0.64
13X-3, 72-74	118.72	1.61	2.66	64.9	42.9	0.65
13X-4, 22-24	119.72	1.64	2.64	62.6	40.6	0.63
14X-1, 74-76	125.34	1.61	2.62	63.7	41.9	0.64
14X-2, 74-76	126.84	1.58	2.74	68.4	46.1	0.68
14X-4, 74-76	129.84	1.57	2.68	67.6	45.7	0.68
14X-5, 13-8	130.58	1.59	2.76	68	45.5	0.68
15X-1, 73-79	135.03	1.61	2.76	66.8	44	0.67
15X-1, 80-82	135.1	1.66	2.57	59.7	38.3	0.6
15X-3, 80-82	138.1	1.61	2.69	65.4	43.2	0.65
15X-4, 13-8	138.88	1.63	2.64	62.8	40.8	0.63
16X-1, 68-70	144.58	1.67	2.65	60.3	38.4	0.6
16X-2, 55-57	145.95	1.69	2.5	55.1	34.5	0.55

Table 10 (continued).

Core, section, interval (cm)	Depth (mbsf)	Bulk density (g/cm ³)	Grain density (g/cm ³)	Porosity (%)	Water content (%)	Void ratio
16X-3, 68-70	147.58	1.66	2.71	62.9	40.3	0.63
17X-1, 67-69	154.27	1.7	2.68	59.5	37.1	0.6
17X-2, 75-77	155.85	1.63	2.65	63.2	41.2	0.63
17X-3, 75-77	157.35	1.59	2.69	66.4	44.3	0.66
17X-4, 75-77	158.85	1.68	2.75	62.7	39.7	0.63
17X-5, 39-41	159.99	1.65	2.57	60.1	38.7	0.6
17X-6, 13-9	161.19	1.65	2.69	62.8	40.4	0.63
18X-1, 72-74	163.92	1.64	2.46	57.5	37.3	0.58
18X-2, 47-49	165.17	1.66	2.62	66.3	42.5	0.66
18X-CC, 14-12	165.8	1.72	2.71	59.1	36.5	0.59
19X-1, 46-48	173.36	1.68	2.8	63.4	40	0.63
19X-2, 46-48	174.86	1.65	2.78	64.5	41.4	0.65
19X-3, 32-34	176.22	1.66	2.64	61.3	39.3	0.61
19X-4, 32-34	177.72	1.57	2.39	60.6	41	0.61
19X-CC, 20-22	178.15	1.66	2.87	66.1	42.3	0.66
20X-1, 48-50	182.98	1.6	2.56	63.2	42	0.63
20X-1, 20-22	192.3	1.65	2.65	61.8	39.7	0.62
21X-2, 20-22	193.8	1.66	2.7	62.7	40.2	0.63
21X-3, 34-36	195.44	1.63	2.78	65.9	42.9	0.66
21X-4, 64-66	197.24	1.71	2.77	61.2	38	0.61
21X-5, 61-63	198.71	1.76	2.76	63.6	38.5	0.64
22X-1, 72-74	202.52	1.7	2.59	57.3	35.7	0.57
22X-CC, 39-41	203.35	1.71	2.85	62.8	38.9	0.63
23X-1, 99-101	212.49	1.64	2.71	64	41.4	0.64
23X-2, 52-54	213.52	1.52	2.46	66.2	46.3	0.66
23X-3, 46-48	214.96	1.63	2.66	63.3	41.2	0.63
23X-4, 15-17	216.15	1.6	2.65	64.9	43	0.65
23X-5, 68-70	218.18	1.62	2.47	59.3	38.8	0.59
23X-6, 87-89	219.87	1.67	2.63	60	38	0.6
23X-7, 13-15	220.63	1.97	2.2	91.7	49.5	0.92
24X-1, 72-74	221.72	1.64	2.69	63.3	40.9	0.63
24X-2, 25-27	222.75	1.63	2.6	61.9	40.3	0.62
25X-1, 73-75	231.43	1.59	2.45	68.9	45.9	0.69
25X-2, 56-58	232.76	1.62	2.7	64.7	42.3	0.65
25X-3, 64-66	234.34	1.63	2.62	62.5	40.7	0.62
25X-4, 57-59	235.77	1.62	2.65	64.2	42.2	0.64
25X-5, 47-49	237.17	1.6	2.67	65.6	43.5	0.66
25X-6, 74-76	238.94	1.61	2.66	64.6	42.5	0.65
26X-1, 67-71	240.97	2.06	6.44	81.3	41.9	0.81
26X-2, 50-52	242.3	1.66	2.59	59.8	38.2	0.6
26X-2, 51-53	242.31	1.7	2.71	60.3	37.6	0.6
26X-4, 96-98	245.76	1.71	2.64	58.2	36.2	0.58
26X-5, 60-62	246.9	1.68	2.58	58.3	36.8	0.58
26X-6, 60-62	248.4	1.66	2.74	63.3	40.4	0.63
26X-7, 37-39	249.67	1.64	2.61	61.5	39.8	0.62
27X-1, 84-86	250.84	1.68	2.75	62.5	39.5	0.63
27X-2, 73-75	252.23	1.64	2.57	60.8	39.4	0.61
27X-3, 27-29	253.27	1.65	2.56	59	37.7	0.59
27X-CC, 13-15	253.81	1.6	2.72	66.5	44.1	0.66
28X-1, 78-80	260.38	1.73	2.75	59.4	36.4	0.59
28X-2, 62-64	261.72	1.6	2.58	63.5	42.1	0.64
28X-3, 65-67	263.25	1.58	2.74	67.9	45.7	0.68
28X-4, 65-67	264.75	1.57	2.61	66.2	44.8	0.66
28X-5, 73-75	266.33	1.62	2.79	66.9	43.9	0.67
28X-6, 56-58	267.66	1.67	2.85	65	41.3	0.65
28X-1, 56-58	269.76	1.65	2.64	62.1	40.1	0.62
29X-2, 47-49	271.17	1.63	2.7	64.5	42.1	0.65
29X-3, 58-60	272.78	1.65	2.74	63.8	40.9	0.64
29X-4, 59-60	274.29	1.66	2.72	62.8	40.2	0.63
29X-5, 50-52	275.7	2.1	3.26	52.3	26.5	0.52
29X-6, 63-65	277.33	1.66	2.69	62.6	40.2	0.63
29X-7, 28-30	278.48	1.65	2.71	63.3	40.8	0.63
30X-1, 74-76	279.54	1.81	2.78	56.1	33	0.56
30X-2, 34-36	280.64	1.78	2.75	56.4	33.6	0.56
30X-CC, 22-24	281.67	1.75	2.77	59	35.9	0.59
31X-1, 37-39	288.87	1.8	2.85	58.3	34.5	0.58
31X-2, 54-56	289.52	1.82	2.71	53	30.8	0.53
31X-2, 68-70	289.66	1.8	2.91	59.3	35	0.59
32X-1, 69-70	294.69	1.75	2.6	54.5	33.1	0.55
32X-2, 65-67	296.15	1.91	2.87	52.5	29.2	0.5

Table 10 (continued).

Core, section, interval (cm)	Depth (mbsf)	Bulk density (g/cm ³)	Grain density (g/cm ³)	Porosity (%)	Water content (%)	Void ratio
35X-4, 133-135	328.33	1.83	2.79	55.1	32.1	0.55
35X-5, 138-140	329.88	1.59	2.92	70.6	47.1	0.71
35X-6, 60-62	330.6	1.88	2.73	50.3	28.5	0.5
35X-7, 13-8	331.58	1.84	2.73	52.8	30.5	0.53
35X-CC, 13-3	332	1.92	2.8	50	27.7	0.5
36X-1, 66-68	332.76	1.84	2.8	54.2	31.2	0.54
36X-2, 76-78	334.36	1.83	2.93	58.2	33.7	0.58
36X-3, 62-64	335.72	1.83	2.73	53.3	31	0.53
36X-4, 50-52	337.1	1.76	2.68	56.3	34.1	0.56
36X-5, 13-9	338.19	1.91	2.91	52.3	29	0.52
36X-CC, 28-30	339.74	1.82	2.62	50.7	29.6	0.51
37X-1, 113-115	342.73	1.88	2.83	52.7	29.7	0.53
37X-2, 75-77	343.85	1.86	2.68	50	28.6	0.5
37X-3, 36-37	344.96	1.89	2.91	54.7	30.8	0.55
37X-4, 88-90	346.98	1.88	2.75	51.1	28.9	0.51
37X-5, 89-91	348.49	1.68	2.46	54.8	34.7	0.55
37X-6, 119-121	350.29	1.83	2.78	54.6	31.7	0.55
37X-7, 46-48	351.06	1.68	2.35	51.1	32.3	0.51
37X-CC, 29-31	351.35	1.53	2.19	56.8	39.4	0.57
39X-1, 136-138	362.26	1.84	2.79	54.2	31.3	0.54
39X-2, 29-31	362.69	1.92	3.15	58.1	32.1	0.58
40X-1, 142-144	371.92	1.8	2.94	62.8	37	0.63
40X-2, 81-83	372.81	1.7	2.51	55.1	34.5	0.55
40X-3, 62-64	374.12	1.69	2.77	62.5	39.3	0.62
40X-4, 82-84	375.82	1.72	2.66	57.8	35.7	0.58
41X-1, 94-96	381.14	1.81	2.69	53.3	31.3	0.53
41X-2, 37-39	382.07	1.87	2.81	53	30.1	0.53
41X-3, 44-46	383.64	1.76	2.78	58.7	35.5	0.59
41X-4, 96-98	385.66	1.97	3.25	57.7	31	0.58
41X-6, 41-43	388.11	1.83	2.88	57.2	33.2	0.57
41X-7, 13-10	389.3	1.83	2.57	48	27.8	0.48
42X-1, 88-90	390.68	1.89	2.76	50.4	28.3	0.5
42X-CC, 13-6	392.77	1.92	2.66	45.7	25.3	0.46

the Pliocene and Pleistocene sections and the greatest vitric ash influx in those of the upper Eocene and Oligocene.

REFERENCES

- Backman, J., Duncan, R. A., et al., 1988. *Proc. ODP, Init. Repts.*, 115: College Station, TX (Ocean Drilling Program).
- Beccalua, L., Macciotta, G., Savelli, C., et al., 1980. Geochemistry and K/Ar ages of volcanics dredged in the Philippine Sea. In Hayes, D. E. (Ed.), *The Tectonic and Geologic Evolution of Southeast Asian Sea and Islands*: Washington (Am. Geophys. Union), 247-270.
- Berggren, W. A., Kent, D. V., Flynn, J. J., and Van Couvering, J., 1985. Cenozoic geochronology. *Geol. Soc. Am. Bull.*, 96:1407-1418.
- Bleil, U., 1982. Paleomagnetism of Deep Sea Drilling Project Leg 60 sediments and igneous rocks from the Mariana Region. *Init. Repts. DSDP*, 60: Washington (U.S. Govt. Printing Office), 855-873.
- Bloomer, S. H., 1983. Distribution and origin of igneous rocks from the landward slopes of the Mariana Trench. *J. Geophys. Res.*, 88:7411-7428.
- Bloomer, S. H., and Fisher, R. L., 1987. Petrology and geochemistry of igneous rocks from the Tonga Trench—a non-accreting plate boundary. *J. Geol.*, 95:469-495.
- Bloomer, S. H., Hawkins, J. W., 1983. Gabbroic and ultramafic rocks from the Mariana Trench: An island arc ophiolite. In Hayes, D.E. (Ed.), *The Tectonic and Geologic Evolution of Southeast Asian Seas and Islands, Part II*. Geophys. Monogr. Ser., 27: Washington (Am. Geophys. Union), 294-317.
- Ewart, A., Brothers, R. N., and Manteen, A., 1977. An outline of the geology and geochemistry, and the possible petrogenetic evolution of the volcanic rocks of the Tonga-Kermadec-New Zealand island arc. *J. Volc. Geotherm. Res.*, 2:205-250.
- Fryer, P., Langmuir, C. H., Taylor, B., Zhang, Y., and Hussong, D. M., 1985. Rifting of the Izu arc, III, Relationships of chemistry to tectonics. *EOS, Trans. Am. Geophys. Union*, 66:421.
- Gill, J. B., Stock, A. L., and Whelan, P. M., 1984. Volcanism accompanying backarc basin development in the southwest Pacific. *Tectonophysics*, 102:207-224.
- Honza, E., and Tamaki, K., 1985. Bonin Arc. In Nairn, A.E.M., and Uyeda, S. (Eds.), *The Ocean Basins and Margins, Vol. 7, The Pacific Ocean*: New York (Plenum Press), 459-499.
- Hussong, D. M., and Uyeda, S., 1981. Tectonic processes and the history of the Mariana Arc: A synthesis of the results of Deep Sea Drilling Project Leg 60. In Hussong, D. M., Uyeda, S., et al., *Init. Repts. DSDP*, 60: Washington (U.S. Govt. Printing Office), 909-929.
- Johnson, L. E., and Fryer, P., 1988. Oceanic plate material on the Mariana Forearc. *EOS, Trans. Am. Geophys. Union*, 69:1471.
- Karig, D. E., 1975. Basin genesis in the Philippine Sea. In Ingle, J. C., Karig, D. E., et al., *Init. Repts. DSDP*, 31: Washington (U.S. Govt. Printing Office), 857-879.
- Karig, D. E., and Moore, G. F., 1975. Tectonic complexities in the Bonin arc system. *Tectonophysics*, 27:97-118.
- Karig, D. E., and Ranken, D., 1983. Marine geology of the forearc region, southern Mariana island arc. In Hayes, D. E. (Ed.), *The Tectonic and Geologic Evolution of Southeast Asian Seas and Islands, II*: Washington (Am. Geophys. Union), 266-280.
- Keating, B., Kodama, K., Uyeda, S., and Hellsley, C. E., 1983. Paleomagnetic results of the Bonin and Mariana Islands. *Advances Earth Planet. Sci. Ser.*, 245-260.
- Ogawa, Y., and Naka, J., 1984. Emplacement of ophiolitic rocks in forearc areas: examples from central Japan and Izu-Mariana-Yap island arc system. *Geol. Soc. London, Spec. Publ.*, 13:292-304.
- Pearce, J. A., Lippard, S. J., and Roberts, S., 1984. Characteristics and tectonic significance of supra-subduction zone ophiolites. *Geol. Soc. London, Spec. Pub.*, 16:77-94.
- Peccerillo, A., and Taylor, S. R., 1976. Geochemistry of Eocene calc-alkaline rocks from the Kastamonu area, northern Turkey. *Contr. Mineral. Petrol.*, 58:63-81.
- Prell, W. L., Niatsuma, U., et al., 1989. Site 723. In Prell, W. L., Niatsuma, et al., *Proc. ODP, Init. Repts.*, 117: College Station, TX (Ocean Drilling Program), 319-384.
- Reagan, M. K., and Meijer, A., 1984. Geology and geochemistry of early arc-volcanic rocks from Guam. *Bull. Geol. Soc. Am.*, 95:701-713.
- Scott, R. B., and Kroenke, L. W., 1981. Periodicity of remnant arcs and back-arc basins of the South Philippine Sea. *Oceanologica Acta*, 4:193-202.
- Shiraki, K., Kuroda, N., Urano, H., and Maruyama, S., 1980. Clinostite in boninite from the Bonin Islands, Japan. *Nature*, 285:31-32.
- Stern, R. J., Smoot, N. C., and Rubin, M., 1984. Unzipping of the volcano arc, Japan. *Tectonophysics*, 102:153-174.
- Wood D. A., Marsh, N. J., Tarney, J., Joron, J.-L., Fryer, P., and Treul, M., 1981. Geochemistry of igneous rocks recovered from a transect across the Mariana Trough, arc, fore-arc, and trench, Sites 453 through 461, Deep Sea Drilling Project Leg 60. In Hussong, D. M., Uyeda, S., et al., *Init. Repts. DSDP*, 60: Washington (U.S. Govt. Printing Office), 611-646.

Ms 125A-110

NOTE: All core description forms ("barrel sheets") and core photographs have been printed on coated paper and bound as Section 4, near the back of the book, beginning on page 383.

Table 11. Physical properties for Hole 782A.

Core, section, interval (cm)	Depth (mbsf)	Thermal conductivity (W/mK)	Resistivity (ohms)	Formation factor	"A" velocity (km/s)	"B" velocity (km/s)
125-782A-1H-1, 75-77	0.75	1.026				
1H-2, 76-78	2.26	1.058				
1H-3, 76-78	3.76	1.05				
1H-4, 76	78	5.26	1.101			
1H-5, 76-78	6.76	1.041				
1H-6, 76-78	8.26	1.043				
1H-7, 29-30	9.29	0.902				
1H-CC, 13-9	9.69	0.973				
2H-1, 76-78	10.56	1.093				
	13.2		19.6	2.29		
2H-3, 76-78	13.56	1.148				
2H-4, -76-78	15.06	1.126				
	16.1		22.4	2.61		
2H-5, 76-78	16.56	1.142				
2H-6, 38-40	17.68	1.414				
	18.3		22.2	2.59		
2H-7, 38-40	19.18	1.121				
	19.4		21.8	2.54		
2H-CC, 13-5	19.7	1.181				
3H-1, 76-78	20.06	1.078				
3H-176-78	20.06	1.07				
3H-2, 76-78	21.56	1.139				
3H-3, 76-78	23.06	1.039				
3H-4, 76-78	24.56	1.061				
3H-5, 76-78	26.06	1.157				
	27.39		23	2.68		
3H-6, 76-78	27.56	1.162				
3H-7, 39-40	28.69	1.125				
3H-CC, 14-12	29.24	1.096				
4H-1, 76-78	29.56	1.088	16.6	1.94		
4H-2, 76-78	31.06	1.124				
4H-3, 76-78	32.56	1.026				
	32.8		20.2	2.36		
4H-4, 55-57	33.85	1.009				
4H-5, 75-77	35.55	1.127	22	2.57		
4H-6, 75-77	37.05	1.223				
4H-7, 40-42	38.2	1.109				
4H-CC, 14-16	38.74	1.059				
5H-1, 78-80	39.08	1.088	20.1	2.35		
5H-2, 78-80	40.58	1.113				
5H-3, 78-80	42.08	1.092	19.7	2.3		
5H-4, 78-80	43.58	1.006				
5H-5, 77-79	45.07	1.099	20.6	2.4		
5H-6, 77-79	46.57	1.088				
	47.41		17.7	2.07		
5H-7, 37-39	47.67	1.106				
5H-CC, 13-11	48.19	1.034				
6H-1, 76-78	48.56	1.108				
	49.6		19.2	2.24		
6H-2, 76-78	50.06	1.41				
6H-3, 76-78	51.56					
	52.4		17.3	2.02		
6H-4, 76-78	53.06	1.068				
6H-5, 77-79	54.57	1.064				
	55.5		19.5	2.28		
6H-6, 77-79	56.07	1.016				
6H-7, 36-38	57.16	1.038				
	57.4		21.3	2.49		
6H-CC, 13-10	57.68	1.034				
7H-1, 75-77	58.05	1.038				
7H-2, 75-77	59.55	1.002				
	60.4		21.7	2.53		
7H-3, 75-77	61.05	1.264				
7H-4, 75-77	62.55	0.999				
	63.4		19.5	2.28		
7H-5, 46-48	63.76	1.096				
7H-6, 46-48	65.26	1.254				
	66.4		22.4	2.61		
7H-7, 46-48	66.76	1.064				
	67.06		21.2	2.47		
8H-1, 65-67	67.45	1.193				
8H-2, 73-75	69.03	1.057				
	70.06		18.4	2.15		
8H-3, 73-75	70.53	0.82				
8H-4, 73-75	72.03	1.108				
8H-5, 73-75	73.53	1.052	23.5	2.74		

Table 11 (continued).

Core, section, interval (cm)	Depth (mbsf)	Thermal conductivity (W/mK)	Resistivity (ohms)	Formation factor	"A" velocity (km/s)	"B" velocity (km/s)
8H-6, 73-75	75.03	1.054				
8H-7, 44-46	76.24	0.953				
	76.49		17.7	2.07		
9H-1, 74-76	77.04	1.031				
	77.26		21.3	2.49		
9H-2, 74-76	78.54	1				
9H-3, 74-76	80.04	1.007				
9H-4, 74-76	81.54					
9H-5, 74-76	83.04	1.116				
9H-6, 74-76	84.54	1.104				
9H-7, 34-36	85.64	1.008				
10X-1, 13-7	85.87	1.073				
9H-CC, 13-10	86.08	0.952				
10X-2, 37-39	87.67	0.978				
10X-CC, 13-7	88.12	0.814				
11X-1, 74-76	96.44	1				
	96.76		19.2	2.24		
11X-2, 51-53	97.71	0.931				
11X-3, 38-40	99.08	1.036				
	99.26		19.7	2.3		
11X-CC, 13-6	99.65	0.955				
12X-1, 74-76	106.04	0.991				
	106.38		23.5	2.74		
12X-2, 74-76	107.54	1.02				
	108.6		18.8	2.19		
12X-3, 74-76	109.04	1.146				
12X-4, 13-10	109.9	1.016				
13X-1, 74-76	115.74	1.103				
	116.18		19.3	2.25		
13X-2, 49-51	116.99	1.042				
13X-3, 74-76	118.74	1.157				
	119		18.3	2.14		
13X-4, 19-21	119.69	1.147				
14X-1, 74-76	125.34	1.112	17.4	2.03		
14X-2, 74-76	126.84	0.992				
	128		22	2.57		
14X-3, 74-76	128.34	1.072				
14X-4, 74-76	129.84	1.052				
15X-1, 74-76	135.04	0.993	19.9	2.32		
15X-2, 74-76	136.54	1.105				
	137.8		20.6	2.4		
15X-4, 13-9	138.89	1.031				
16X-1, 74-76	144.64					
16X-2, 47-49	145.87	1.183				
	146		21.5	2.51		
16X-3, 47-49	147.37	1.102	23.5	2.74		
17X-1, 74-76	154.34	1.123				
	154.8		22.4	2.61		
17X-2, 74-76	155.84	1.103				
17X-3, 74-76	157.34	1.065	20.1	2.35		
17X-4, 74-76	158.84	1.146				
	159.96		29.5	3.44		
17X-5, 74-76	160.34	1.109				
17X-6, 13-7	161.17	1.21				
	163.4		23.2	2.71		
18X-1, 73-75	163.93	1.138				
18X-2, 44-46	165.14	1.135				
18X-CC, 14-16	165.82	1.286				
	173.13		21.9	2.56		
19X-1, 73-75	173.63	1.087				
19X-2, 48-50	174.88	1.106				
	176.13		28.1	3.28		
19X-3, 74-76	176.64	1.071				
19X-4, 28-30	177.68	1.024				
19X-CC, 13-15	178.08	1.095				
20X-1, 30-32	182.8	0.914				
20X-CC, 13-15	183.29	0.926				
	192.25		24.4	2.85		
21X-2, 74-76	194.34	1.147				
	195.2		21.6	2.52		
21X-4, 74-76	197.34	1.293				
	198.2		24.6	2.87		
22X-1, 80-82	202.6	1.228	26.1	3.05		
	211.68		30.8	3.59		
23X-1, 80-82	212.3	1.04				
	214.8		22.5	2.63		

Table 11 (continued).

Core, section, interval (cm)	Depth (mbsf)	Thermal conductivity (W/mK)	Resistivity (ohms)	Formation factor	"A" velocity (km/s)	"B" velocity (km/s)
23X-3, 80-82	215.3	1.064				
	217.6		41.7	4.87		
23X-5, 80-82	218.3	1.014				
	220.6		31.7	3.7		
24X-1, 78-80	221.78	0.814				
	230.8		17.6	2.05		
25X-2, 77-79	232.97	1.228				
	233.86		26	3.03		
25X-4, 77-79	235.97	1.159				
	237.1		31.5	3.68		
25X-6, 77-79	238.97	1.358				
26X-1, 78-80	241.08	0.943				
26X-2, 51-53	242.31				1.67	1.69
	243.9		28.5	3.33		
26X-3, 78-80	244.08	0.995				
26X-5, 78-80	247.08	0.89	27	3.15		
26X-7, 32-34	249.62	1.181				
27X-1, 36-38	250.36	1.106	28.1	3.28		
	251.32		21.3	2.49		
	252.06		23.3	2.72		
27X-3, 44-46	253.44	1.101				
28X-1, 44-46	260.04	1.003	21.9	2.56		
28X-3, 48-50	263.08	1.055				
	263.5		23	2.68		
28X-5, 48-50	266.08	1.05				
	266.62		23	2.68		
29X-1, 48-50	269.68	1.039				
	270.26		27.5	3.21		
29X-3, 48-50	272.68	1.073	36.1	4.21		
29X-4, 118-120	274.88				1.75	1.73
29X-5, 47-49	275.57	1.118	21.3	2.49		
29X-7, 28-30	278.48	1.031	30.5	3.56		
30X-1, 75-77	279.55				1.75	1.73
30X-2, 46-48	280.76	0.56				
31X-1, 37-39	288.87				1.74	1.72
31X-1, 43-45	288.93					
31X-2, 47-49	289.45	0.992				
31X-2, 68-70	289.66				1.72	1.73
31X-3, 54-56	291.02			1.77	1.76	
31X-4, 47-49	292.45					
32X-1, 60-62	294.5	0.809			1.81	1.85
32X-2, 65-67	296.15				1.8	1.84
32X-3, 65-67	297.65				1.69	1.69
32X-4, 42-44	298.92				1.75	1.8
32X-5, 60-62	300.6	1.148			1.74	1.73
32X-6, 58-60	302.08				1.72	1.75
33X-1, 32-34	303.82	1.079			1.76	1.75
33X-2, 16-18	305.16				1.67	1.74
33X-3, 32-34	306.82	1.143				
33X-4, 29-31	308.29				1.67	1.7
33X-5, 32-34	309.82	1.037				
33X-6, 37-40	311.37				1.68	1.72
33X-7, 32-34	312.82	1.127				
33X-CC, 25-28	313.21				1.7	1.7
34X-1, 74-76	313.84	1.017				
34X-CC, 25-27	314.84	0.999				
35X-1, 3-5	322.53				1.62	1.63
35X-1, 40-42	322.9				1.68	
35X-1, 74-76	323.2					
35X-2, 37-39	324.37				1.75	1.73
35X-2, 74-76	324.74	1.072				
35X-3, 48-50	325.98	1.129			1.78	1.78
35X-4, 73-75	327.73	1.2				
35X-4, 133-135	328.33				1.8	1.77
35X-5, 73-75	329.23	1.185				
35X-5, 138-140	329.88				1.74	2.49
35X-6, 73-75	330.73	1.427			2.49	
35X-7, 22-24	331.72	1.435				
36X-1, 72-74	332.82	1.206			1.94	1.86
36X-2, 72-74	334.32	1.236			1.95	
36X-3, 72-74	335.82	1.29			1.88	1.86
36X-4, 50-52	337.1				1.9	1.97
36X-4, 74-76	337.34	1.282				
36X-5, 9-11	338.19				1.97	1.92
36X-5, 58-60	338.68	1.292				
36X-CC, 13-11	339.57	1.27				

Table 11 (continued).

Core, section, interval (cm)	Depth (mbsf)	Thermal conductivity (W/mK)	Resistivity (ohms)	Formation factor	"A" velocity (km/s)	"B" velocity (km/s)
37X-1, 74-76	342.34					
37X-1, 113-115	342.73				1.92	1.91
37X-2, 74-76	343.84	0.913			1.91	1.82
37X-3, 36-38	344.96				2.05	2.09
37X-3, 74-76	345.34	1.304				
37X-4, 74-76	346.84	1.258				
37X-4, 88-90	346.98				1.79	1.75
37X-5, 74-76	348.34	1.118				
37X-6, 74-76	349.84	1.031				
37X-6, 119-121	350.29				2.09	2.19
37X-7, 21-23	350.81	1.124				
39X-1, 70-72	361.6	1.059				
39X-1, 136-138	362.26				2.1	2.01
39X-2, 37-39	362.77	1.087				
39X-CC, 18-20	363.4	1.192				
40X-1, 74-76	371.24	1.187				
40X-2, 74-76	372.74					
40X-3, 54-56	374.04	1.157				
40X-4, 74-76	375.74	1.263				
40X-CC, 14-12	376.62	1.118				
41X-1, 74-76	380.94	1.052				
41X-1, 94-96	381.14				2.23	
41X-2, 74-76	382.44	1.117				
41X-3, 44-46	383.64				2.37	2.29
41X-4, 74-76	385.44					
41X-5, 74-76	386.94	1.05				
41X-6, 41-43	388.11				2	
41X-6, 74-76	388.44	1.243				
41X-7, 15-17	389.35				2.06	2.02
42X-1, 60-62	390.4	1.34				
42X-1, 88-90	390.68				2.07	2.04
42X-2, 61-63	391.91	0.69				
42X-CC, 6-8	392.77				1.84	1.87

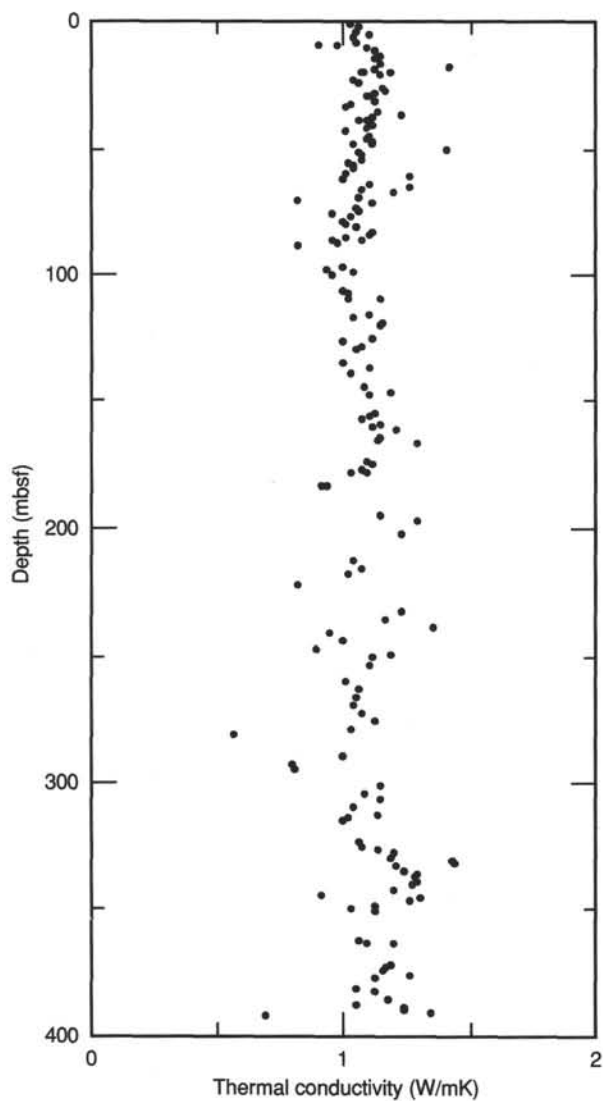


Figure 18. Plot of thermal conductivity vs. depth. Although the data are scattered, conductivities increase with depth.

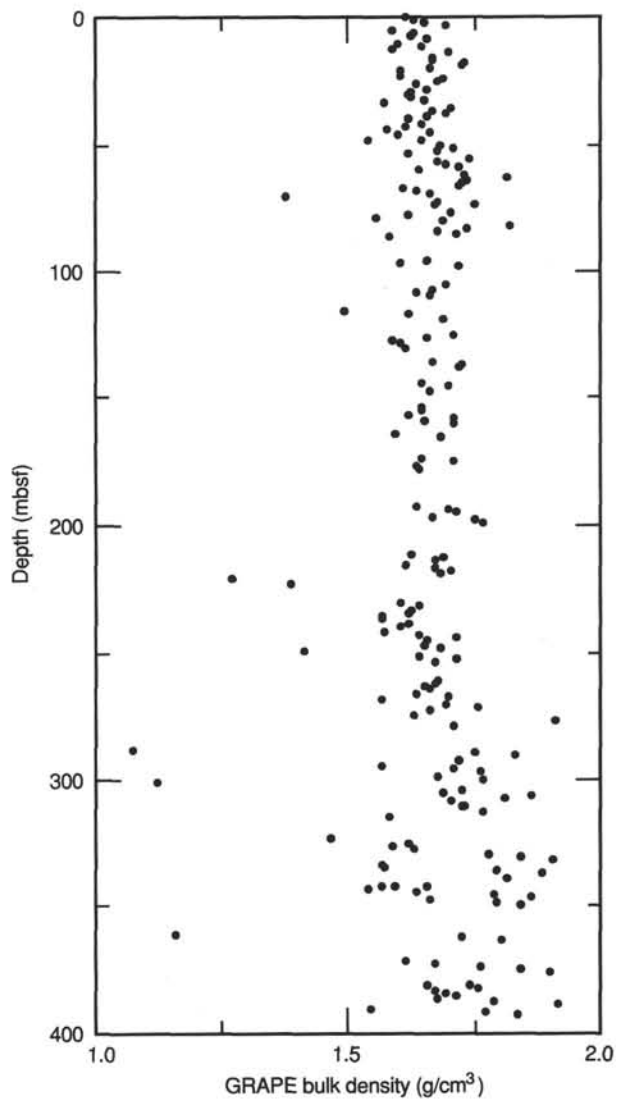


Figure 19. Plot of filtered GRAPE bulk densities vs. depth. The original GRAPE files were edited to reduce the number of data points. Density increases with depth. Increasing scatter in the data with depth probably resulted from drilling disturbance.

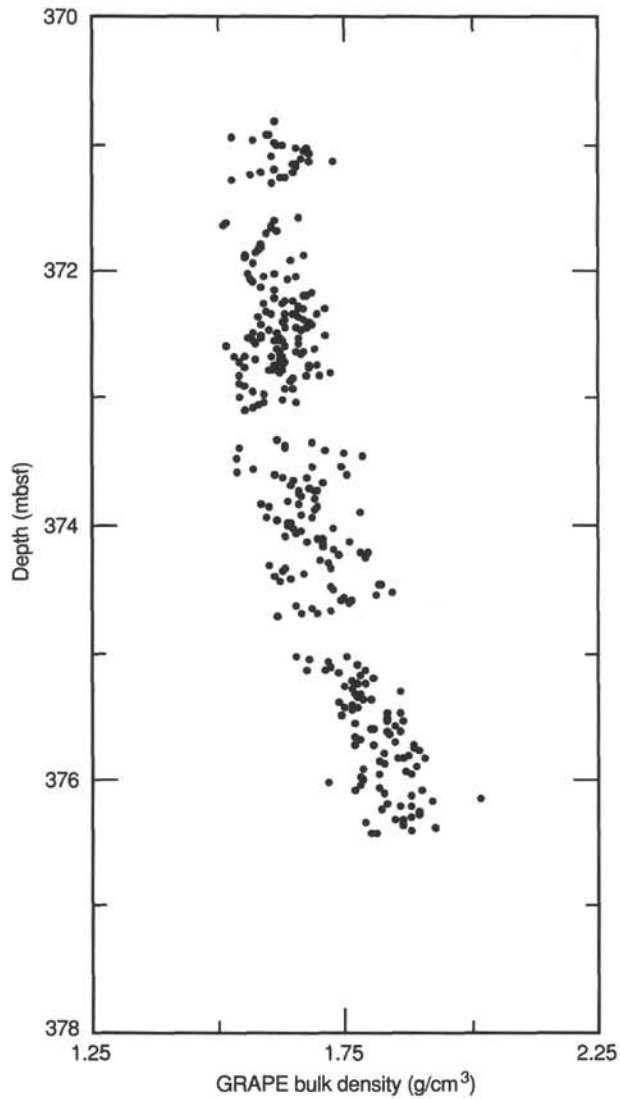


Figure 20. GRAPE bulk density plots for Cores 125-782A-3H, 125-782A-25X, and 125-782-39X through 125-782-40X from Hole 782A. Plots for Cores 125-782A-3H and 125-782A-25X are similar. A significant change in density is apparent at 373 mbsf in these cores.

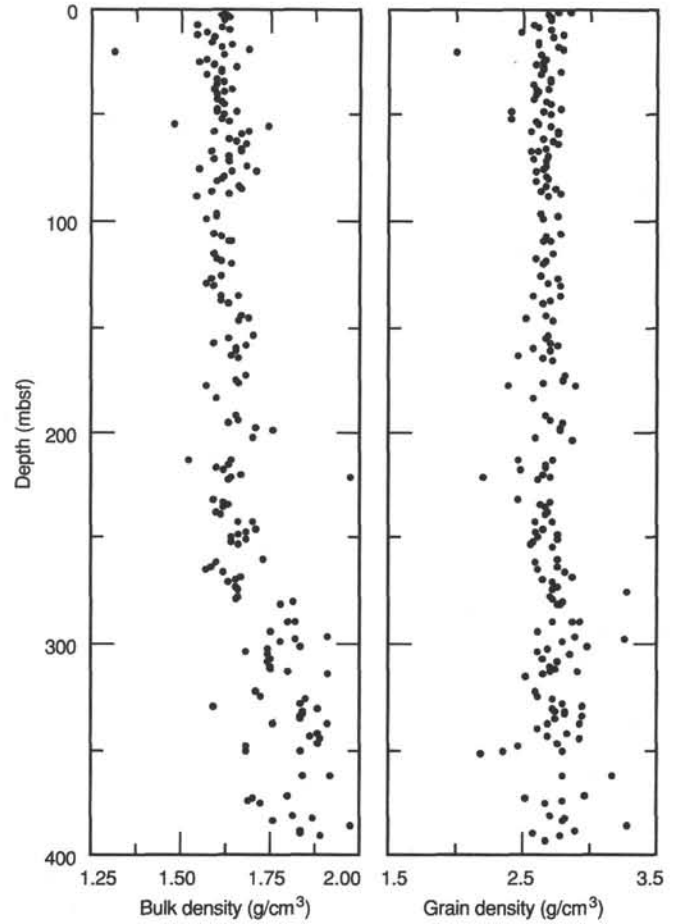


Figure 21. Variation of index properties with depth. Note the similarity of the index bulk-density plot to that from the GRAPE (Fig. 19). Bulk densities show a discontinuity at 280 mbsf, where sediment induration increases.

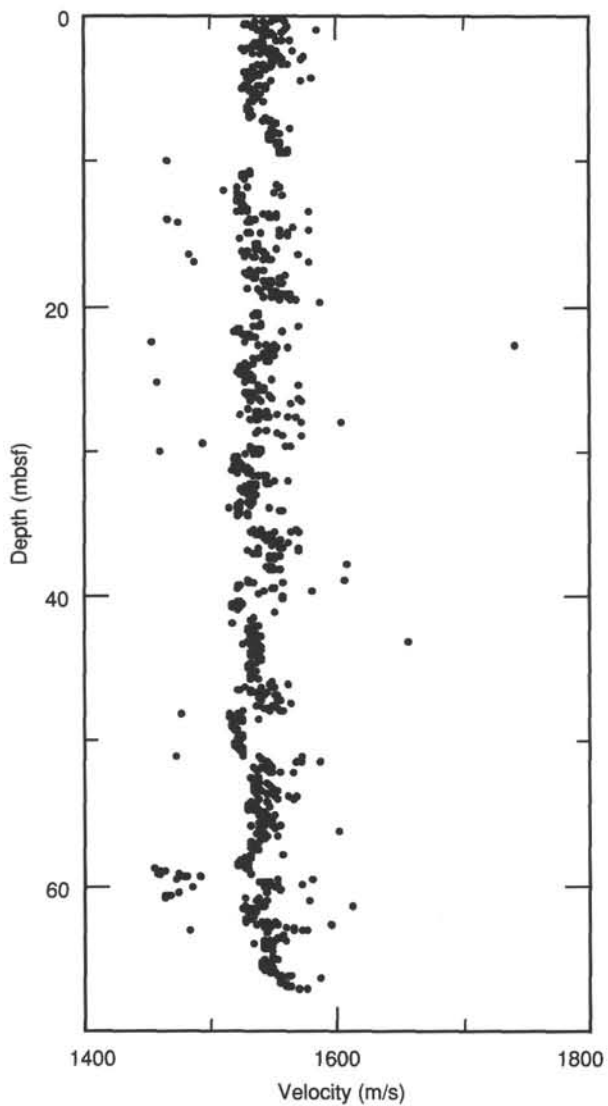


Figure 22. Plot of depth vs. compressional-wave velocities obtained from the *P*-wave logger on the MST for APC cores (125-782A-1H through 125-782A-8H). Velocity is nearly constant over this depth range.

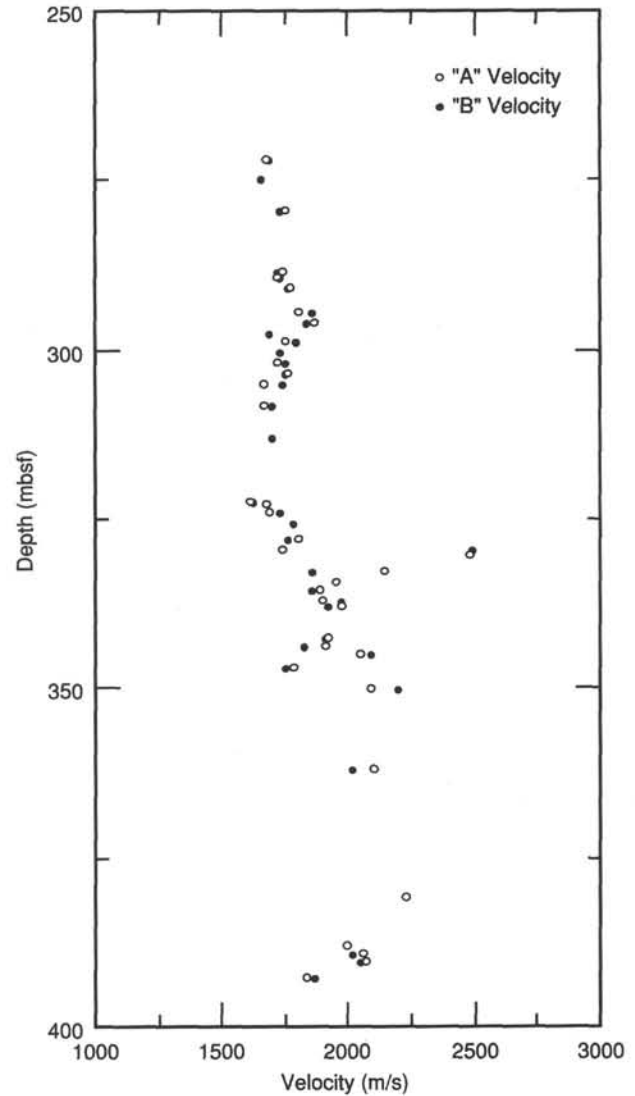


Figure 23. Plot of depth vs. velocities from the Hamilton frame for well-consolidated sediment (depths greater than 278 mbsf). The "A" direction denotes propagation along the core axis, and the "B" direction indicates propagation normal to the core axis. Velocities for "A" and "B" directions are nearly equal, indicating that these sedimentary rocks are isotropic. Velocity increases from 1700 to 2000 m/s over this depth interval.

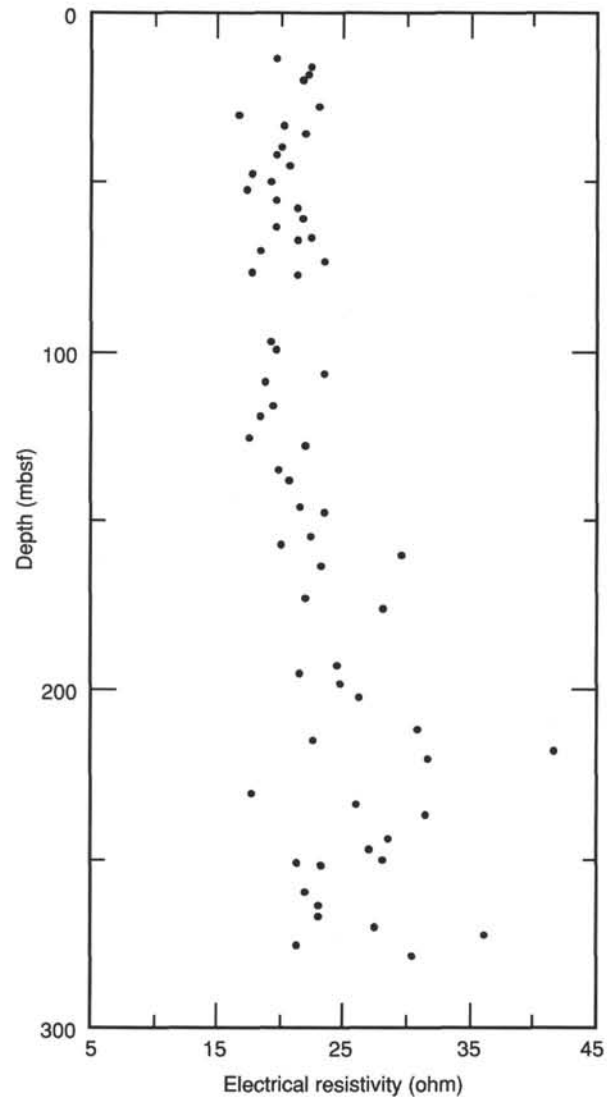


Figure 24. Plot of electrical resistivity vs. depth. Although scattered, these data show higher resistivity with increasing depth.

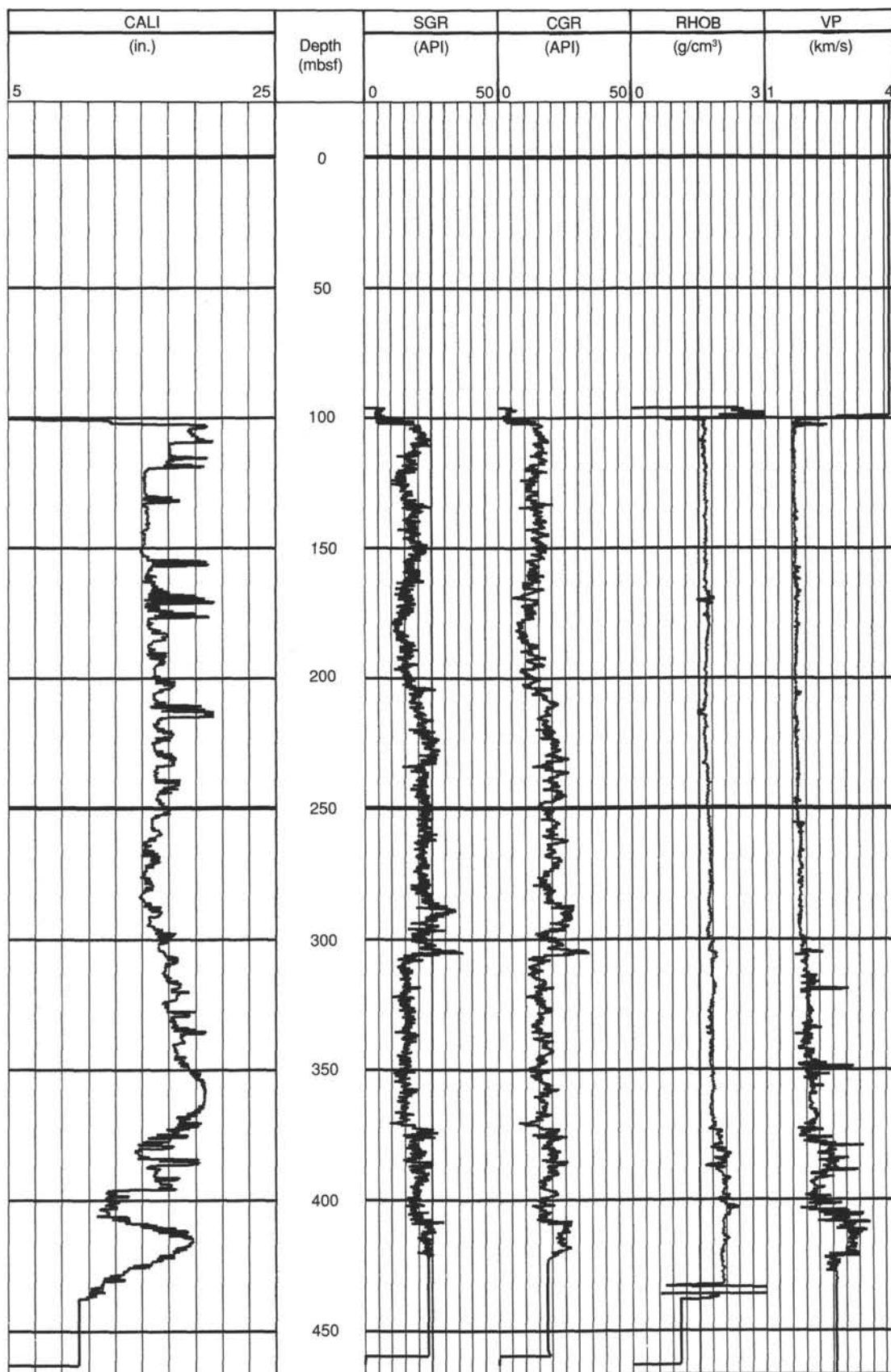


Figure 25. Plot of logs for Hole 782B as a function of depth. Logs shown are caliper (CALI), the gamma ray (SGR and CGR), density (RHOB), and velocity (VP).

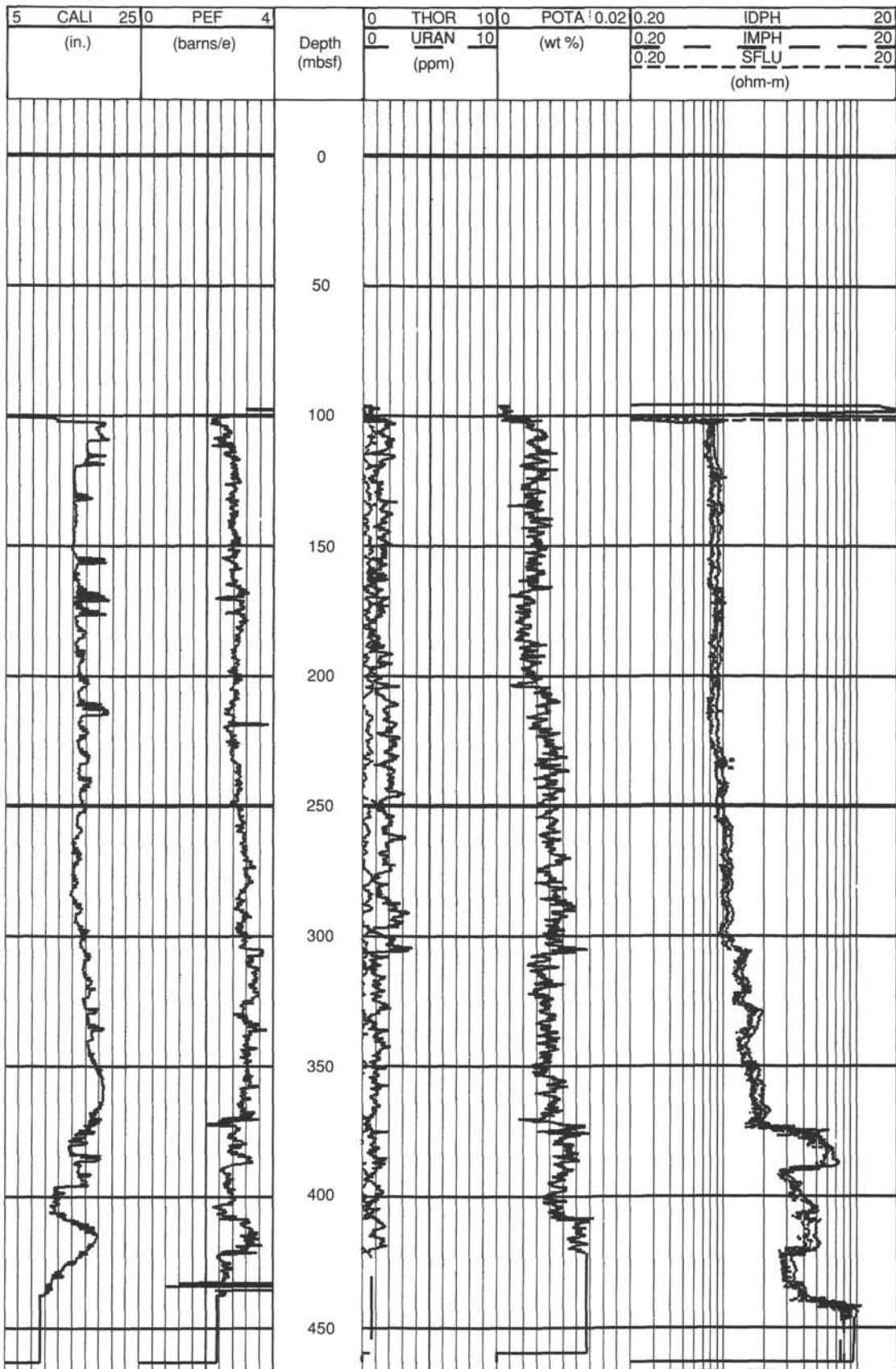


Figure 26. Plot of logs for Hole 782B as a function of depth. Logs shown are caliper (CALI), photoelectric effect (PEF), thorium (THOR), uranium (URAN), potassium (POTA), and resistivity (deep induction: IDPH; medium induction: IMPH; spherically focused: SFLU).

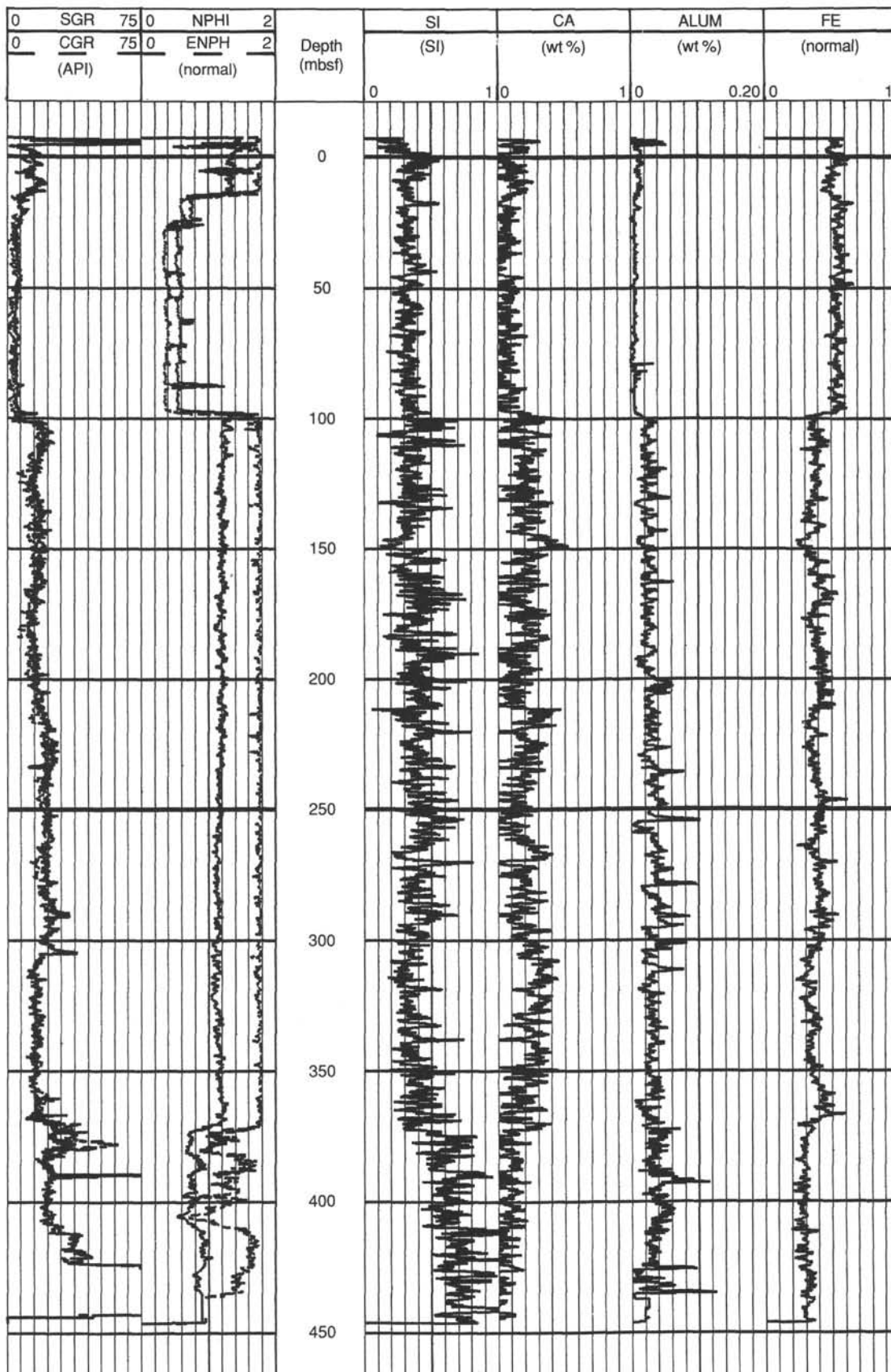


Figure 27. Plot of logs for Hole 782B as a function of depth. Logs shown are gamma ray (SGR and CGR), neutron porosity (NPHI), and epithermal neutron porosity (ENPH) on a relative scale, normalized (see text) silica (SI), normalized calcium (CA), aluminum (ALUM), and normalized iron (FE).

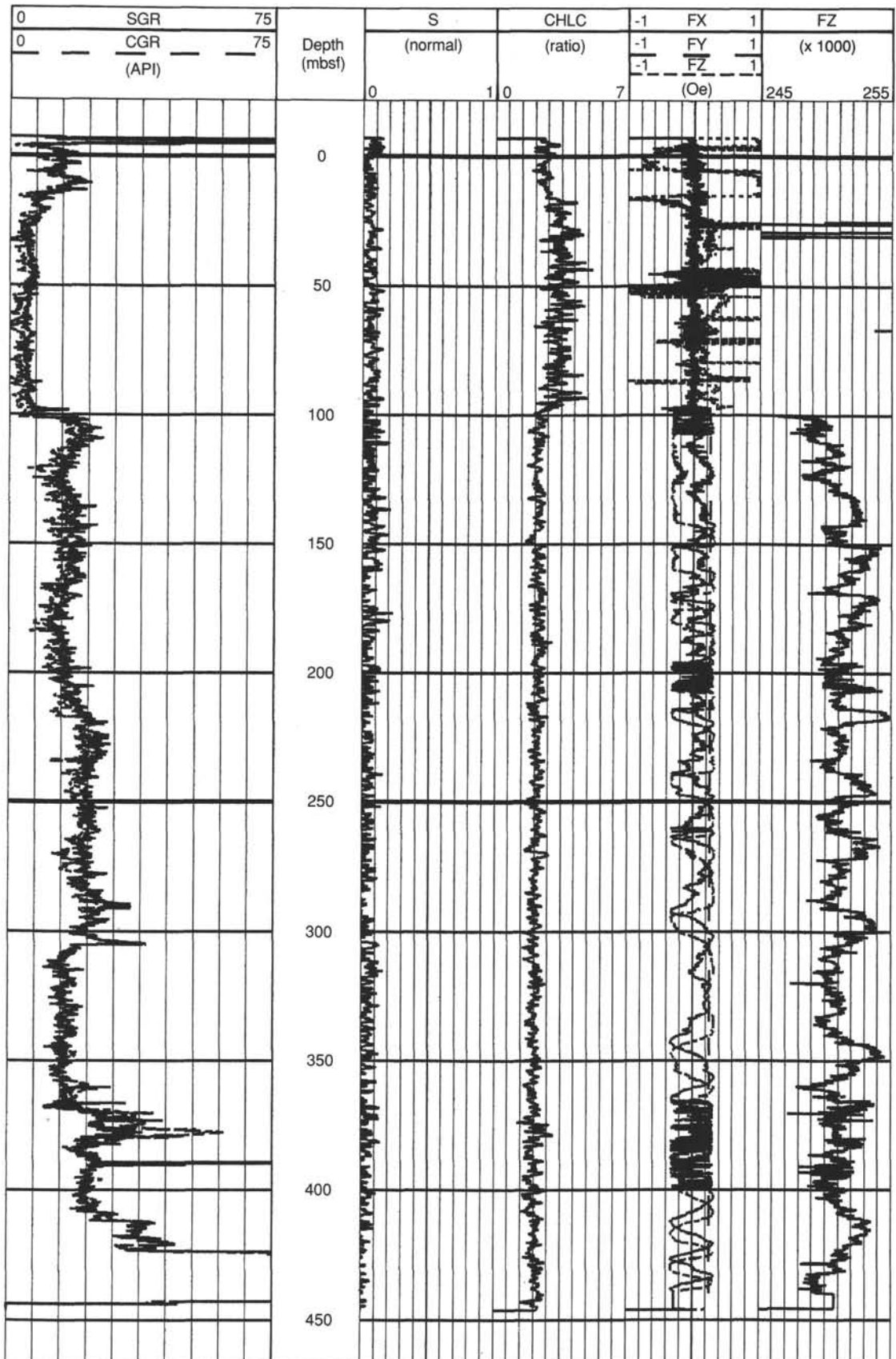


Figure 28. Plot of logs for Hole 782B as a function of depth. Logs shown are gamma ray (SGR and CGR), normalized (see text) sulfur (S), chlorine/hydrogen ratio (CHLC), magnetic field strength (FX, FY, and FZ), and the vertical magnetic field strength $\times 1000$ (FZ10).

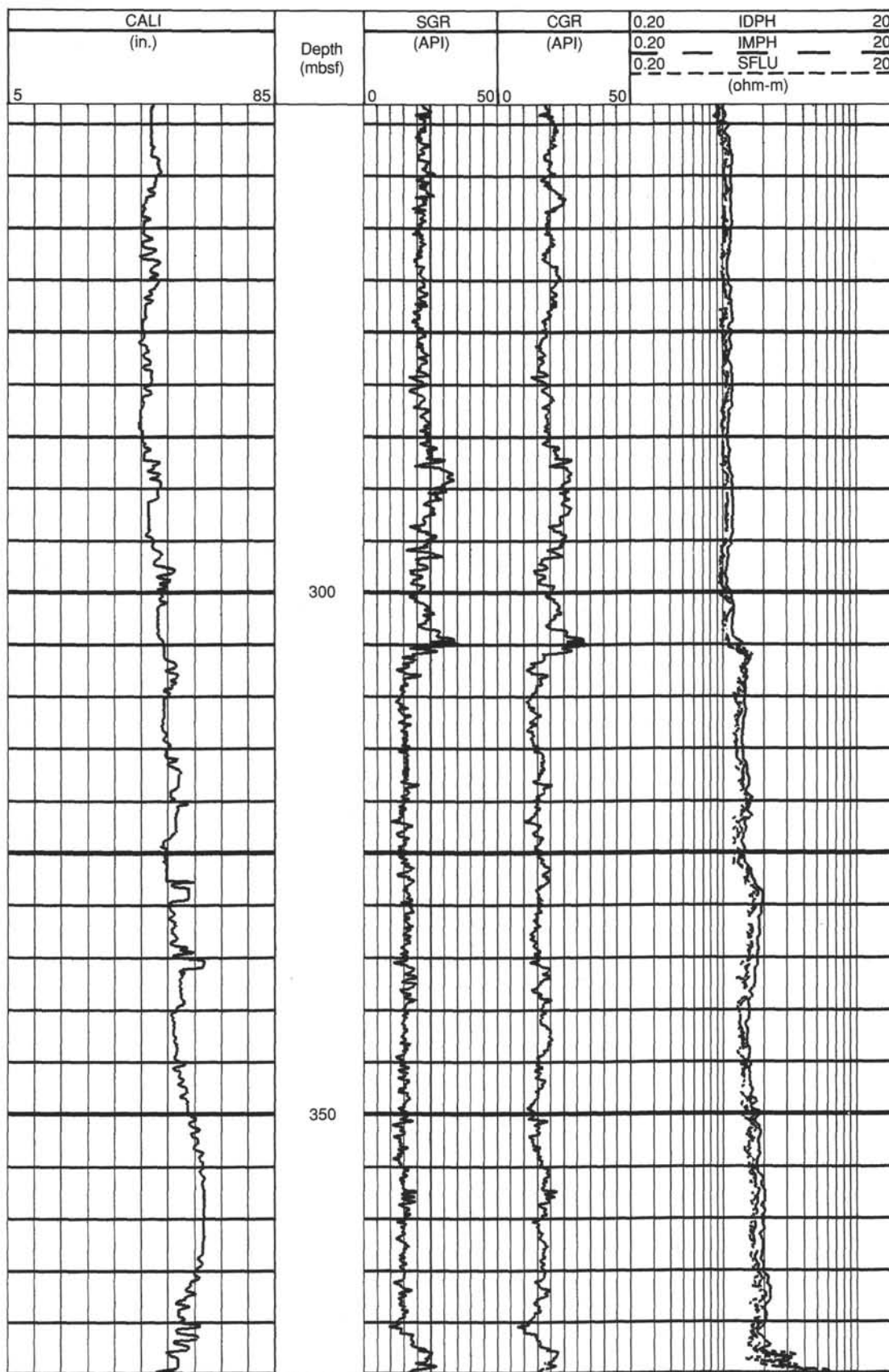


Figure 29. Enlarged plot of logs for second unit (208-305 mbsf) and for the third unit (305-373 mbsf). Logs shown are caliper (CALI), gamma ray (SGR and CGR), and deep (IDPH), medium (IMPH), and spherically focused (SFLU) resistivity.

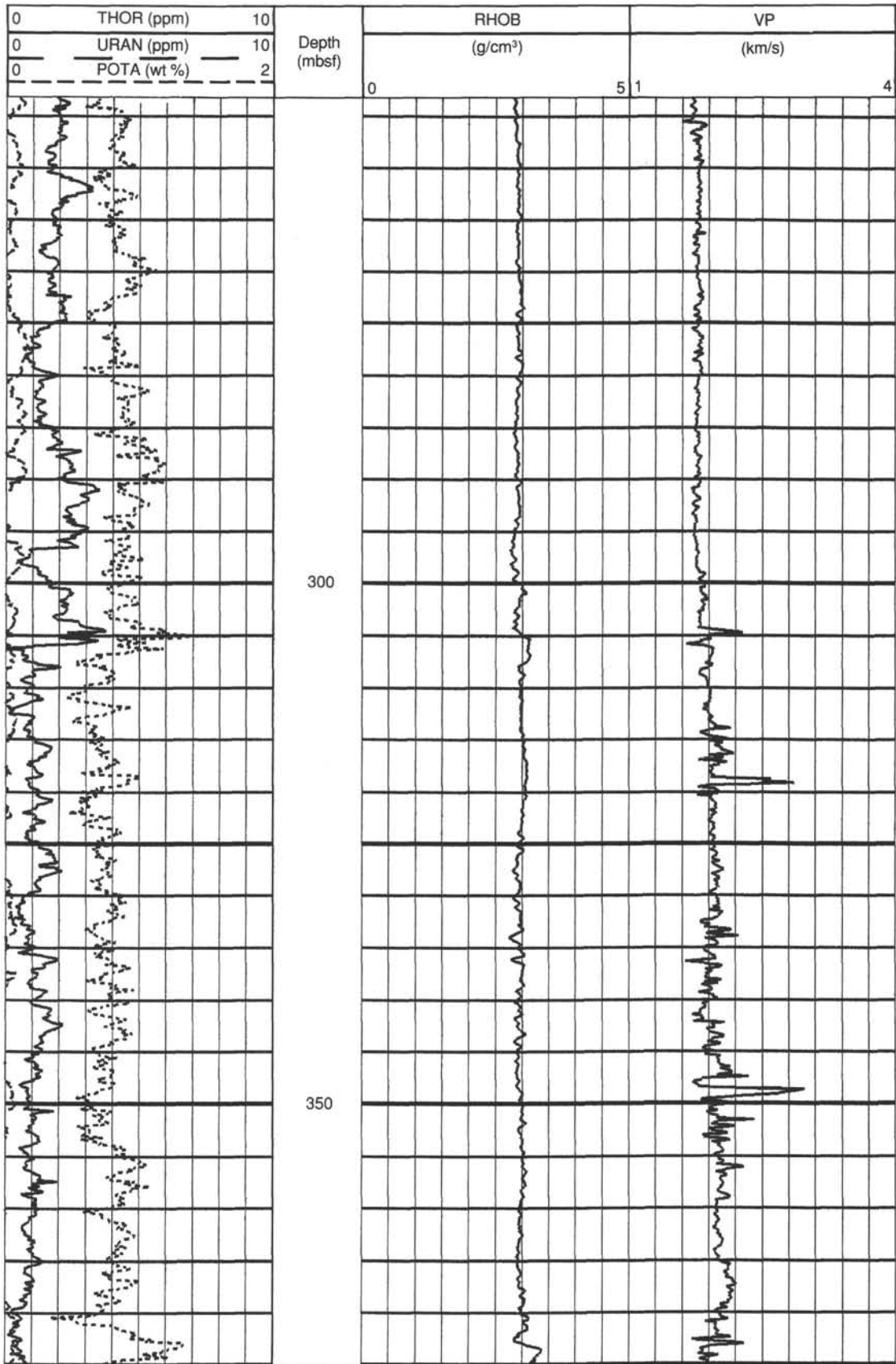


Figure 30. Enlarged plot of logs for the second unit (to 300 mbsf) and for the third unit (305-373 mbsf). Logs shown are thorium (THOR) and uranium (URAN), potassium (POTA), density (RHOB), and sonic velocity (VP).

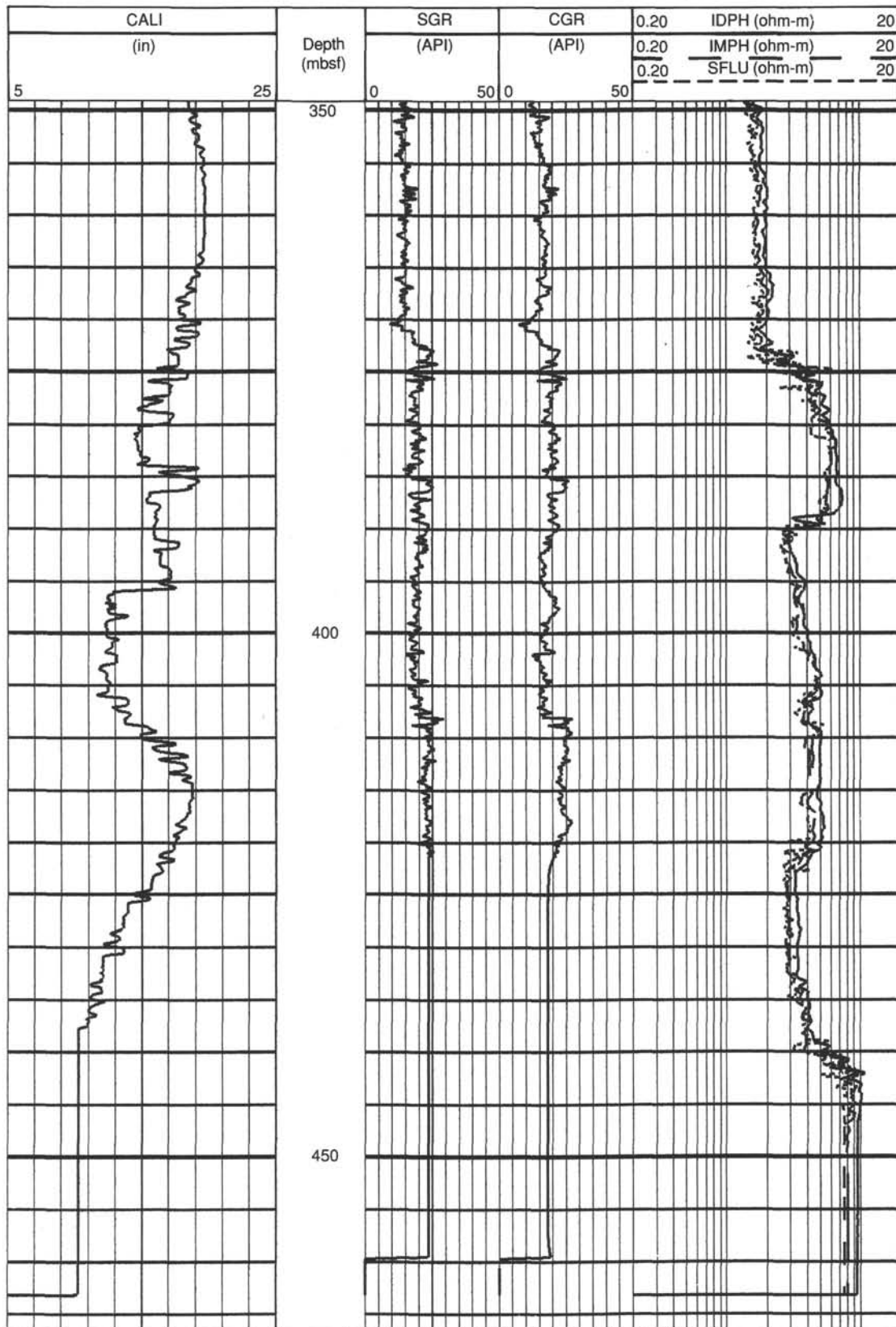


Figure 31. Enlarged plot of logs for the fourth unit (373–409 mbsf) and for basement (409 mbsf to bottom). Logs shown are caliper (CALI), gamma ray (SGR and CGR), and deep (IDPH), medium (IMPH), and spherically focused (SFLU) resistivity.

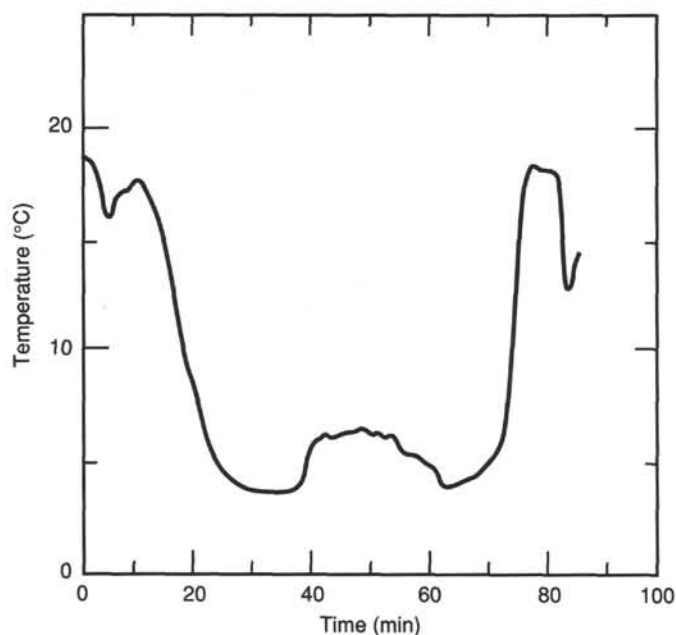


Figure 33. Record of temperature vs. time for Barnes-Uyeda Run 05H at 38.3 mbsf. The irregular temperature record between 40 and 60 min shows that the probe was being moved while it was in the sediment.

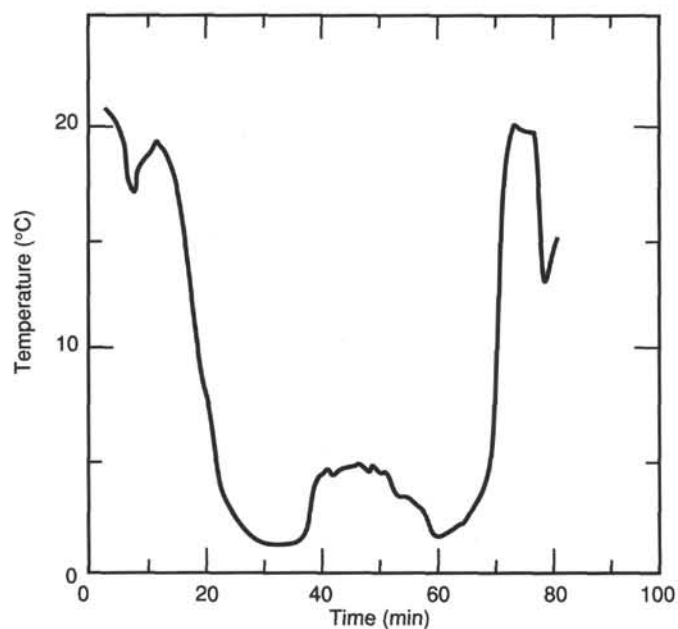


Figure 34. Record of temperature vs. time for Barnes-Uyeda Run 08H at 66.8 mbsf. The irregular temperature record between 50 and 60 min shows that the probe was being moved while it was in the sediment.

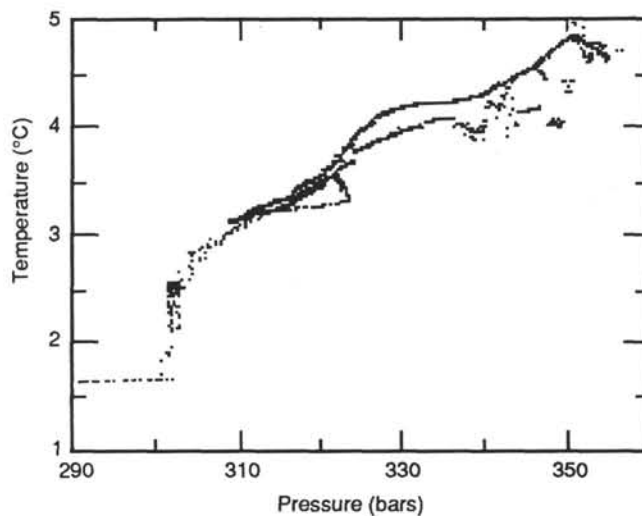


Figure 35. Record of temperature vs. pressure for the first run of the temperature logging tool (TLT). The upper, more solid, line of data is from the slower part of the logging run from the bottom of the hole upward and represents the best data from the run.

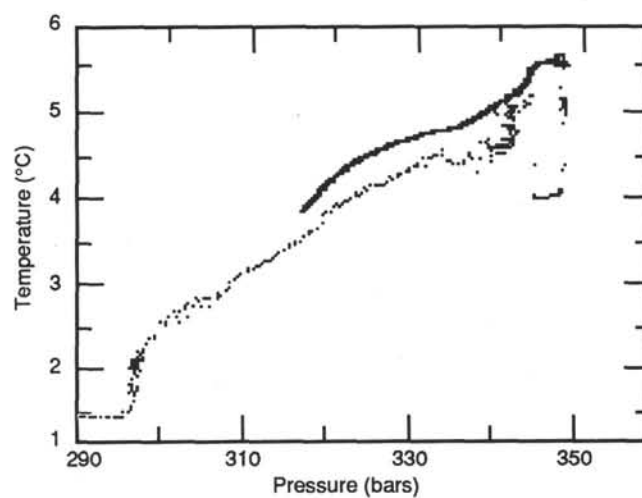


Figure 36. Record of temperature vs. pressure for the second TLT run. The bottom of the hole has warmed by about 1°C relative to the data presented in Figure 38.

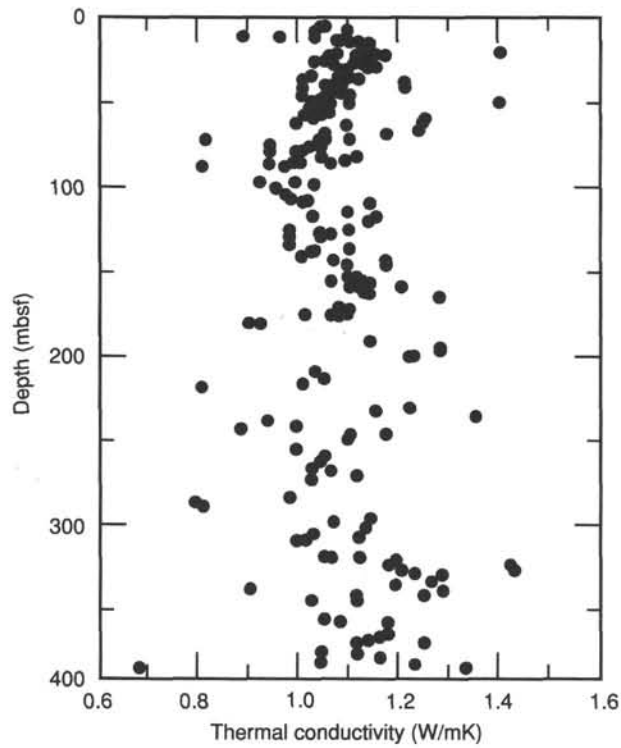


Figure 37. Thermal conductivity vs. depth for Hole 782B. There is little trend with depth.

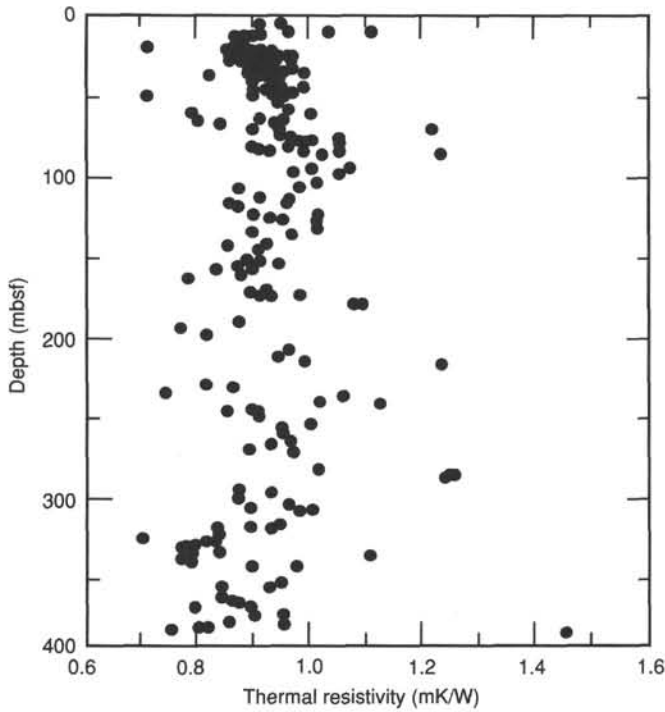


Figure 38. Thermal resistivity (the inverse of thermal conductivity) for Hole 782B.

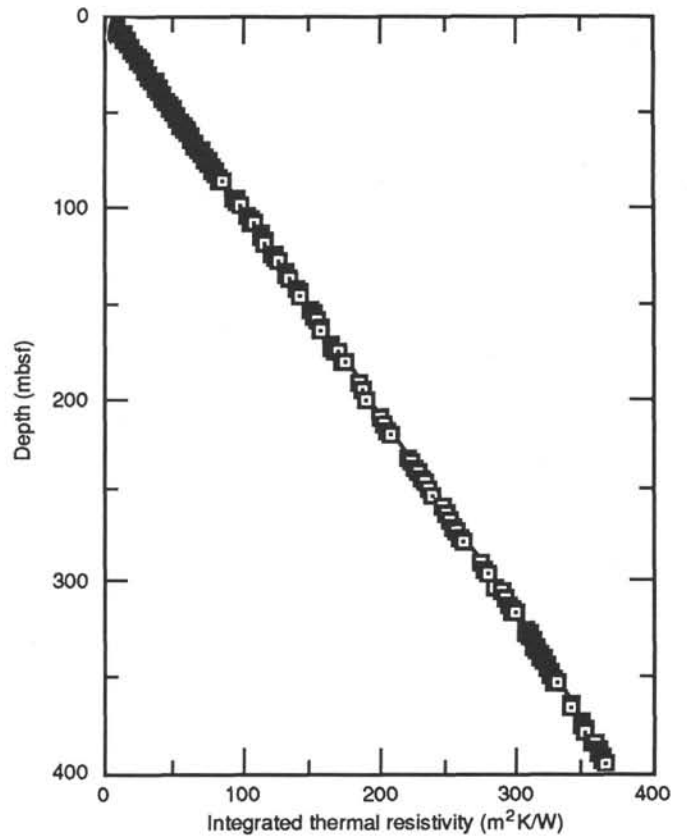


Figure 39. The depth integral of thermal resistivity vs. depth for Hole 782B. This will be combined with a calculated equilibrium temperature profile to determine the heat flow at this site.

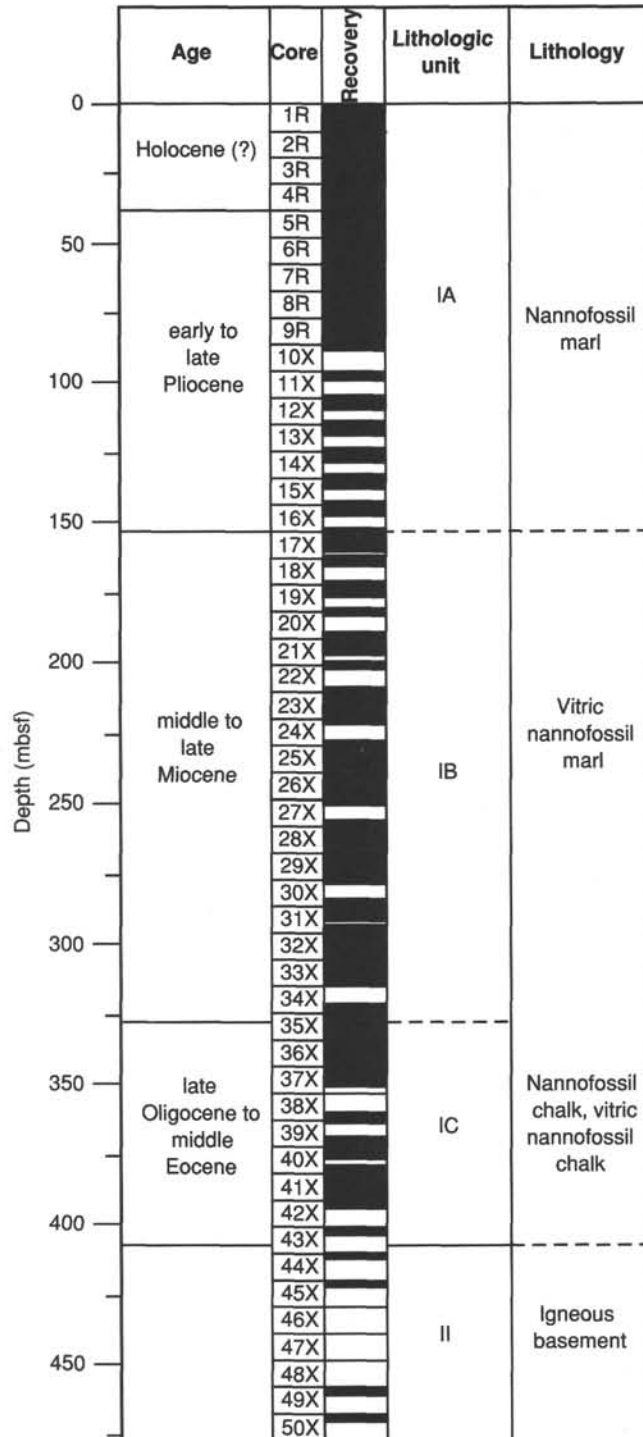
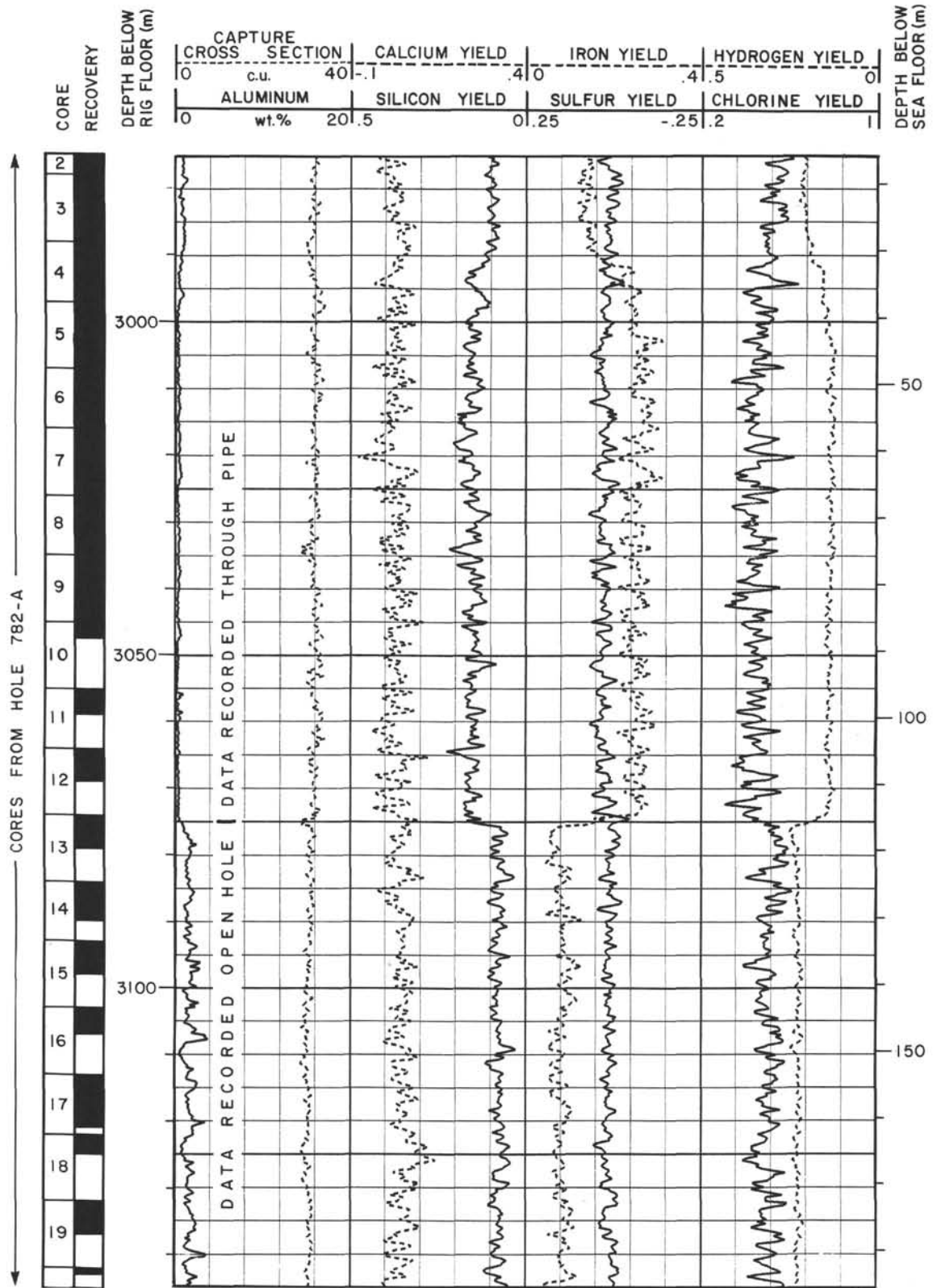
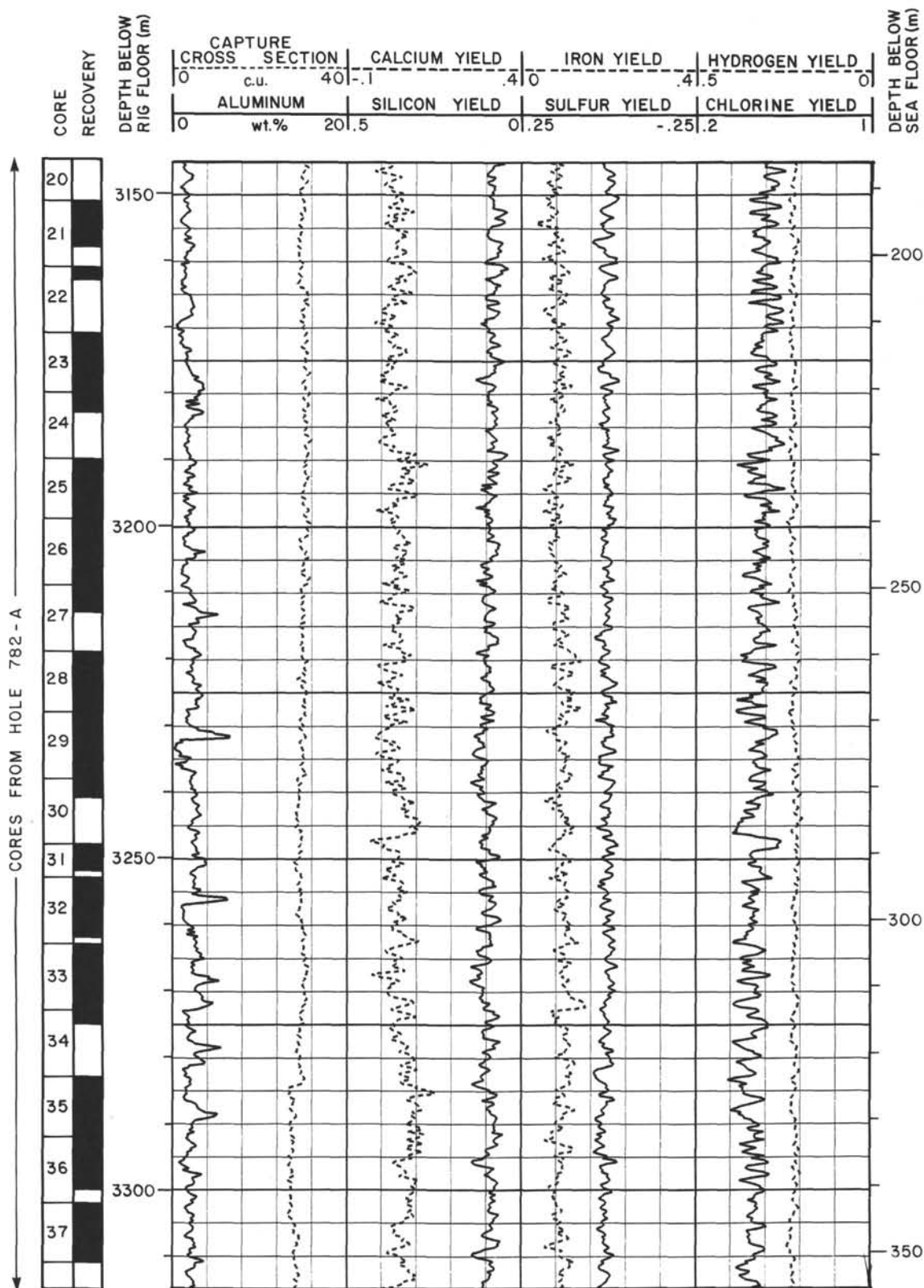


Figure 40. Core recovery and lithologic summary, Hole 782A.

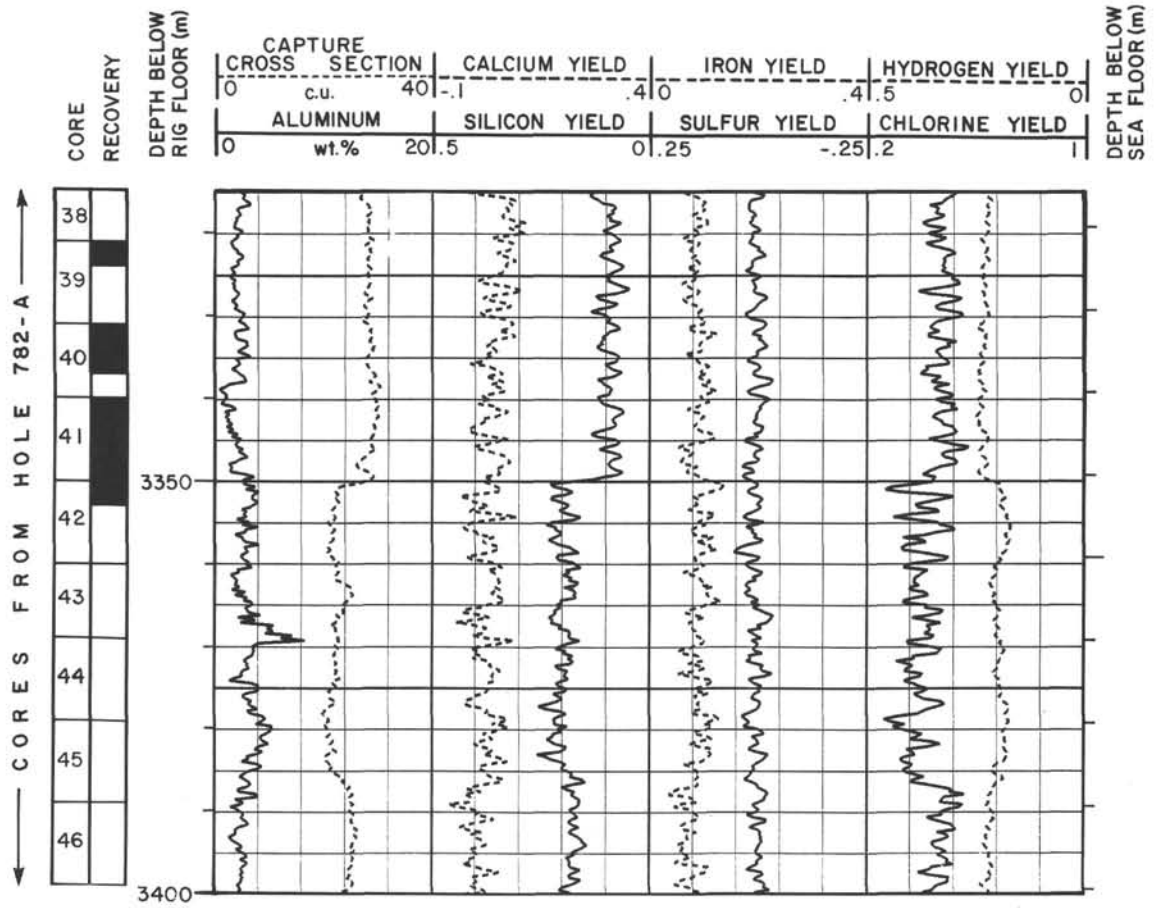
Summary Log for Site 782



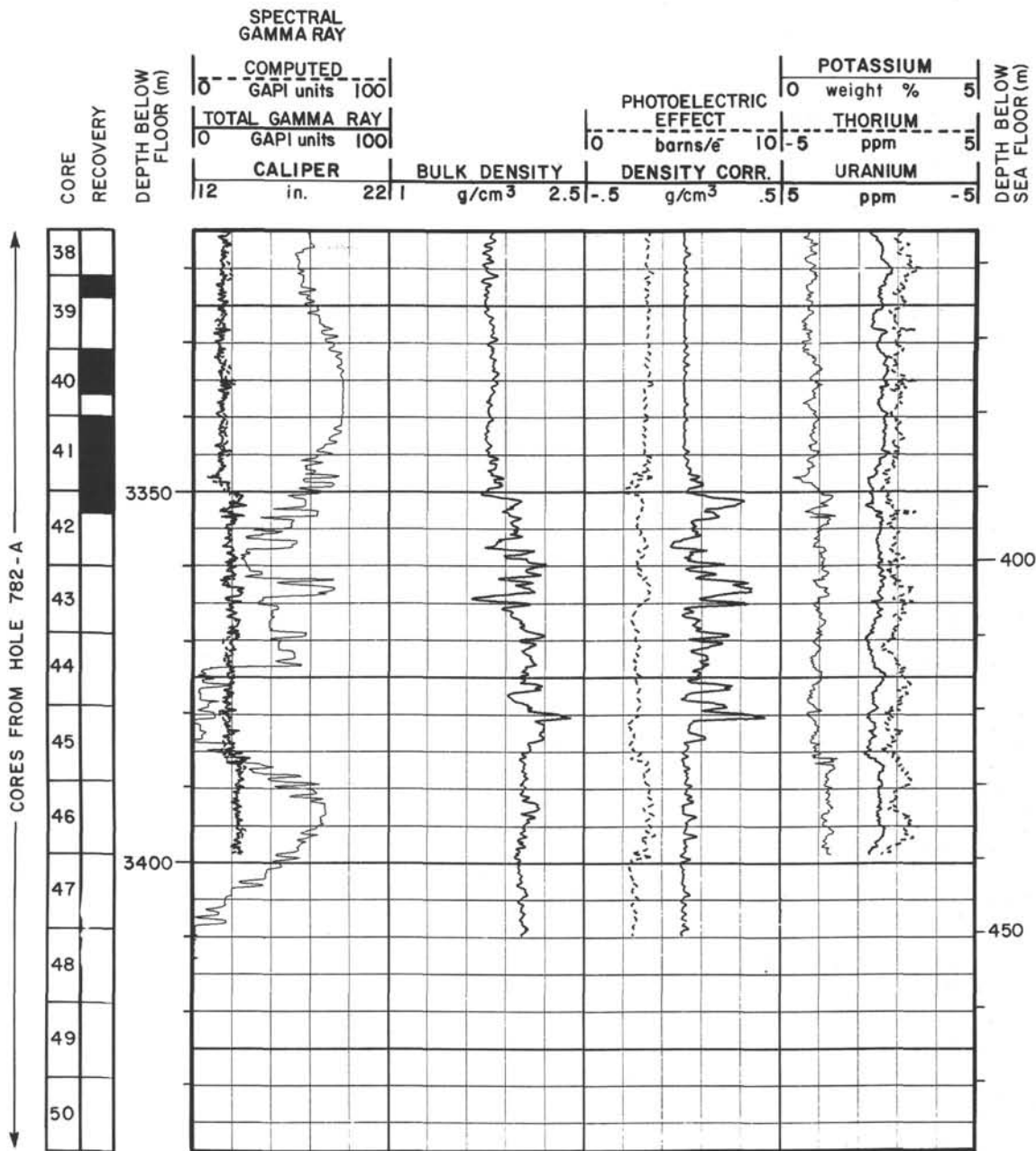
Summary Log for Site 782 (continued)



Summary Log for Site 782 (continued)

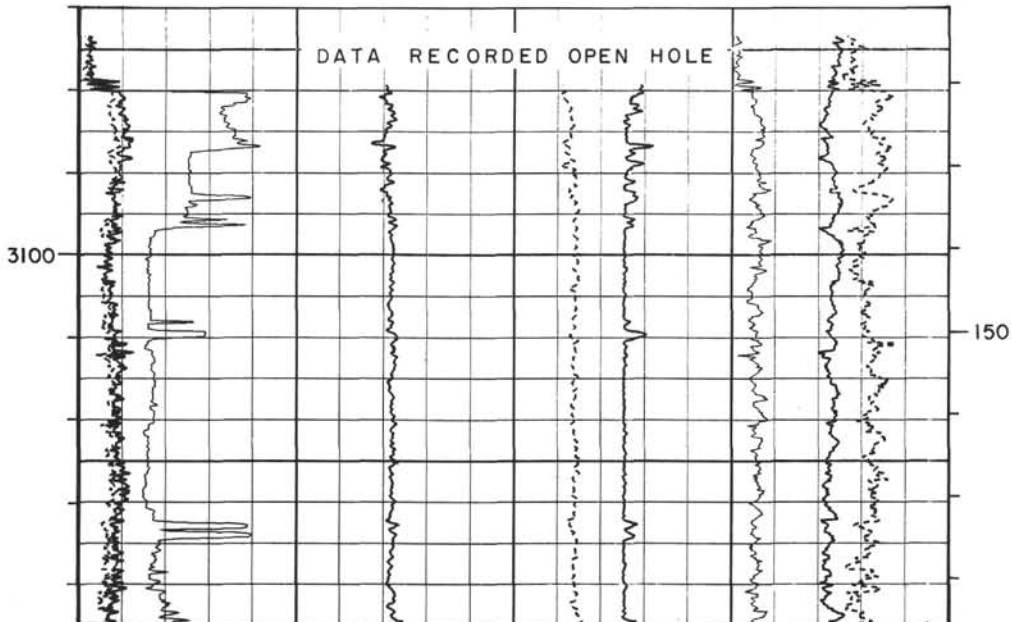
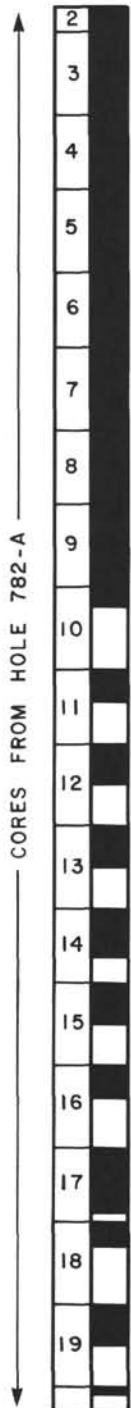


Summary Log for Site 782 (continued)

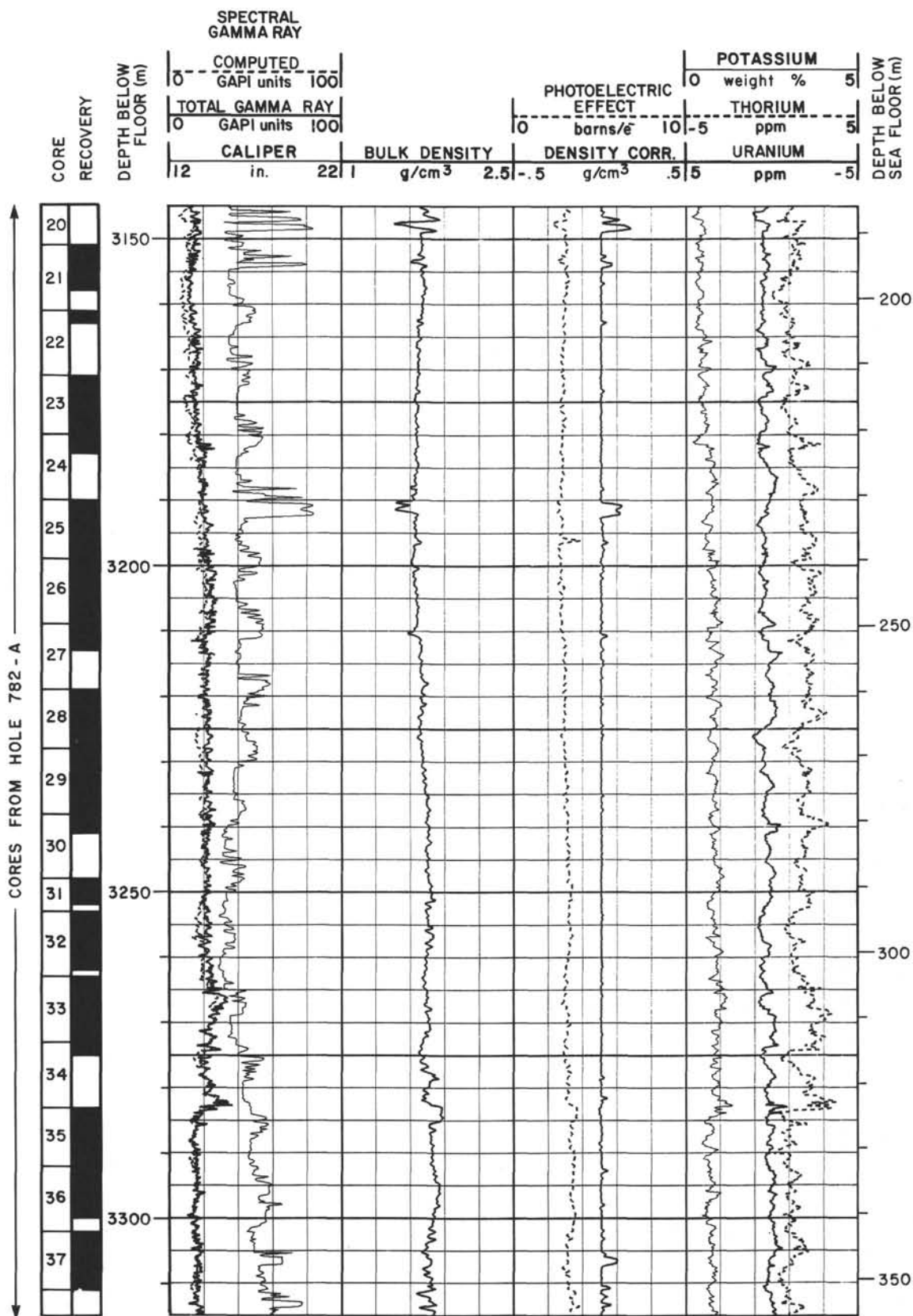


Summary Log for Site 782 (continued)

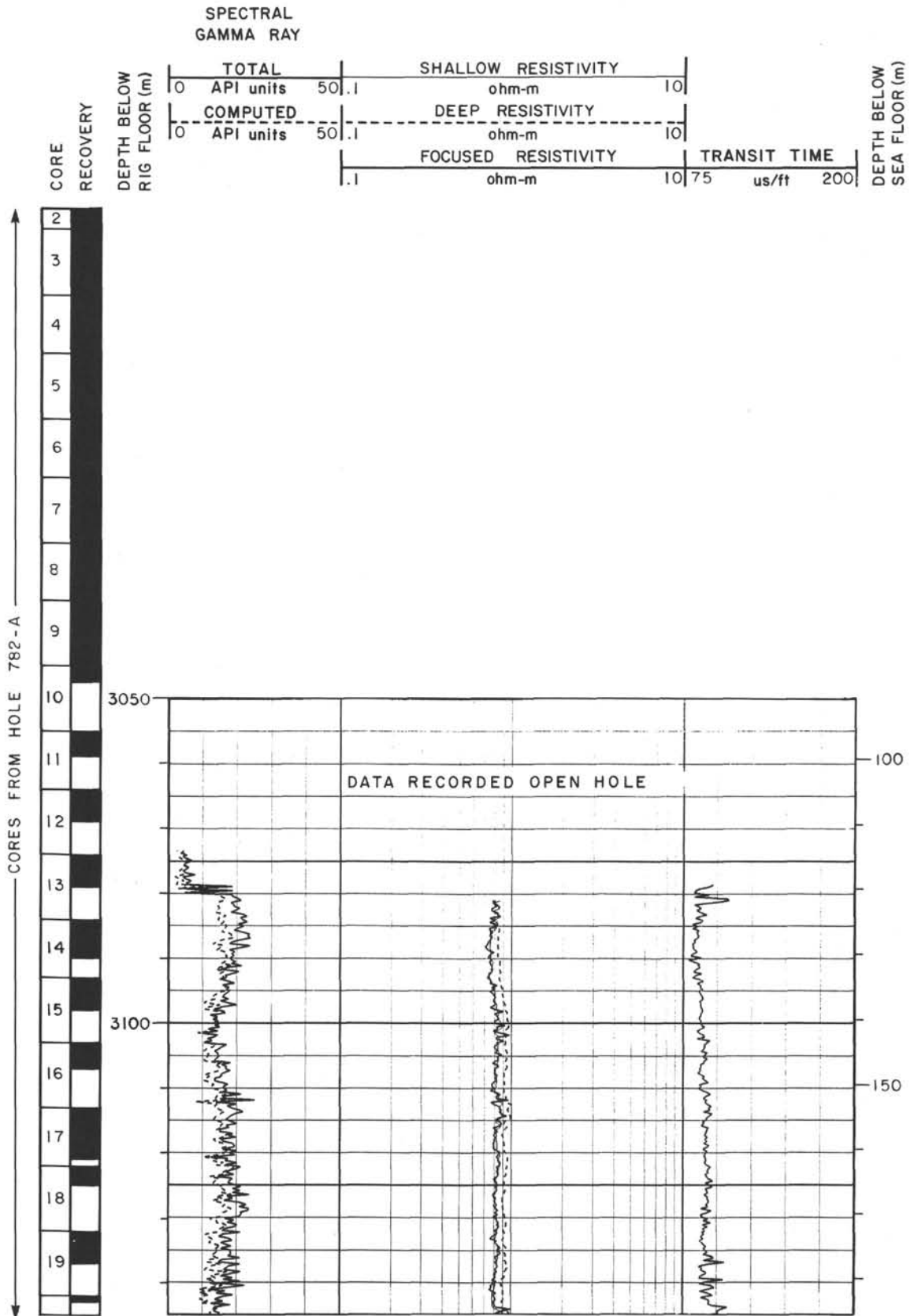
CORE RECOVERY	SPECTRAL GAMMA RAY										DEPTH BELOW SEA FLOOR (m)						
	COMPUTED GAPI units		TOTAL GAMMA RAY		PHOTOELECTRIC EFFECT		POTASSIUM		THORIUM								
	0	100	0	100	0	10	0	5	0	5							
	GAPI units		GAPI units		barns/e		weight %		ppm								
	12	in.	22	1	BULK DENSITY	g/cm ³	2.5	-	5	DENSITY CORR.	g/cm ³	.5	5	URANIUM	ppm	-	5



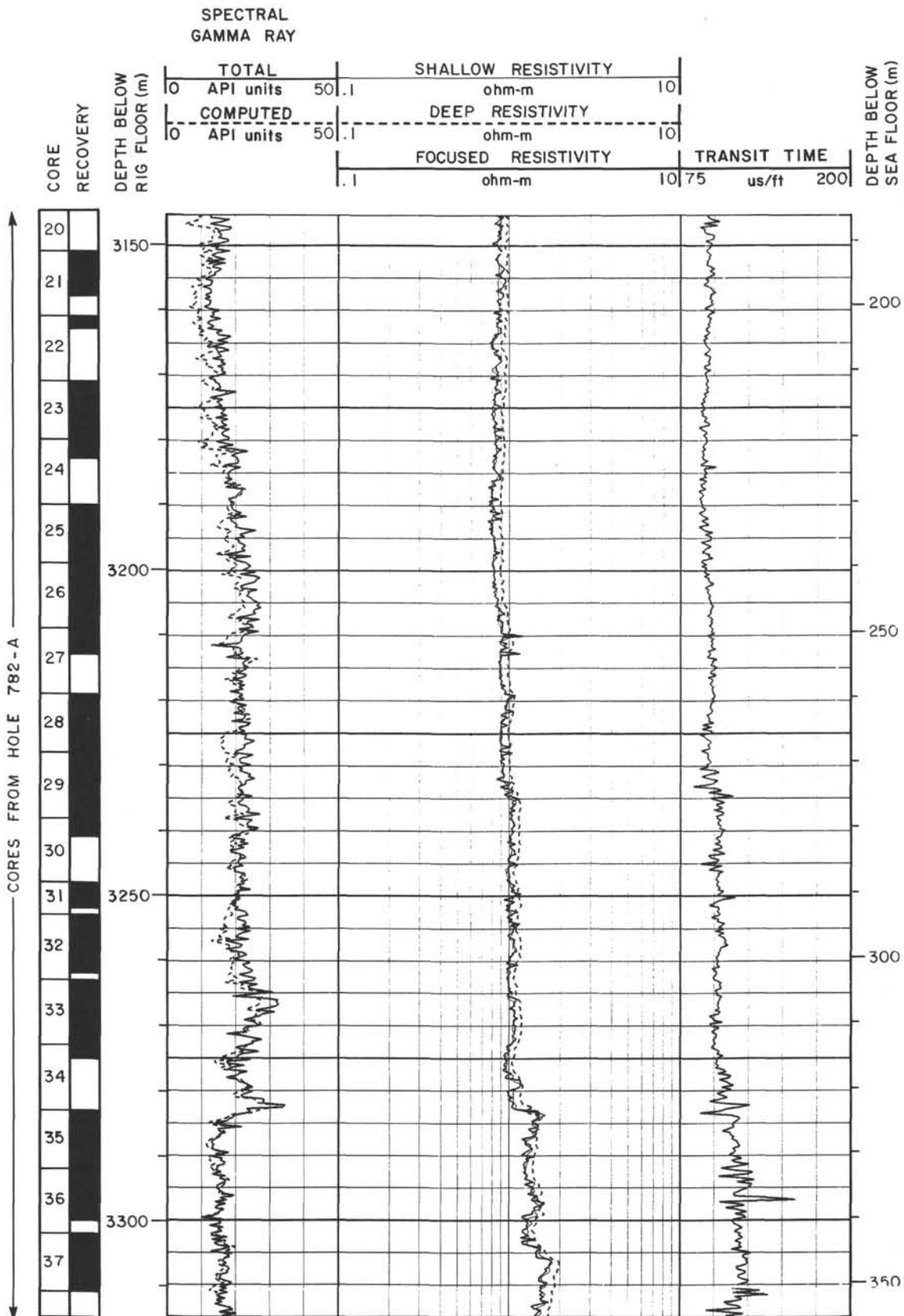
Summary Log for Site 782 (continued)



Summary Log for Site 782 (continued)



Summary Log for Site 782 (continued)



Summary Log for Site 782 (continued)

